Faster than the Blink of an Eye

New insights into neuromuscular activations of arboreal snakes

Grady William Jensen

Graduate School of
Systemic Neurosciences

LMU Munich

Dissertation
der Graduate School of Systemic Neurosciences
der Ludwig–Maximilians–Universität München

June 2020

Supervisor:
Prof. Dr. Patrick van der Smagt
Argmax.ai, Machine Learning Research Lab
Volkswagen AG

First Reviewer: Prof. Dr. Patrick van der Smagt
Second Reviewer: Prof. Dr. Hans Straka
External Reviewer: Prof. Dr. Horst Bleckmann

Date of Submission: 4 June, 2020
Date of Defense: 18 September, 2020

Contents

Acknowledgement

I wish to thank various people for their contribution to this project: Dr. Alexandros Paraschos, for his help configuring and running the Franka Emika robotic arm; Rommy Petersohn and Ingrid Weiss, from the Friedrich-Schiller University of Jena, for their help in collecting the X-ray data; Dr. Maximilian Bothe for providing the Matlab script used to control the turntable; Yvonne Schwarz for much needed assistance with animal care; Prof. Dr. Hans Straka for his insights and guidance when encountering research, as well as bureaucratic, issues; and finally Dr. Tobias Kohl who invested an immense amount of time and personal involvement which directly enabled the research for this thesis.

Special thanks should be given to Prof. Dr. Patrick van der Smagt, my research project advisor, for seeing something in me worth nurturing, for his guidance, and for his unwavering support through the many twists and turns of the research that supports this thesis.

Finally, I wish to thank my wife, Elisabeth, for being a strong researcher role model, my editor-in-residence, for giving me the confidence to pursue my crazy ideas, and supporting me when I sometimes, or most of the time, bite off more than I can chew.

Danke.

Summary

Arboreal snakes such as the amazon tree boa (*Corallus hortulanus*) are able to cantilever large sections of their body for very long periods of time with seemingly minimal muscular effort. From this cantilevered position they exert quick strikes as well as compensate for any movement of the object from which they cantilever. The mechanisms of muscle coordination required for the dynamic switch between resting and strike have been hypothesized for terrestrial puff adders (*Bitis arietans*) to result from the vast and unique musculo-tendon arrangement of the snake's epaxial muscles put under pre-strike tension, i.e. a spring-like mechanism where the snake is able to store a large amount of energy in tendons which can then be later quickly released. Furthermore, while muscle activity during gap crossing or extension activities has been described for an arboreal species, it is not clear how the stationary snake's muscles compensate for perturbations of the anchoring object, e.g. as happens in the wild with a branch swaying in the breeze. Using a self-built high-speed 3D tracking system along with a novel method for collecting chronic multi-electrode bipolar electromyography (EMG) information, my data is not only unsupportive of the elastic energy-storing strike hypothesis but provides insights to the muscle coordination required for stabilization in a moving, as well as stationary, environment.

This dissertation is split into two main parts. The first part focuses on the hardware and methods established to allow the capture of the novel data presented in the second part. The first part is composed of two chapters. One contains the content of a manuscript that has been accepted for publication (Ch.1), and the other the content of a manuscript in the process of submission. The second part of the dissertation focuses on deeper analysis of data collected during a pilot study in which the methods of part one were leveraged. The content of part two will be submitted for publication at a later time.

List of Figures

List of Tables

Introduction

Snakes are infamous in the general public for their perceived danger, and famous for their method of locomotion. This method of transport, and their body structure, has interested the fields of biomimetics and robotics for decades (Wright et al. (2007); Liljebäck et al. (2014); Crespi and Ijspeert (2008); Nilsson (1998); Bayraktaroglu (2009)). This interest is mainly focused around trying to extract insights from their method of locomotion. A method that is ideally suited to a wide variety of habitats and terrains. Typically, robot locomotion involves a wheeled base, which has limited terrain capacity. Though, more recently vertebrate or, more common, humanoid paradigms have been used. These humanoid models typically require robots of much larger size as they have more pieces devoted to keeping the robot upright.

Snake-like robotic design benefits from the inherent stability that a snake has, i.e. it can't fall over unless it falls off of an object, it can traverse a variety of terrains, and it has good traction properties. Snake robots are ideal for situations of extraction or inspection tasks where a small wheeled robot is not able to venture. The downside is that they have a slower speed than other types of robots, such as wheeled robots, on their suitable terrain, e.g. an autonomous vehicle on a roadway can achieve very high rates of speed. Furthermore, they cannot usually carry a large payload, and they are challenging to develop as they have a large number of degrees of freedom. Therefore, new insights into the movement mechanisms of snakes that could improve robotic design and performance would be greatly beneficial. Actions such as climbing or gap crossing are very interesting for robot development as they dramatically increase the applicability of a robot to otherwise challenging terrains. Understanding how snakes are able to cantilever themselves, i.e. in gap crossing or resting configurations of arboreal species, and not sacrifice performance in other areas of their behavior could be deeply beneficial for robotic design, e.g. in robotic arms. Furthermore, although it has yet to be proven, it is widely believed that the energy consumption of the biological snake to complete these tasks is low. Insights into the snake's mechanism could improve energy efficiency for similar tasks in robotic models. Knowledge

concerning the ability of arboreal snakes to handle perturbations to their environment while staying focused on a task might also generalize to help stability issues in larger robots.

While neurosciences such as neuroethology and systems neuroscience have been primarily investigating snake sensory systems (Goris (2011); Simões et al. (2016); Catania et al. (2010); Catania (2010); Christensen et al. (2012); Westhoff et al. (2005); Martínez-Marcos et al. (2002)), their interest in movement behavior has been just as notable. Locomotion research on snakes has enabled us to decipher how snakes propel themselves forward without limbs. This skill involves coordination between the movements of the snake and the friction of their skin on the surface the snake is attempting to traverse using specific muscle motor patterns. This behavior falls into four categories of movement according to (Gray (1946); Jayne (1986); Hu et al. (2009); Jayne (1988); Newman and Jayne (2018); Lissmann (1950); Moon and Gans (1998)): lateral undulation, concertina, sidewinding, and rectilinear. These discoveries were made possible by the recording of these movements using single cameras and a defined experimental setup with known distances or by using two or more cameras. Recently, the work of Gart et al. (2019) used multiple cameras to record and analyze the techniques used by kingsnakes (*Lampropeltis mexicana*) to traverse step inclinations with height up to 30% of the snout–vent length (SVL) of the animal, and discover useful insights into the strategies employed by the snakes for covering diverse terrain. The SVL is a common measurement metric when working with snakes as the distance from the tip of the snake to the cloaca is a better measure of the size of the snake than the tip to tail measurement. The cloaca to tail tip length can vary greatly across species. Cantilevering has also been investigated with the use of cameras (Lillywhite et al. (2000)) and later using both cameras and electromyography (EMG) to get a fused view of how muscle activation correlates with animal movement (Jorgensen and Jayne (2017)). These studies have been vital in providing the base understanding of how axial muscles of the snake contribute not only to movement, but to interesting problem solving strategies at a slow rate of movement, i.e. cantilevering and gap-crossing.

Data fusion of camera and EMG information has proven vital for the understanding of snake movement behavior (Jayne (1988); Young (2010); Newman and Jayne (2018)). A major reason for this is the complicated body structure and musculature of the snake. The

[†]The μCT-scans were collected in collaboration with Dr. Tobias Kohl at the Chair of Zoology at the Technical University of Munich along with Dr. Bernhard Ruthensteiner at the Zoologische Staatssammlung München (ZSM).

[††]Background subtracted image. Original image captured and used with permission from Dr. Tobias Kohl.

Figure I-1: **Left**: Cross-section of an amazon tree boa (*Corallus hortulanus*). The four main axial muscles of the snake *M. semispinalis-spinalis* (blue), *M. longissimus dorsi* (orange), *M. iliocostalis* (green), and *M. multifidus* (yellow) are shown in a μCT image from the midsection of the snake. This view makes it clear how hard it is differentiating muscles other than the four main axial muscles. † **Right:** A juvenile amazon tree boa in a stereotypical cantilevered resting configuration. This position can be held for hours at a time and a transition to strike movement often requires no visible configuration change.††

skeletal and muscular structure of a snake forms a quasi-continuum and is highly articulated. While there are four clear main axial muscles of the snake (fig. I-1), i.e. *Musculus longissimus dorsi* (LD), *Musculus semispinalis-spinalis* (SSP), *Musculus iliocostalis* (IL), and the *Musculus multifidus* (Jayne and Riley (2007)), the remaining muscles in the trunk of the snake are very small and difficult to differentiate. Furthermore, even though these muscles are quite prominent, the tendons attached to these muscles can span upwards of 20–24 vertebrae in the case of the SSP, or 7–8 vertebrae in the cases of the LD and IL of the brown tree snake (*Boiga irregularis*). Though, if true morphology is being taken into account, the LD connects to the IL, which means that from the posterior attachment of the LD to the anterior attachment of the IL as many as 24 vertebrae can be spanned (Jorgensen and Jayne (2017)). It is known, however, that the distances these tendons span vary across species of snakes, e.g. the LD-IL system spans 20 vertebrae in gopher snakes (*Pituophis melanoleucus affinis*) (Moon and Gans (1998)).

This makes the decoupling of motion and muscle activation a very hard task in snakes.

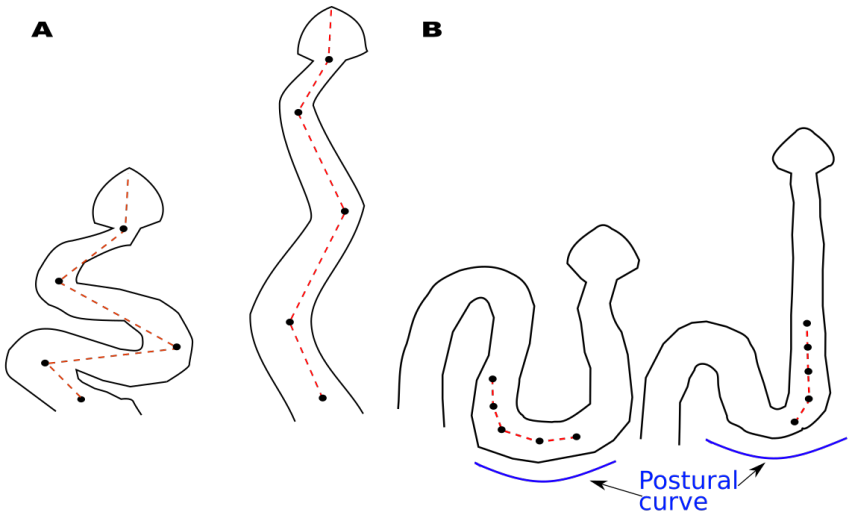

Figure I-2: The methodology for categorizing parts of the snake strike of a boid snake, adapted from Kardong and Bels (1998). (**A**) The gate model of snake strike. The snake decreases its distance to an anterior target by moving the black dots, i.e. the gate hinges, medially. This causes the segments of body between hinges to elongate in the anterior direction. (**B**) The tractor-tread model of snake strike. To move towards its target, the segments of the snakes body flow through the postural curve, thus decreasing the distance between the head and the target.

Combining video and EMG allows the reconstruction of movement as the EMG show the muscles that are activated and the video shows how that activation affects the positioning or movement of the snake. This was shown to great effect when using video and EMG together to validate the hypothesis for the method of rectilinear motion (Lissmann (1950)) almost 70 years after it was stated (Newman and Jayne (2018)). The combination of video capture and EMG has furthered the understanding of a variety of other snake behaviors as well. For example, jaw and mandible muscle activity has been investigated in post-prey capture feeding behaviors (Cundall (1983); Cundall and Gans (1979)), muscle coordination needed for constriction (Moon (2000)), as well as the drinking of water (Jena et al. (1995)).

In all of snake behavior, however, it is the strike which draws largest mixture of fear and awe. This mixture comes from the perceived peril presented by the strike as well as the very fast speeds in which the strike occurs. For example, strikes from the black rat snake (*Pantherophis obsoletus*) can reach speeds of 2.67 m/s with maximum accelerations of 190 m/s^2 (Penning et al. (2016)). There are two models for the snake strike (Kardong and Bels (1998)), the gate model and the tractor-tread model. For a visual guide, see figure I-2. The gate model occurs when the apex of the coiled curves of the snake serve as a pivot point (i.e. a gate hinge) that swings open the internal angle of the coiled curve which

extends the anterior portion of the snakes body forwards. The tractor-tread model occurs when the body of the snake stays fairly rigid at the postural curve and the segments of the body 'flow' around the curve. The tractor-tread model shows similarity to movement of undulatory locomotion (Kardong and Bels (1998)). This coincidence could mean that the neuromuscular activation patterns used for the two types of behavior are similar. This begs the question of whether the gate-model uses similar neuromuscular patterns as the concertina movements of the snake, as they also share a similar movement. This is interesting as concertina movements might be the evolutionarily oldest mode of snake locomotion (Gans (1986)).

Though there are two forms a strike can take, a single snake strike can be composed of one or both forms. The ability to split the strike motion between forms of strike lends credibility to the idea that a snake strike is not an all-or-nothing ballistic movement. Frazzetta (1966) described the ability of a striking python to change its strike vector, though this behavior has not been seen in any other studies. Additionally, it has been shown that posture does not affect viperid strikes (Kardong and Bels (1998); Young (2010)), which is very surprising given the neural coordination presumed to be required to modulate the behavior, the speed of the process, and the complexity of muscle activation (Cundall and Greene (2000)). This lends support to the idea that open-gate strikes are faster than tractor-tread strikes, the latter which would require more continuous motor control, while the former could be done in a more ballistic manner without adjustment via feedback (Moon et al. (2019)).

The progression of a strike can be further broken down into distinct phases along a timescale, though this categorization differs across researchers. Kardong and Smit (2002) broke the strike into 3 main scenes (pre-strike, strike, and post-strike) with phases and even stages in some phases for a total of 14 distinct parts, while de Cock Buning (2015) used 9 phases without hierarchy. This work uses the hierarchy of Kardong and Smit (2002), but in a modified manner, as shown in figure I-3. 'Pre-strike' entails the period of time from when the stimulus is first presented to the snake, through the first movement of the snake being seen in the videographic record following the introduction of a prey stimulus and ending at the start of the strike. This first movement seen in the video comprises small head movements to orient towards the stimulus or slight movement forwards towards the stimulus. The 'Strike' phase encompasses the visual start of the strike up to the point of maximum extension of the strike towards the prey. The 'Post-strike' phase consists of the small amount of time following the point of maximum extension until the snake is again

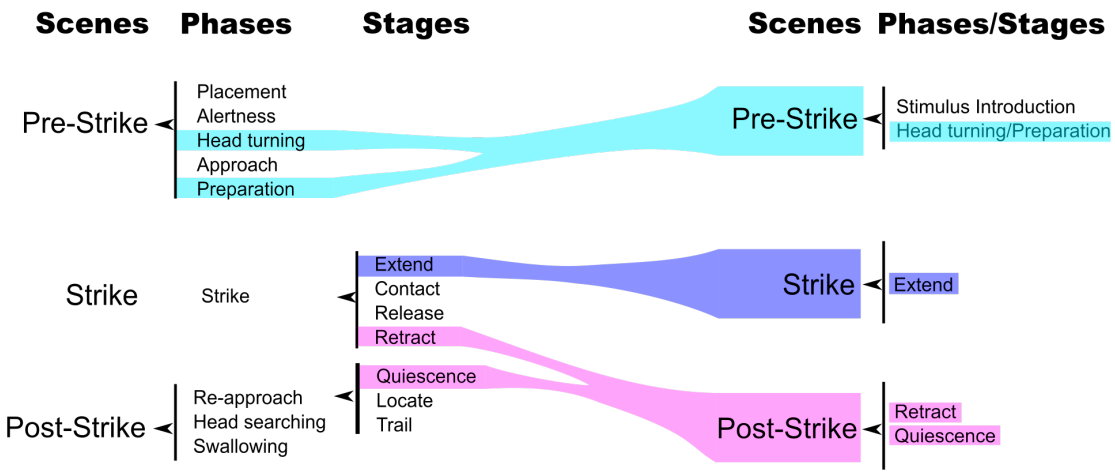

Figure I-3: The methodology for categorizing parts of the snake strike of a boid snake. On the left is the methodology of Kardong and Smit (2002), a very comprehensive description. For the purposes of this work, a simplified model (right) is assumed as the snake is not in a natural setting. All phases of the reduced model are easily verifiable from video captures. The left side of this figure is adapted from Kardong and Smit (2002).

coiled in a form similar to pre-strike and is no longer visibly moving. This modified form is used because all data collections performed were in a laboratory setting with artificial stimulus. This automatically precludes most of the phases/stages of the Kardong and Smit (2002) model. The phases used in this work were also easily verifiable using the video record.

In the research that has been conducted, there is consensus in the idea that there are two motivations for striking: predatory and defensive. While the purpose of a predatory strike is straightforward and the main motivation for defensive strikes is as well, i.e. to keep a potential threat at bay, in the latter case the specific goal is not clear. It has been hypothesized for terrestrial vipers that the goal of defensive strikes could be to startle or fake a threat to maintain this distance, to cause pain to a potential predator, or some other reason (Moon et al. (2019)). Furthermore, classifying the two types of strikes is not straightforward as the literature already shows species-specific differences in behavior. The western diamondback rattlesnake (*Crotalus atrox*) strikes farther and faster in its defensive strikes than in its predatory (LaDuc (2002)), while the puff adder (*Bitis arietans*) does the opposite (Young (2010)). Differentiating these strikes through performance characteristics is thus not possible. As Moon et al. (2019) states, the aspects or indicators of strikes that best describe strike performance are not yet clear and very may well differ according

to species or environmental differences, i.e. temperature. The top candidates for these indicators are currently strike velocity, distance, acceleration, duration, and success rate. These indicators, however, are correlated in many respects. The further a strike extends the higher the maximal velocity of the strike (Herrel et al. (2011)).

Research in snake strikes has benefited greatly from the availability of progressively faster cameras with which to capture the snake's motion. This leads to some confusion when comparing the results of different studies as a 'high-speed' camera in one study could refer to 100 frames a second, while in another it could mean 2000 frames a second. When a time from strike initiation until contact with the prey only takes 0.05 s (Kardong and Bels (1998)), the difference between 5 frames and 100 frames of the same strike is enormous. Typically, the higher the frame rate of the camera, the higher the cost of the camera. This creates a situation where access to this equipment is limited. Furthermore, while these cameras have been utilized to understand the mechanics of snake bites and envenoming strategies, the analysis of the data is almost always done in two dimensions (2D) as only a single camera is used, or in the case where two cameras are used point triangulation is not implemented to track the the snake in three dimensions (3D). More recently there have been a few studies that use multiple cameras to track points on snakes in 3D (Gart et al. (2019); Jorgensen and Jayne (2017)), also known as motion capture. These snakes movement tracking methods have been very helpful in observing slow snake movements, but no study to date has used motion capture technology to capture the fast kinematics of the strike. The studies by Gart et al. (2019) and Jorgensen and Jayne (2017) focused on slow moving behavior where fast image sequence were not required. For many researchers buying multiple high-speed cameras is not beneficial as many do not have the expertise in programming or computer vision to put together a system capable of doing 3D motion capture using such cameras. Commercial options exist, but for multiple high-speed cameras (>500 Hz) the cost for the entire vendor setup is often out of reach. Likewise, opensource options exist, but one must cobble together several different software solutions from data collection through data processing; this often requires expertise in programming or computer vision.

Single or perpendicularly-positioned high-speed video cameras have been used to record strike dynamics and distill performance indicators such as strike speed, maximum velocity, etc. The majority of this research focuses on the terrestrial snakes such as viperids or large pythons (Ryerson and Tan (2017); Kardong and Bels (1998); Cundall and Deufel (1999); Penning et al. (2016)). The research focusing on arboreal snake strikes is much less

diverse with a single study of arboreal pit vipers (Herrel et al. (2011)). Research on boid snakes' strikes and other arboreal snakes is limited to tracking of the head and jaws and does not include the axial motion dynamics of the body (Cundall and Deufel (1999)). This leaves a major gap in the understanding of strike motion dynamics. The cameras used in these studies were between 30–500 frames per second, with the study by Ryerson and Tan (2017) being an exception by using a single camera at 2000 Hz. The camera setup usually consisted of a single camera or a single camera with a planar setup with known distances. In those without the planar setup, the 3D movement of the snake could not be determined. In the case of Cundall and Deufel (1999), the frame rate of the camera was so low that multiple strikes were superimposed over each other in order to get a better idea of what the full strike trajectory looked like.

Unlike in research focusing on snake locomotion behavior and gap crossing behavior, there has only been a single study where the combined tools of video tracking and EMG were used simultaneously for investigating strike behavior (Young (2010)). This study looked at the striking action of puff adders (*Bitis arietans*). The lack of muscle coordination data observed for a strike could be due to challenges associated with keeping multiple electrodes in a snake. For slow snake behavior, 4–12 electrodes have been successfully used (Newman and Jayne (2018); Jayne (1988); Cundall and Gans (1979); Jorgensen and Jayne (2017); Moon (2000)). But in the only study that has shown EMG information in snakes strikes, only four electrodes were able to be inserted. Furthermore, the insertions were inconsistent, involving a variety of different muscle configurations, and the recordings could not be done over multiple days (Young (2010)).

Science is often held back not by a dearth of ideas but rather a lack of technology or methods to support investigating those ideas. This limitation is often encountered because the use of the technology requires its own expertise separate from the expertise of the researcher. Access to these technologies can help answer questions already posed, but can also inspire new questions. Packaging these technologies in a form usable by non-experts while keeping overall technology costs low increases the ability of researchers to investigate new research ideas. Further research into snake strike dynamics has been prevented, as discussed above, because of limited access to high-speed motion capture equipment and a stable method for EMG recordings that prevents the snake from hurting themselves and removing electrodes.

The following chapters focus on technologies that the author, along with others, has brought to fruition to enable the capturing of novel data that add a vital counterpoint

for muscle coordination studies in snakes. These data describe several behaviors for the first time as well as show how the muscle activity correlates with this activity. In the case of a snake strike, the data presented in this work are the first of their kind for non-viperid snakes and provide a wider view of muscle coordination during strike than the single previous study.

Chapter 1 presents an open source software framework that combines the full pipeline of data processing from data collection through triangulation of marker positions in 3D. Using this system the first strike meta-data for an arboreal species of snake not from the viperid family, the amazon tree boa *Corallus hortulanus*, is presented.

Chapter 2 presents a method for multi-electrode chronic EMG implantation in snakes. This technique keeps the electrodes inserted over several days with minimal detriment to the animal. Furthermore, the method supports the use of numerous electrode sites, which can span the length of the snake trunk. Here, first descriptions of compensatory activation to a sinusoidal perturbation stimulus are presented.

Chapter 3 uses the methods from the previous chapters along with the experimental setup from chapter 2 to understand the neuromuscular activation of the gate model by comparing the activity of several snakes over multiple days. It is shown that snakes modify their body position to compensate for the motion of the turntable following a model similar to the gate model described by Kardong and Bels (1998). This compensation is driven by a head fixation towards a stimulus strategy of the snake.

There is limited research focused on the axial kinematics of the snake during striking. The research that does exist is primarily focused on viperid snakes. Furthermore, only one study so far has attempted to describe the mechanisms that produce and control strikes. Young (2010) was able to show that there are muscles active prior to the initiation of a defensive strike movement and, furthermore, that the prestrike posture does not appear to affect strike kinematics. Chapter 4 investigates the neuromuscular activations of the amazon tree boa during striking behavior. This is the first work to present this information for an arboreal snake not part of the viperid family. Furthermore, as described in detail in the chapter, these data shown do not support the current elastic energy storing hypothesis of snake striking kinematics (Young (2010)).

Part I

Tools and Methods for Novel Data Collection

The contents of the following chapter comprise a manuscript that has been accepted for publication.

Jensen, G. W., van der Smagt, P., Heiss, E., Straka, H., and Kohl, T. (2020a). Snakestrike: A low-cost open-source high-speed multi-camera motion capture system. *Frontiers in Behavioral Neuroscience*, 14:116, doi: 10.3389/fnbeh.2020.00116

This author's contributions were as follows:
- Conceptualization: together with HS, PvdS, and TK
- Methodology
- Software
- Validation
- Formal analysis: together with HS, EH, PvdS, and TK
- Investigation: together with TK and EH
- Data curation
- Writing - original draft
- Writing - review editing: together with HS, EH, PvdS, and TK
- Visualization: together with TK

Chapter 1

SnakeStrike: A Low-cost Open-source High-speed Multi-camera Motion Capture System

Current neuroethological experiments require sophisticated technologies to precisely quantify the behavior of animals. In many studies, solutions for video recording and subsequent tracking of animal behavior form a major bottleneck. Three-dimensional (3D) tracking systems have been available for a few years but are usually very expensive and rarely include very high-speed cameras; access to these systems for research is limited. Additionally, establishing custom-built software is often time consuming - especially for researchers without high-performance programming and computer vision expertise. Here, we present an open-source software framework that allows researchers to utilize low-cost high-speed cameras in their research for a fraction of the cost of commercial systems. This software enables researchers to record video data from multiple high-speed cameras and perform 3D position tracking on a variety of animals, including snakes. A snake strike can be as short as 50 ms, literally twice as fast as the blink of an eye, which is too fast for faithful recording by most commercial tracking systems and therefore represents a challenging test to our software for quantification of animal behavior. Therefore, we conducted a case study investigating snake strike speed to showcase the use and the integration of the software in an existing experimental setup.

1.1 Introduction

High-speed video recording is a common tool to visualize and subsequently quantify fast behavioral performances such as in snakes (Herrel et al. (2011); Kardong and Bels (1998); Penning et al. (2016); Ryerson and Tan (2017); Young (2010)), or other fast moving animals (Seid et al. (2008); Patek et al. (2004); Tobalske et al. (2007)), or insect flight (e.g. Altshuler et al. (2005); Boeddeker et al. (2010); Geurten et al. (2010); Straw et al. (2011)).

However, in most snake studies only one camera or a maximum of two are used to capture such rapid motion, with the one exception of a recent study where multiple cameras with only moderate temporal resolution, were used to investigate locomotor maneuvers (Gart et al. (2019)). Software such as DLTdv (Hedrick (2008)), Tracker (Open Source Physics, http://www.compadre.org/OSP/), ImageJ (Schneider et al. (2012)), or Didge (Alistair Cullum, Creighton University) have usually been used to process the captured images. These open source solutions are suitable tools to use when capturing with a single camera and with a known distance to the recorded object(s), with an exception for DLTdv as it performs triangulation when combined with calibration information provided by a different software. Single camera capture, however, creates some limitations. Using a mirror allows a single camera to perceive multiple views of the snake such as done by Kardong and Bels (1998), but any time a single camera is used to capture three-dimensional (3D) information, the camera must be placed in a setup that is stereotypically well-defined in a way that the distances such as between camera sensors or from the camera sensor to the object are known. The inflexibility of these well-defined setups can be troublesome for the use in multiple experiments, requires extra expertise, and entails extra costs for building and storage.

Motion capture technology using multiple infrared cameras has been available for experimental studies already for decades. While one of the principal fields of employment for these systems was and still is the capture of human motion, this technology has been used in more recent years for the tracking of animal locomotion (Dahmen et al. (1984); Fry et al. (2000); Robie et al. (2017); Straw et al. (2011); Theunissen and Dürr (2013); Theunissen et al. (2017); Tian et al. (2011). Systems such as Vicon, Optitrack, Motion Analysis, Qualisys, or XSense are largely comparable and use infrared reflective spherical surface markers on the subject of interest that are tracked by multiple spatially fixed cameras and allow triangulating the positions of various body parts in virtual 3D space. In contrast, active marker-based tracking systems such as Dari Motion, Myomotion, NDI, or marker-less systems, commonly use depth information and a wire-frame, or similar, model of the tracked object mostly for applications involving humans. These model-based systems are expensive with costs that range from $10,000 to $100,000, though some open source algorithms are available for human pose estimation in video recordings (e.g. OpenPose (Cao et al. (2018)), DeepPose (Toshev and Szegedy (2014)), ArtTrack (Insafutdinov et al. (2016a)), and DeeperCut (Insafutdinov et al. (2016b)). While commercial systems work well with low reconstruction error and ease of use, this technology is rather insufficient for high-

speed motion capture, mostly because of the typically low maximal camera frame rates of 100–250 Hz. Accordingly, details of ultrafast movements such as strikes of rattlesnakes, which from initiation to target contact are completed within ∼0.05 seconds (Kardong and Bels (1998); Penning et al. (2016)) require a camera with a capture frame rate well beyond 200 Hz. At such a frame rate, and using a state-of-the-art tracking procedure, optical recordings of a rattlesnake strike would comprise a mere 10 frames of triangulated trajectory. Accordingly, many details about the kinematic profile would be unavailable and thus invisible apart from the fact that raw images are usually not stored. Though often done to save disk space as well as to minimize bandwidth saturation, it prevents any re-analysis of the triangulated motion trajectory.

Here, we present a multi-camera system that allows high-speed motion capture of ultrafast animal movements such as snake strikes using low priced cameras with high frame rates of 750 Hz and sufficient spatial resolution. The developed software provides a suite of functions that encompass the entirety of data collection, processing, and storage of motion capture with a special focus on processing speeds for high-speed camera capture. The amount of data that is generated by high-speed cameras grows quite rapidly with the number of cameras, their speed, and their resolution. This software processes the data to the full extent of the available computer system resources; a feature not available in other tracking software such as DLTdv (Hedrick (2008)), but which greatly diminishes the time required for processing. Although this system was developed in order to capture snake strike motion dynamics, it can easily be employed for motion studies of other animals than snakes. SnakeStrike is an open source framework written to allow users to harness the power from other open source libraries for image manipulation, camera interaction, and computer vision (Bradski (2000); Guennebaud et al. (2010); Moulon et al. (2013); Rusu and Cousins (2011); Schroeder et al. (2006)). Thus, besides assisting in the resource-intense and time-critical initial collection of images at high frame rates with multiple cameras, SnakeStrike performs image processing for triangulation and data visualization. Color thresholding is used for marker identification, allowing simultaneous tracking of multiple animals or body parts when markers with different colors are used. If infrared cameras are used, then infrared markers can subsequently also be used. Marker types need not be spherical or 3D in form. Something as simple as a piece of colored tape can be used, and no wire-frame, or similar model, is required. A major advantage of SnakeStrike is the storage of all original images as reference. This permits repeated off-line data re-interpretation in case new automatic tracking methods or sequential modeling methods become avail-

able. Because of the open source code and the modular structure of SnakeStrike, other annotation and pose estimation tools such as DeepLabCut (Mathis et al. (2018)) or LEAP (Pereira et al. (2019)) can be incorporated into the processing pipeline.

1.2 Materials and Methods

This section describes the requirements to use the system and how we fulfilled those requirements, how to use the software from a user's perspective, as well as give a high-level overview of how the images are processed such that 3D triangulated points of the markers become available. The order of the sections follows the order the user will generally interact with the interface. This order is reinforced by the software to create a consistent pipeline for the user. Where appropriate we include suggestions for solutions to problems that can arise during use. Furthermore, we describe the experimental setup used for each of our two experimental settings.

1.2.1 Hardware Requirements

For effective recording of high-speed videos for 3D tracking, it is important to use cameras that are fast enough to capture every detail of the motion of interest and can function together. The only absolute requirements to run the SnakeStrike software are a 64-bit computer running 64-bit Linux. To ensure faithful data transfer to the computer, enough bandwidth on a single bus or multiple busses for the communication protocol is required to save data without dropping individual frames. Therefore, it should be thoroughly calculated which camera communication protocol (e.g. USB3, Ethernet, etc) is most beneficial given the respective requirements. The only requirements are that the camera adheres to the GenICam standard and has an application programming interface (API).

Since very large amounts of data need to be transferred and stored, a computer equipped with sufficient sized RAM and hard drives that have enough storage space to store the recorded raw images is required. However, the precise camera and computer configuration generally depends on the speed of the motion of interest and total recording time necessary to capture every detail. An example data set of only 1 sec recording time from a setup equipped with 5 USB 3.0 cameras with a resolution of 640x480 with lossless data compression requires $\sim$700 MB of disk space, while $\sim$3.2 GB of RAM is the minimal requirement for the images from the data capture, assuming that the images are returned from the camera in RGB8 format. If the format is changed to something like Bayer BG8, then the

amount of required RAM decreases by a third. Sufficient RAM for running the software should also be included in the calculation. Since AC powered lights flicker when recorded with high-speed cameras, lights for the experimental setup need to have a flicker frequency that is higher than the camera speed or are non-flickering. Note that not all LED lights are non-flickering.

To satisfy secondary requirements of our experiments, we used a computer with multiple CPU cores, 64 GB RAM, and several Terabytes of available hard disk storage. Furthermore, we used multiple USB 3.0 cameras. Consequently, a PCI card that expanded the available USB 3.0 ports and ensured that each new port had its own controller was utilized. A separate controller for each port guaranteed that the port would not share bandwidth with other USB 3.0 ports. When running a high-speed camera, it is very easy to saturate these buses with a single camera, let alone multiple. For triggering the cameras, a software trigger is usually available, although this does not guarantee synchronized images when using a USB connection. If a hardware trigger is required while using USB cameras, an external hardware trigger must be added. We chose Basler Ace acA1300-200uc cameras (Basler AG, Ahrensburg, Germany), which have a maximum image size of 1280 x 1024 pixels. At full spatial resolution, the maximum speed is 203 Hz, however, if the resolution is decreased to 640x480 pixels, a frame rate of 750 Hz can be achieved. With camera speeds this high, light flickering of the illumination can be a major issue. Accordingly, surgical lights were used when recording snake strikes in the 3D X-ray setup. However, AQ Aquaflora 54-watt fluorescent bulbs (D-D The Aquarium Solution Ltd, Ilford, UK) are cost-efficient and have successfully been applied in initial tests. When available, non-flickering LED-technology can be used as an alternative. The used cameras were connected to the computer by USB 3.0. To exclude potentially dropped images due to saturation of the bus, a Startech PEXUSB3S44V card (StarTech.com, London, Ontario, Canada) was used.

For correct triangulation during our experiments, USB camera synchronization was essential. Accordingly, a Labjack U3 (Lakewood, CO, USA) AD/DA converter with custom-built housing to synchronize the cameras via three available digital ports was used. A maximum of three cameras can be triggered per port, without critical attenuation of the TTL signal. As long as the camera speed is less than 25,000 fps, i.e one frame per 40 μs, the 20 μs delay between each of the pulses of the three triggers does not affect camera synchronization. If only one trigger is available, another solution to allow all cameras to be triggered is to use a buffer amplifier; this prevents the signal from being affected by load

currents.

1.2.2 User Interface

SnakeStrike is currently only available for 64-bit Linux. The C++ source code and installation instructions are available at "https://github.com/gwjensen/SnakeStrike", while the main user and code documentation can be found at "https://gwjensen.github.io/SnakeStrike/". Since compiling C++ source code with many dependencies is not an easy task, a docker image with the required dependencies as well as SnakeStrike pre-installed is available on DockerHub at gwjensen/snake_strike with the requisite source for building the Docker image manually located at "https://github.com/gwjensen/SnakeStrikeDocker". Information regarding plugins or specific functions is available at "https://gwjensen.github.io/SnakeStrike/".

The main method of interacting with SnakeStrike is through a basic graphical user interface (GUI). The interface manages folder structure and encapsulates the many steps behind the actions of calibration, capture, and triangulation tasks. The functionality of the interface is divided into three separate tabs in the top left corner of the window (Figure 1.1A). First, the user creates a new project/experiment, where a project/experiment comprises a single data collection. This ensures consistent data annotation output and reduces workload for the user by automatically organizing created files. After the project is created, new options become available guiding the user along the GUI. For instance, if the cameras are not connected, the user is unable to use any recording options until establishing the connections and pressing 'Refresh Camera Connection'. The 'Collect Data' tab as well as the side toolbar provides the user with a live preview from the cameras, to initially position the cameras and perform the fine tuning of the focus.

Camera parameters, such as frame size, frame rate, and exposure length need to be set by the software provided by the camera manufacturer and has to be saved in an external configuration file that adheres to the GenICam programming standard. This standard is a generic programming interface that is supported by all compliant cameras and guarantees that a configuration file is transferable between cameras produced by different manufacturers. To set the camera parameters within SnakeStrike, the configuration file must be loaded using the 'Load Camera Config' button. Further information, i.e. whether the camera is USB 3.0 or Ethernet-connected, are automatically abstracted. After the configuration of the cameras, the calibration can be started by pressing the 'Calibrate Cameras' button that opens the calibration dialogue (Figure 1.1B). Using the technique described by Li et al. (2013), the intrinsic calibrations, i.e. finding the optical center, focal length, and

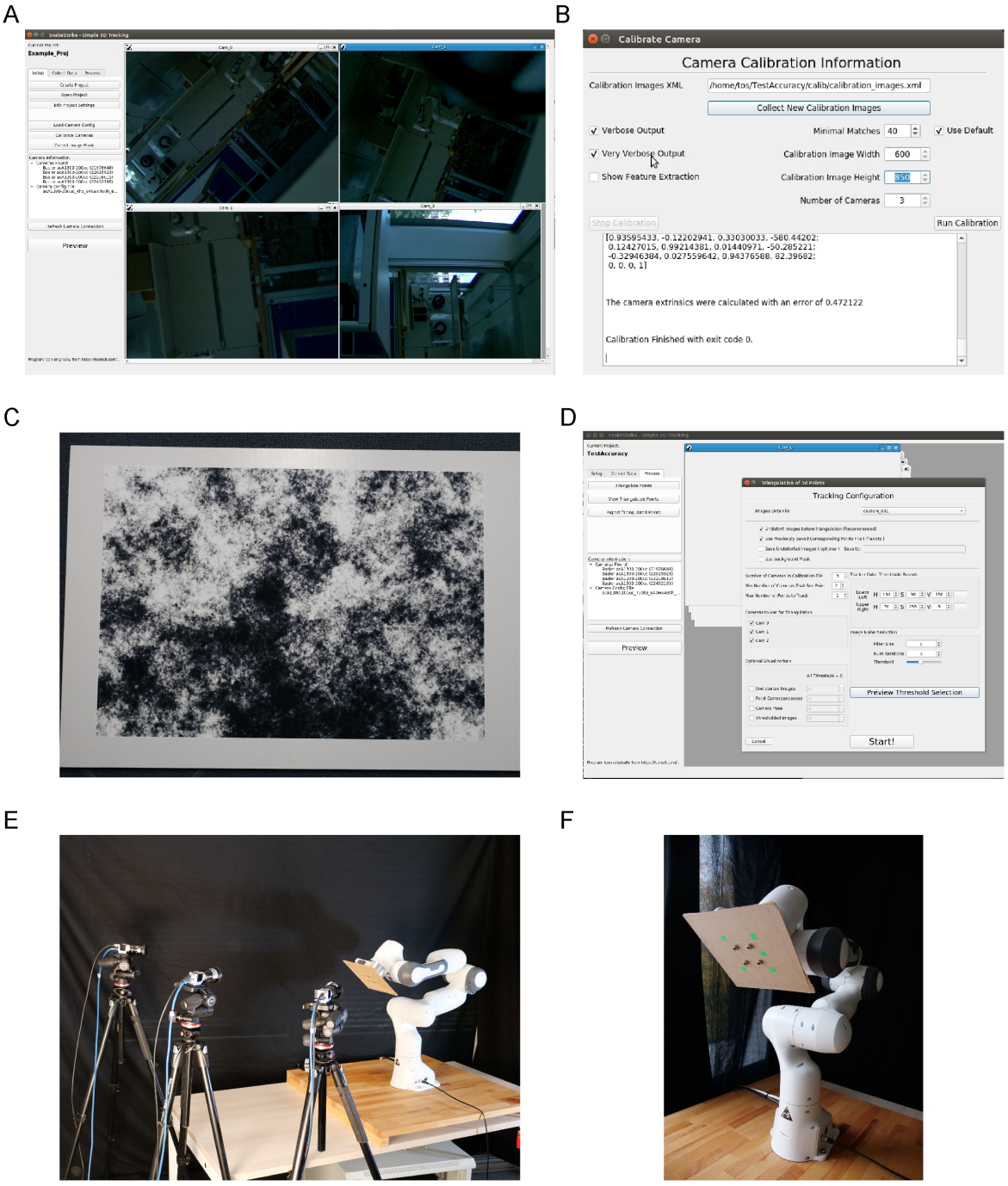

Figure 1.1: User Interface of the SnakeStrike software and view of the experimental setup used for study 1. (**A**) Main screen of the software depicting simultaneous previews from four connected cameras. (**B**) Calibration dialog window after a successful calibration attempt. (**C**) DIN A1-sized calibration image adopted from Li et al. (2013), affixed to a 1 cm thick cardboard for calibration. (**D**) Example of the dialog window used to triangulate the markers encountered in the images. (**E**) Overview of the experimental setup used for study 1, depicting the arrangement of three low-cost Basler cameras and a Franka Emika Panda robotic arm. (**F**) Close-up of the robotic arm with green markers affixed to a piece of fiberboard. Image source: Jensen et al. (2020a).

lens distortion of the individual camera, as well as the extrinsic calibrations, i.e. how the cameras are positioned relative to each other in 3D space, are performed.

1.2.3 Undistortion and Calibration

The size of the image used for calibration depends on the angles between the cameras and the viewing space covered by the cameras. A large viewing angle and/or a large viewing space requires a calibration image that is sufficiently large to be viewed by more than one camera at a time. Optimal calibration objects allow finding correspondences at multiple levels of resolution. The calibration object must be affixed to a movable planar surface such that the image remains flat, but still can be moved through the cameras' field of view (Figure 1.1C). It is not necessary for the calibration image to be fully viewable by each camera or that all cameras see the calibration image at the same time. More important for a successful extrinsic calibration is that the cameras can be linked across images that are shared. For example, in a setup with three cameras (A, B, C), where A and B can see the calibration image in a few image captures, and B and C can see the calibration image in a few captures, it is unnecessary for A and C to also share image captures when capturing the calibration image.

Calibration images should be recorded at low frame rates (e.g. 4 Hz in the current study). This reduces the amount of multiple copies of identical images that would be recorded if the movement of the calibration object is too slow with respect to the camera frame rate. Identical images lead to instabilities in the calibration calculation and unnecessarily increase computation time. Generally, it is recommended to use a slow capture frame rate, and make sure that the calibration object is presented with multiple different orientations relative to the cameras. For a detailed and mathematical explanation of the calibration procedure see Hartley and Sturm (1997) and Kanatani et al. (2016).

To undistort the images from individual cameras, and to calculate the relative camera positions, we used the technique described by Li et al. (2013). One camera sensor will always be used to define the origin of world space. After collection of the images, the user can choose to see the text output of the calibration and can set the lower boundary for the number of matches. The SURF-like (Bay et al. (2008)) difference of Gaussian filter (Li et al. (2013)) detectors must find a pair of images that can be paired for further calibration. If the calibration returns with no errors, then a root-mean square error (RMS) of camera positions in space relative to each other is provided (Figure 1.1B). As the positioning is an optimization and not a closed-formula solution, the error depends on different parameters,

such as camera resolution, quality of focusing, number of recorded images, and number of Gaussian filter matches. After calibration, a mask of the experimental setup can be saved (although not required) along with the project information, to improve post-processing such as thresholding.

1.2.4 Marker Detection and Tracking

After configuration and calibration of the cameras, the 'Record' button in the 'Collect Data' tab becomes available and the recording can be started. Once a recording has been completed, data processing can be started by pressing the 'Process' tab. Pressing 'Triangulate Points' brings up the dialog window for thresholding the markers from each camera's image and triangulating those points into world coordinates (Figure 1.1D). Our marker detection method is analogous to how commercial tracking systems work in that a specific color range, as supplied by the user, is thresholded to detect the markers in an image. This thresholding combined with the grouping of pixels close to each other and then returning the center of that group is how a colored marker on the object/animal is transformed into a marker position. Typically, commercial systems rely on the markers being IR reflective and of a spherical shape to allow the use of ellipse fitting algorithms. Our approach does not have these restrictions.

To decrease computational complexity in our software, the initial correspondence of marker position in relation to the different cameras and the colored marker in 3D space are provided by the user. All subsequent correspondences are performed automatically as described below. For thresholding, a range of colors according to the HSV scale can be chosen. To help remove noise, which can pose a severe problem when using this rudimentary approach, a small configurable filter is available. The preview dialog allows the user to fine tune the values for a particular capture session before proceeding to the triangulation. Images being used for triangulation will automatically be undistorted according to the camera distortion matrices that were calculated separately for each particular camera during calibration.

Markers are not required to be 3D in form when capturing data, i.e. the IR reflective spheres used by commercial systems, however, when capturing data, it must be ensured that at least two cameras see the tracked points. While two cameras are the minimal requirement for 3D triangulation, the quality of triangulation is considerably improved using three cameras (Stewenius et al. (2005)). The benefit of using non-3D markers, like tape or paint, on animals that are difficult to handle such as snakes, is that such 2D markers

are more likely to remain attached to the animal. This benefit is offset by the need for more cameras if markers are obscured from one or more cameras. The optimal marker size depends on the camera resolution and size of the object to be tracked. Markers and lighting need to be adjusted to each other. Markers must appear bright enough to allow a dissociation from other low light background colors. On the other hand, markers must not be too bright, because of a potential confoundment with reflections or glare from other surfaces in the experimental environment. We thus recommend choosing colors that have a very high value and saturation in the HSV color space. This facilitates segmenting with both small and large amounts of light. Using a less vibrant color for a marker is possible, but requires that the color is non-glossy; otherwise, reflections on the marker surface can optically change the shape of the marker and thus impair the function of the thresholding algorithm. This could lead to larger errors such as the mid-point of the marker shifting, or even optically splitting the marker into two. In this case, noise smoothing operators in the thresholding dialog are required to rejoin the marker. Accordingly, the larger the markers, the larger the potential error that can occur during triangulation, due to the number of pixels that the marker covers and the problem of finding a representative pixel for this group. When several pixels enter or leave the group, the representative center pixel will most likely change as well. This splitting can also occur because of changes in illumination of the marker, i.e. slight shadow on the marker. This is a source of error related to the lighting of the setup, that cannot be fixed by non-flickering lights.

In a perfect situation, where the cameras in a setup have perfect intrinsic and extrinsic calibration matrices, i.e. the parameters of the camera and its position to every other camera is perfectly known, the triangulation of corresponding pixels across cameras is straightforward. A ray extends from each camera sensor through the corresponding pixel in question. In a perfect setup, these projection rays would intersect in 3D space. In reality, however, there are many sources of noise that prevent an intersection of these lines. These sources include noise in the calibration of the camera, noise in how the camera sensor converts light information, noise caused by the viewing of a 3D object from different positions that might not view the object in the same way, etc. When the lines don't intersect, as is usually the case, a method for finding the 3D point of intersection is required. This means that a new pixel in each image needs to be found such that all the projection lines through those pixels intersect in 3D space. There are many metrics that can be used for determining where this new pixel in each image is located.

To help correct for noise inherent in marker location triangulation we used a technique

described by Kanatani et al. (2008) as 'optimal correction', but using the specific implementation from Kanatani et al. (2016), that translocates the marker's center pixel in the image space a minimal amount such that all projection lines from the cameras intersect again in 3D space. This is known as minimizing the geometric error, i.e. the error in pixel space of the data point and its reprojection. In other words, this method finds a pixel as close to the original pixel in the pixel space for each camera such that the projection lines through those pixels will intersect. Once the lines intersect again, the algorithm of Direct Linear Transformation (DLT) (Sutherland (1974)) can be used to calculate the 3D point represented by the corresponding marker locations in each image. If DLT is used without the geometric correction afforded by 'optimal correction', or by another correction algorithm, then the algorithm minimizes the sum of least squares distance not in the pixel space, but in 3D space from the projection lines of the data points to the point in 3D space that satisfies the intersection constraint.

When using three or fewer cameras, the globally optimal translocation of data points according to geometric correction can be provided by the polynomial algorithms of Hartley and Sturm (1997) for two cameras, which was later extended by Stewenius et al. (2005) to three cameras. However, as the number of cameras grows, the size of the polynomial function to solve becomes unwieldy. As described by Hartley and Kahl (2007), Stewenius and Nister, in an unpublished work, calculated the degree of the polynomial that would need to be solved for views 2 to 7. They found 6, 47, 148, 336, 638, and 1081 to be the respective order of the polynomial for calculating the global optimal solution. This shows how quickly the number of local optima of the cost function increases.

For more than three cameras, the search for a global optimal solution is commonly done with optimization of a cost function or gradient descent algorithms. These solutions, however, as mentioned by Hartley and Zisserman (2003) can be quite computationally expensive as well as difficult to program. Quite often these methods also rely on assumptions regarding the source of the noise, e.g. Gaussian distributed. We used the iterative method of Kanatani et al. (2008) to minimize the geometric error without minimizing a cost function or relying on any assumptions regarding the source of the noise. Furthermore, as was shown in Kanatani et al. (2008), since this method starts as an approximation of the solution, it typically requires only a couple of iterations to converge and, in the case of 3 or less cameras, to provide the same solution as the closed form polynomial equations in less time. In our experience with 5 cameras the algorithm performs quickly and produces high quality results even with the additional noise that is contributed by the movement of

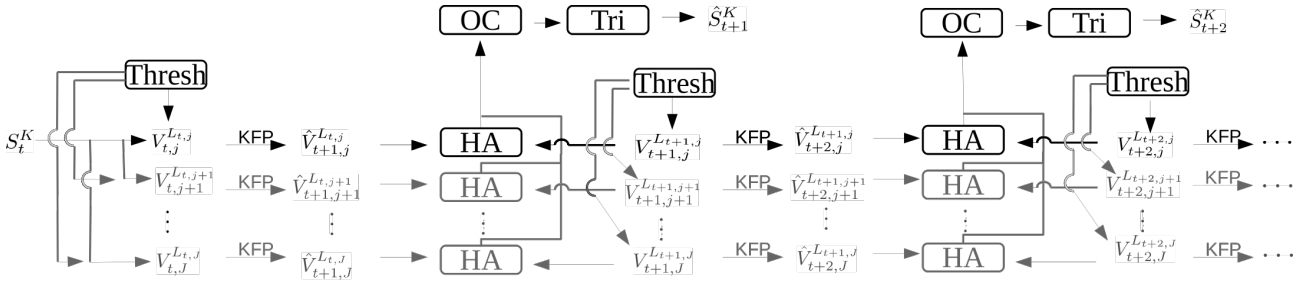

Figure 1.2: Diagram depicting the flow of data during the processing of images which results in a 3D triangulated point of the markers being tracked. The variable S is the set of markers as they exist in the real world with $S_{t=0}$ being the first time step in the image capture series. The information for initial point correspondence is input by the user manually using the provided labelling GUI. The variable $V_{t,j}$ is the image pixel position of the markers for time step t and camera j. Variables with a hat such as $\hat{V}_{t,j}$ or $\hat{S}_t$ represent calculated guesses as to the true values $V_{t,j}$ and S_t, respectively. The arrow with the marking 'KFP' is a Kalman filter prediction, and the boxes 'Thresh', 'HA', 'OC', and 'Tri' indicate the color thresholding algorithm, the Hungarian algorithm, the optimal correction algorithm, and the triangulation algorithm, respectively. Image source: Jensen et al. (2020a).

marker center positions. These errors are discussed further in Study 1 below.

Matching multiple points across multiple cameras is not a trivial problem, as Munkres (1957) demonstrated. If we have M cameras, finding the corresponding point from one camera in the set of all other points in each of the other $M-1$ cameras is a computationally intensive task. This problem can be solved for two sets in $\mathrm{O}(N^3)$, i.e. the time required to solve the problem scales cubically with the number of inputs, assuming that there are no further constraints to the matching. For more than two sets and when there are additional constraints, such as that the assignment over time stays consistent, these problems are still an active area of research. A general solution to the problem of triangulation of occluded points during tracking has also proved elusive. Only basic methods for the tracking of points are available in our implementation at the moment. Currently, for a triangulation attempt, the user has to select the visible markers in images from a single time step manually using an intuitive GUI. The selection does not need to be pixel precise as the closest visible marker will automatically be selected. This initial marking helps to decrease the computational complexity of assigning matching points across camera views to a more manageable problem.

These starting positions are then used as the initial starting positions for points in a Kalman filter (Kalman (1960)). Using this initial configuration, the Hungarian algorithm, also known as the Munkres-Kuhn algorithm (Bourgeois and Lassalle (1971); Kuhn (1956);

Munkres (1957)), along with the Kalman filter, which receives its step update information from the matching of the Hungarian algorithm, are used to keep the point assignments consistent through time. These algorithms are only used to support the correct assignment of correspondence, while the pixel positions of the marker come from the thresholding and not from the steps of the filter. A high-level diagram of this processing pipeline is shown in figure 1.2. The user has the option to force the algorithm to skip timesteps where not all markers for each camera are visible. When the setup consists of more than two cameras, the user can fall back to a set of fewer cameras that have no occlusion for that timestep. An algorithm library for correspondence is used to match corresponding points from images taken at different angles. In the default case this library is the Kalman filter and Hungarian algorithm combination mentioned above. However, since this library is dynamically loaded, the user has the option to write a correspondence plugin for keeping the identity of thresholded points unique through time, making it unnecessary to rely on the basic method described above.

Our framework provides an API where these new algorithms can be supplied to the framework without re-compiling the codebase. This interface is basic in the sense that it provides the points for each timestep, and expects the points to return in ordered lists for each timestep. This creates an interface that puts a minimal amount of constraints on the algorithms that are used to process the point tracking data. More information regarding the API for these algorithms can be found on "https://gwjensen.github.io/SnakeStrike/". This is where software such as DeepLabCut (Mathis et al. (2018) or LEAP (Pereira et al. (2019)) can be integrated into SnakeStrike. This also allows data to be processed by many different algorithms, if necessary. It further offers the possibility for the user to maximize the constraints such as how to handle obscured points, what to do when point labels are swapped, etc.

1.2.5 Viewing Tracking Data

After triangulation, the data can be viewed by the built-in 3D point cloud viewer. This generates an animation of the movement through time, and also allows stepping through each individual timestep. A line connects the points in the order as indicated by the user for disambiguation. This line is useful for relating triangulated points to the body of the animal, but does not directly reflect pose information of the animal. For example, in the case of a snake, the line won't follow the contours of the snake unless the markers are spaced with minimal distance to each other. The points are also of different colors to prevent

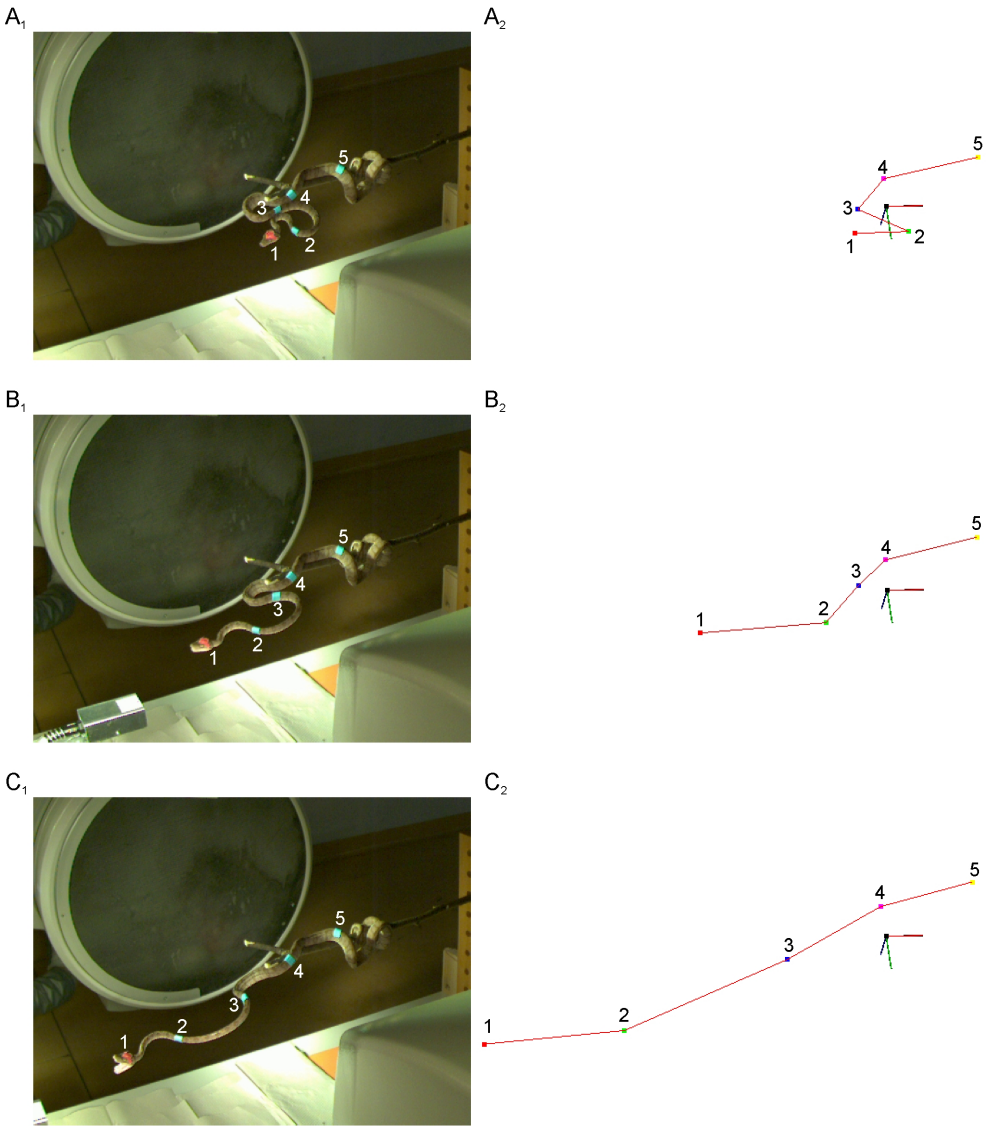

Figure 1.3: Experimental setting for capturing and analyzing snake strikes in study 2. (**A**–**C**) Raw images of a strike of an amazon tree boa (*Corallus hortulanus*) at three different time steps: at a stationary position (A_1), and approximately in the middle of the strike (B_1, C_1). The large black circle behind the snake is the horizontal X-ray emitter, while the vertical X-ray emitter above the snake is out of view. Corresponding triangulation is plotted as output by the SnakeStrike software for the corresponding images (A_2, B_2, C_2). The coordinate system has been rotated such that triangulated points and images have the same viewpoint. Each marker (1–5) on the snake is depicted by a different color label in the triangulated data, starting with the red (1) point and ending with the yellow point (5) in images A_2, B_2, C_2; a red line connects all points in the triangulation. This line corresponds to the marker positions on the snake from rostral to caudal and is not based on pose estimation. The direction of the line is defined by the user during triangulation. The data shown in plots **B** and **C** are 86 images (114.7 ms) apart. Image source: Jensen et al. (2020a).

ambiguity when viewing the motion of the points through time (Figure 1.3A_2,B_2,C_2). The triangulation performed by SnakeStrike does not perform any direct filtering or smoothing on the triangulated points over time. It only provides a simple forward-backward filter as part of the GUI window to allow the user to see how filtering or smoothing could improve the data.

1.2.6 Procedures for study 1: measurement of accuracy

Small Mark Number	1	2	3	4	5
1	0	72	80.5	101.8	72
2	72	0	36	72	101.8
3	80.5	36	0	36	80.5
4	101.8	72	36	0	72
5	72	101.8	80.5	72	0
Big Mark Number	1	2	3	4	5
1	0	84	93.9	118.8	84
2	84	0	42	84	118.8
3	93.9	42	0	42	93.9
4	118.8	84	42	0	84
5	84	118.8	93.9	84	0

Table 1.1: Distance between markers on the calibration object used for Study 1. Measurements are all in mm.

The accuracy of SnakeStrike was determined under particular control conditions, that however differed with respect to the experimental setting used in study 2 for the strike movements of snakes (e.g. cameras, lighting conditions, etc.). The accuracy of the system was determined with a robotic arm that reproducibly moved an artificial object to calculate the error level for the calibration technique and illustrated the effect of different recording conditions. The setup consisted of a robotic arm (Model: “Franka Emika Panda”, Franka Emika GmbH, Munich, Germany) used to move a flat plane with affixed markers in a specific spatial configuration (Figure 1.1E,F, Table 1.1). Robotic arm motion allowed for precise movements with identical trajectories, while parameters such as speed were altered under defined conditions. With this approach two types of camera lenses, two different marker dimensions, and two different movement speeds were tested. The definition of the exact distances between the points allowed calculating the error in 3D triangulation

between all points. The affixation of the points to a plane allowed calculating the error of the points from the plane that fits all points with the least error.

The basic experimental setting was as follows: placement of three cameras, oriented around the robotic arm (Figure 1.1F). Bright neon green markers (small: 10 mm x 10 mm; large: 22 mm x 22 mm) were attached at specific locations on a flat piece of medium-density fiberboard to ensure that the markers were aligned in the same spatial plane; the chosen marker color was unique and did not occur on objects anywhere else in the cameras' field of view. For the Fujinon DV3.4x3.8SA-1 (Fujifilm, Tokyo, Japan) lens, the distance between cameras and marker plane was about 110 cm (Figure 1.1E). For the Ricoh FL-CC0614A-2M (Ricoh, Tokyo, Japan) lens, the distance was increased to ∼175 cm, because of the longer focal length of the lens. As the cameras had to be moved, calibration differences as well as lens differences were tested. Each capture session was completed with the cameras set to an image size of 640 x 480 pixels at a frame rate of 750 Hz. For each capture, 6000 images were recorded. For triangulation, the thresholding viewer tools of SnakeStrike were used and set to a color range with the most correct detection of the markers and minimum false-positive detections.

1.2.7 Procedures for study 2: Strike movement of the amazon tree boa (*Corallus hortulanus*)

The tracking framework was applied for the first time ever on living animals in combination with biplanar X-ray to capture fast snake strikes. The field of view of the X-ray tubes was too small to encompass the entire strike of the snakes while still providing adequate resolution. Therefore, an additional data capturing method was required to compare local information obtained from the biplanar X-ray motion capture with global snake movement information. This multi-modal data and the analysis of the resulting data fusion is not a component of the tracking system, and thus out of scope. Nevertheless, we were able to assess the usage of the system with live animals and to demonstrate that this stand-alone 3D motion tracking system can easily be integrated in existing experimental set-ups to record multi-modal data sets.

The experiment included four amazon tree boas (*Corallus hortulanus*) with a snout-vent-length (SVL) of 100–120 cm. Snakes of either sex and a body mass of 23–69 g were obtained from the in-house animal breeding facility at the Chair of Zoology at the Technical University of Munich. Snakes were kept at a temperature of 22–30°C on a 12 h:12 h light: dark cycle. Permission for the experiments was granted by the respective governmental

institution for animal welfare (Thüringer Landesamt für Verbraucherschutz; code: 15-003/16). For the experiments, five cameras running at 750 Hz at a spatial resolution of 640 x 480 pixels were used resulting in 7500 images per camera per capture. This required ∼11 GB RAM (We used Bayer BG8 image format) and ∼7 GB disk space to record and store one capture, not considering any memory or storage space to run SnakeStrike. The orientation of the snake in space when anchored to a branch represented a difficult condition to reliably capture images as snakes can coil back onto themselves, thus potentially occluding markers. Additionally, the placement of markers on the snake, though spaced out along the body of the snake, can end up next to each other when the snake forms its characteristic S-shaped curves. Therefore, multiple cameras were necessary such that at least two cameras saw the markers at all times.

Avery No. 3320 multipurpose labels (Avery Dennison Corporation, Glendale, California, USA) were used as markers as they can be stained with any suitable color, and have a good adhesion, without irritating the skin. The labels were painted in a light blue color as it would be the only incidence of that color in the experimental setting. There were blue markers on the body and an additional red marker on the head because the head becomes obscured by the opening of the mouth as described by Cundall and Deufel (1999) and the X-ray tubes did not allow for setting up cameras directly above the snake (Figure 1.3A_1,B_1,C_1). To reduce errors and avoid correspondence switching of the markers, the body and head markers had different colors. Accordingly, the two marker colors were triangulated separately and then required post-processing to fuse the data manually using a simple script.

1.3 Results

1.3.1 Study 1: Measurement of accuracy

The accuracy of the tracking system was determined by using a robotic arm for the generation of a movement of the flat plane through the visual field of the cameras (Figure 1.1E,F). Based on the variations of the experimental protocol, it was possible to determine the errors related to the different configurations. To provide an intuitive understanding of the performance abilities of the system, we also converted errors from absolute 3D world space measurements to approximate pixel space equivalencies. Figures 1.4A (appendix figure A-1A) and 1.4B (appendix figure A-1B) illustrate the errors resulting from running the same movement at two different speeds, two different lenses, and two different marker

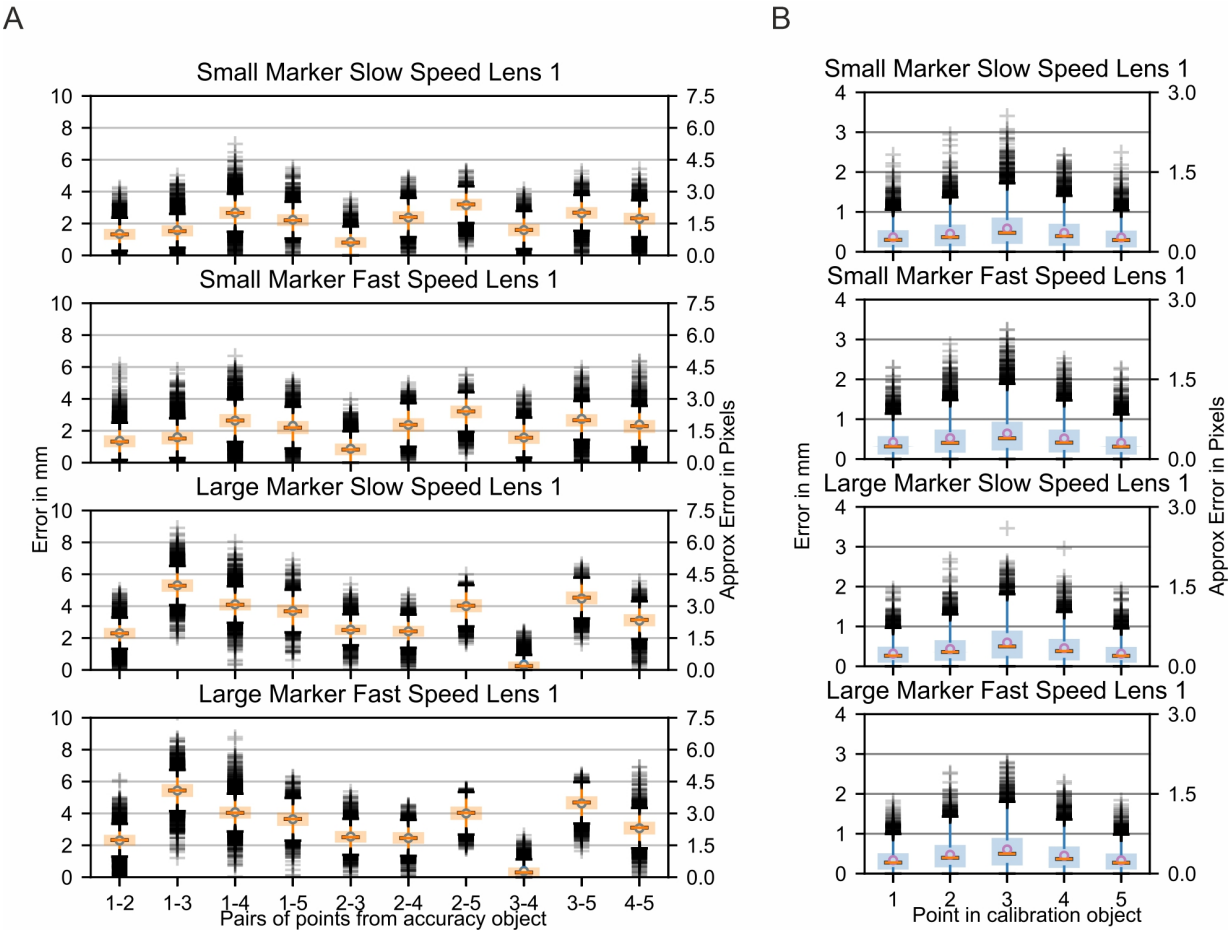

Figure 1.4: Study 1: Error in marker location while the fiberboard with attached markers was moved through space by the Franka Emika Panda robotic arm. Parameters: two marker sizes and two relative speeds of movement of the markers. Data is shown for one camera lens (Fujinon DV3.4x3.8SA-1) only. In appendix figure A-1 additional data recorded with a second camera lens (Ricoh FL-CC0614A-2M) are presented. (**A**) Each boxplot refers to an interpoint distance error between two points of known distance in the calibration object (Table 1.1); the numbers on the x-axis represent the points and are separated by a hyphen. (**B**) Marker distance from the best-fitting plane for all markers. Image source: Jensen et al. (2020a).

sizes. The faster robotic arm speed covered the same motion trajectory as the slower speed, but also covered a slightly different motion at the end due to the faster movement. This was expected as it produces the same trajectory as the movement at the slower speed, but over a shorter amount of time. Details of the results with different marker size, lenses, and movement speed were plotted in the various rows and columns in figure 1.4 and appendix figure A-1. A major outcome of these experiments was the observation that neither the change of lenses nor the speed of the movement has a substantial effect on the accuracy of the reconstruction. The latter finding was also not too surprising given that the movement speed was far slower than the camera frame rate (750 Hz) for these experiments.

The largest visibly observed differences were found for the size of the markers, with an increase of ∼2–3 mm (∼2 pixels) in the average error per point when using larger markers. This was likely due to the fact that the larger the marker, the more the center of the marker potentially shifts. This shifting can be caused by parameters such as changes in illumination, color intensity, or visibility. It is noteworthy, however, that the planar error did not change between the two marker sizes. In order to better understand the effect that aspects such as viewing angle, lighting, or color intensity changes have on the accuracy, stationary images were collected. Figure 1.5A,B show the respective distance errors between points and the distance from the closest fitting plane, respectively. During all captures, 6000 images were acquired at a frame rate of 750 Hz. In this case, small markers were used and each plot represented the position of the fiberboard relative to the main camera. The positions were as follows: 'facing downwards', 'facing perpendicular', 'slanted right', 'slanted left', 'slanted up', and 'slanted up with a sharper angle'. It is noticeable that the error ranges for 'slant right', 'facing downwards', and for 'slanted up with a sharper angle' were considerably larger than for the other capture angles. Variances for both of these positions ranged mostly from 4–6 mm (∼3–4.5 pixels), while other positions tended to have less than 4 mm (∼3 pixels) of variance. The markers perpendicular to the camera as well as the 'slant left' capture error ranges were considerably smaller than reported for moving markers. Markers at other angles relative to the camera had error variances comparable to those during motion captures.

To better explain the source of these errors in the triangulation, the original pictures were reanalyzed to potentially discern differences between the positions that showed a smaller error variance and those that showed a larger variance. The first noticeable difference was that the angle of the marker board relative to the camera was larger in the 'slanted right' compared to the 'slanted left' capture configuration. A similarly sharp angle

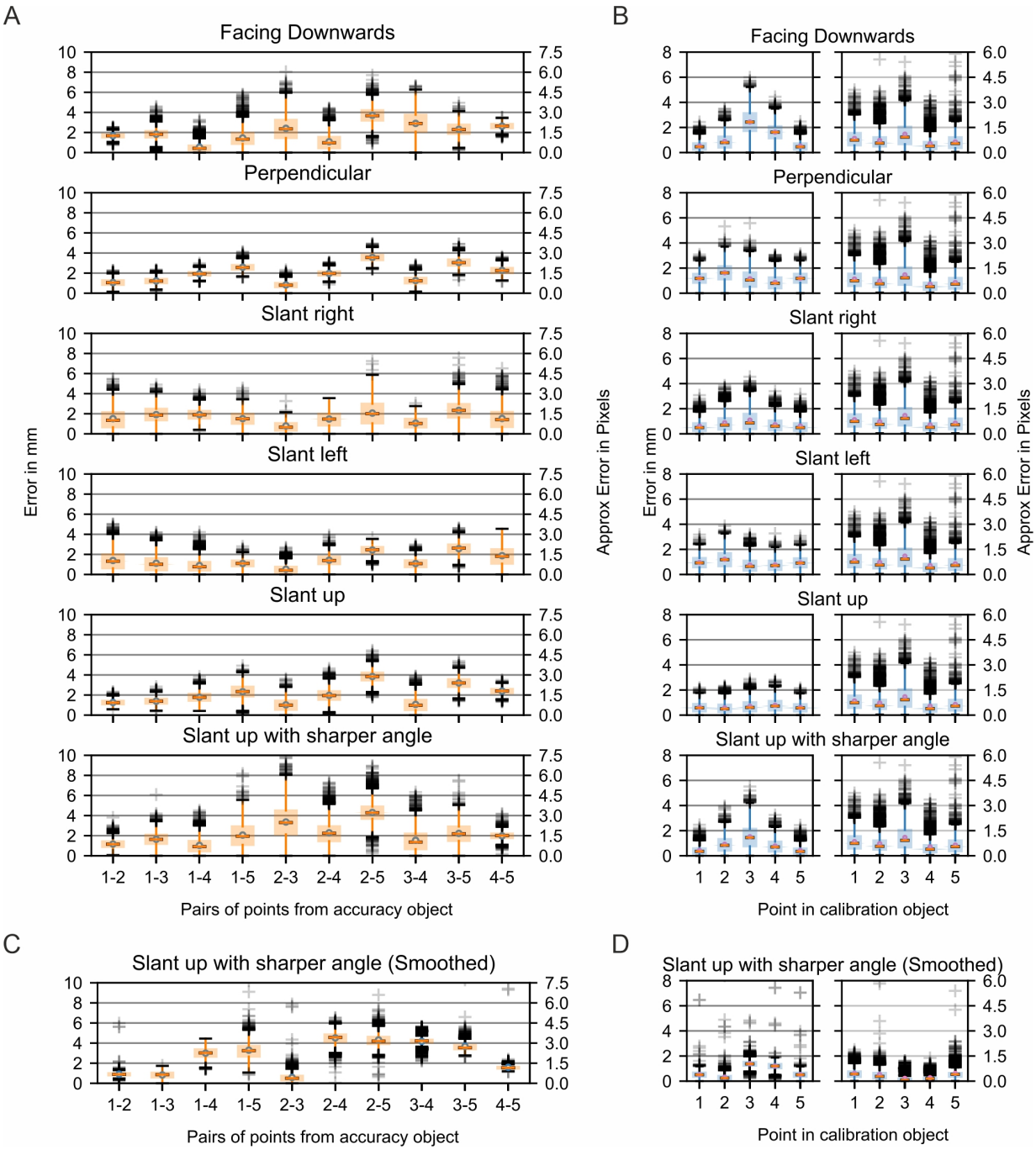

Figure 1.5: Study 1: Error in marker location with a stationary fiberboard across 6000 time steps. (**A**) Stationary markers viewed from different angles by the center camera. Each boxplot refers to an interpoint distance error between two points of known distance in the calibration object (Table 1.1). The numbers on the x-axis represent the points and are separated by a hyphen. (**B**) Distance of markers from the best-fitting plane for all markers (left). Movement of triangulated points in 3D from their mean while markers were stationary (right). (**C,D**) Same data as shown in **A** and **B** but post-processed with a Kalman filter. For plots of the remaining data post-processed with a Kalman filter see appendix figure A-2. Image source: Jensen et al. (2020a).

was also present relative to one of the cameras in the 'slanted up with a sharper angle' capture condition. Thus, the sharper the angle of the camera optical axis relative to the marker, the smaller the marker from the view of the camera. The resulting smaller viewable marker size combined with color intensity differences due to the angle relative to the camera caused the center point of the marker to move with either the flickering of the light source or the change in illumination caused by the angle. Part of the error was likely due to the fact that the triangulated points provided by SnakeStrike have not been filtered or smoothed through time. To demonstrate the effect that a filter would have on the error variance, the data from figure 1.5 were processed by a simple Kalman filter (Kalman (1960)). As illustrated in figure 1.5C,D and appendix figure A-2, it was clear that the use of such a filter drastically reduces the error variance for both the inter-point error as well as the planar error, indicating the necessity to apply such a simple and easy to implement post-processing to obtain even more reliable motion tracking.

Analysis of the data collected from this experimental paradigm showed that even though a high frequency fluorescent bulb was used as the main light source, a minor oscillatory flicker occurred in the image sequence. This introduced a noticeable effect on the accuracy of marker positions as the flicker significantly changed the color characteristics of the markers with respect to saturation and hue. To precisely quantify the error, introduced by the flickering light, a second test of the accuracy object was performed in a new setup where the object remained stationary in a position that was perpendicular to the center of three cameras. In this second experimental setting, data was recorded using a completely separate location with a bright light source consisting of four AQ Aquaflora 54-watt fluorescent bulbs fluorescent bulbs that did not produce any light flickering, and the spacing of the cameras was similar to the original setting. The respective data are presented in appendix figures A-3B and C and A-4B and C and give a clear approximation of the error that the flickering of the light has introduced in the originally collected data (appendix figures A-3A and A-4A), i.e. an average spatial error difference of maximally 1 mm ($\sim$1 pixel) with considerably increased variances, 2–3 mm ($\sim$2 pixels) for the flickering data error. As the errors for both the flickering and the non-flickering light condition show the same trends, there is still a systematic error in the triangulation of the system. Given that the data obtained in the flickering and non-flickering light condition used different camera calibrations, it is more likely that the residual error is derived from inaccuracies in the calibration object, or an error in the triangulation and rudimentary thresholding algorithms, though it is nevertheless still small in magnitude.

1.3.2 Study 2: Strikes of the amazon tree boa (*Corallus hortulanus*)

Snake-Trial	Duration(s)	Distance(m)	Velocity(m/s)	Max Velocity(m/s)
Y4-1	0.0866458717	0.0958	1.1055	1.6393
Y4-2	0.1359673678	0.1731	1.2732	1.8036
Y4-3	0.1506305153	0.2136	1.4182	1.9968
Y4-4	0.0786477912	0.0829	1.0542	1.8137
Y2-5	0.1146391533	0.1461	1.2743	1.6408
Y2-6	0.1066410728	0.2192	2.0556	2.3136
Y2-7	0.1306353142	0.1472	1.1270	2.1715
Y2-8	0.1426324349	0.1567	1.0984	1.6513
Y2-9	0.1652936629	0.1419	0.8583	1.2661
Y2-10	0.1986189981	0.1573	0.7920	1.3879
B5-12	0.1959529713	0.1901	0.9700	1.4633
B5-13	0.1746247567	0.1695	0.9705	1.3763
B5-15	0.1093070996	0.0968	0.8854	1.4035
B5-17	0.1479644885	0.1462	0.9878	1.3030
B5-18	0.155962569	0.1468	0.9411	1.3333
All Mean	0.1396109378	0.1522	1.1208	1.6376

Table 1.2: Strike meta-data as calculated from initial forward movement of strike until start of head retraction.

In the framework of the experimental setting, 20 snake strikes were recorded, out of which 15 were used to provide tracking data that could be fully processed by SnakeStrike (Figure 1.6). The meta-information regarding successful strikes is presented in table 1.2. Captures 19 and 20 derived from a smaller snake and thus were not included. Captures 14 and 16 used a rather strong heat element as infrared target to elicit the strike instead of the IR emitter that was used for the other strikes. This strong heat element produced visible light that affected the ability of SnakeStrike to properly track the markers. Capture 11 did not yield a consistent set of images, likely because of partially missing data from one of the 5 cameras and therefore was excluded from further analysis. Details regarding the velocity of each strike over time is presented in figure 1.6. The dots indicate the calculation of the velocity for each timestep using 3D triangulation information. The value for each individual dot was calculated as the change in distance between two subsequent timesteps, where a timestep was denoted by a captured image. There are two lines for each capture plot with one showing the best fit for the trial data and the other indicating the average best fit for all trials of a particular snake. Data points that did not allow an analysis were

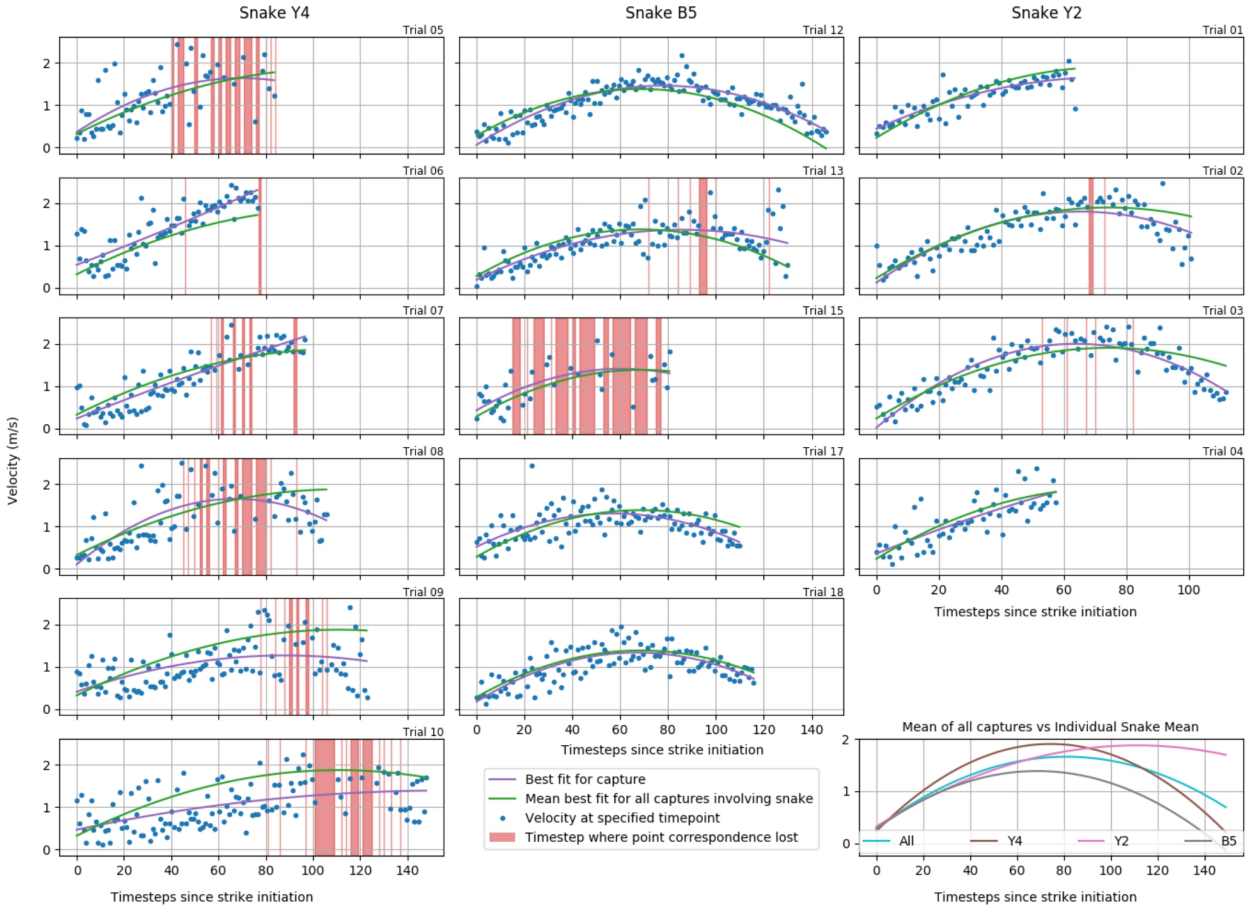

Figure 1.6: Study 2: Snake strike velocity over time (**A**) 3D positions in study 2 of each snake's head for each trial are plotted to illustrate the velocity changes during the strike. In some trials, e.g. Y4, markers were obscured from the view of at least one camera resulting in a loss of correspondence as a new and usually temporary point was assigned to be the marker location. These time steps were removed using a velocity threshold of 2.5 m/s (red vertical bars). (**B**) Group aggregate velocity statistics for all snakes individually and as mean across all snakes tested in this study. Image source: Jensen et al. (2020a).

removed from the plot (red bars) based on a velocity threshold of 2.5 m/s. This omission of data typically occurred when the identity of points was swapped for a few timesteps, or when the thresholding process found a different reflection or source of color than the marker in question and assigned a new — but often only temporary — point as marker for that timestep. An example for the velocity change of a snake strike is plotted at the lower right of figure 1.6 as the best fitting curve for all snake strike trials in comparison to the best fitting curve for all trials of each individual snake.

1.4 Discussion

As indicated previously for machine vision in social interaction studies (Robie et al. (2017)), when individual animals are visually indistinguishable, the task of tracking in the presence of occlusions or partial overlap is an unresolved problem. For snake motion tracking, a similar problem exists as positions on the body surface of the snake are nearly identical, such as when the snake skin consists of a repetitive pattern. This makes markerless tracking methods, such as DeepLabCut (Mathis et al. (2018)), much harder to employ successfully on patterned snakes. Markerless annotation programs such as DeepLabCut further require a set of manually labeled images to train the software. In the case of DeepLabCut, this training can require a couple of hundred images per camera, though in practice a smaller number can be sufficient, and if the camera is moved, it might require re-labeling of a set of new images from that camera. Furthermore, DeepLabCut does not provide 3D triangulations of annotated points. On the other hand, non-patterned skin can also be problematic as large sections of the snake surface look very similar and indistinguishable causing specific positions to be difficult to discern with sufficient spatial resolution.

With the snake moving and changing body shape in a very short period of time, the labels assigned to these markers will be swapped in most cases, unless the system is able to uniquely identify and track a particular marker over time. This is implemented in many systems by using multiple markers as a single marker and putting them into a unique configuration scheme that is identifiable by the system (Theunissen et al. (2017)), thus filling up even more skin space with markers. Unfortunately, the maintenance of the spatial configuration can be also very problematic since some animals (e.g. insects or small birds) are too small to carry an extra payload or are able to remove these markers very easily (e.g. snakes or squids). For example, a snake easily twists itself and effortlessly removes even the smallest markers. This is the major reason why studies, such as that by Theunissen et al.

(2017), used rigid structures attached to the body and head of the animal as markers. This method allows motion capturing of the whole animal as body and head can be tracked, even when there is occlusion of some markers. In a large system with many cameras the triangulation is robust to marker loss through the view of many cameras. Unfortunately, this method is not suitable when attempting to capture the kinematics of the animal or the kinematics of particular appendages.

SnakeStrike is a framework that allows researchers in animal tracking to use one piece of software from experiment start to finish and in combination with high-speed cameras to save time in the processing of 3D triangulation data for animals that can be difficult to track. Our preliminary data set on boid snakes showed that this framework is suitable to track even fast movements such as snake strikes and provides first information about the instantaneous speed during the complete strike of a boid snake. Although this data set primarily serves to demonstrate potential applications of this framework, it already showed that instantaneous strike speed has a similar magnitude, when compared across different individuals. In addition, our data on boid snakes shows similar strike profiles and trajectories as described for strikes of viperid snakes (Herrel et al. (2011); Kardong and Bels (1998)), suggesting the presence of a common motor program for executing strike behavior. Similar experiments with an increased number of markers placed on the snake body, would also allow for a further, more detailed analysis of the contribution of typical loop formations in strike progression.

Collection of data from living animals in study 2 would not have been possible without either this system or spending a vast amount of money on a commercial system. Despite room for further improvement, the system provides scientists with new options and another alternative to existing systems such as DLTdv (Hedrick (2008)) to record novel data sets. Some drawbacks of the system derive from the necessity to simultaneously save the images from multiple high-speed cameras, which requires a large amount of memory for the initial capture, high CPU load for processing, and a large amount of hard drive space for long term storage. This requires a large upfront cost for a computer, although the computer can also be used for other tasks, and still costs only a fraction of a commercial system. However, the storage of the raw data, allows recalculations and reanalysis at any time (see below). Since changes of light intensity, shadowing, and occlusion of markers can occur within a given recording session, thresholding color from the images can be complicated and time consuming. The impact of this issue can be reduced, though not completely eliminated, by pre-tests of the color(s) to be thresholded in the actual setting, as well as

by strict adherence to a consistent experimental environment and regime.

The benefits of this framework considerably compensate for the few disadvantages, also because in many experiments, the latter can be at least partially circumvented. The reduced upfront costs compared to commercial motion tracking systems allows greater ability to incorporate motion tracking at high speed in animal studies. Animals that could previously not be tracked in 3D space because of the speed of the camera or the cost of the system can now be used in respective studies. As shown in study 1, the error in the system is small with regard to normally occurring sources of errors such as flickering lights, color thresholding problems, or marker identity swapping. For animals in which affixing large 3D markers is impossible because the animal might remove the markers or they do not remain affixed, this is a particular improvement.

In studies of animal behavior, the goal usually is to obtain the largest amount of usable data as possible. Being able to store and reassess all originally captured images, rather than having to only rely on calculated 3D points is a very big advantage, since various additional analyses can be performed offline. This indicates that the acquired information can be used not only for the initial, principal aim of a project, but also allows answering novel questions without the necessity to perform a second experiment. Since all 3D points are decoupled from the images, the generation of the points in terms of decrease in error can be improved by new methods in the future. The data generated from older studies can therefore be re-interpreted or interpreted in greater detail, when e.g. new algorithms for coping with occlusion of tracking markers have been developed. Triangulation of data collected today would suffer from this aspect of the current state of the art in algorithms. However, if this problem is improved, these data can be easily re-interpreted with new algorithms and possible new insight can be obtained, without having to re-run tedious and often difficult and time-consuming experiments.

SnakeStrike brings the functionality of several open source projects together in a way that is highly beneficial to researchers who have no access to expensive motion capture systems. Researchers who work with non-standard and especially fast-moving animals now have an affordable option to exploit novel experimental ideas. In addition, those interested in testing new algorithms for object correspondence over time can generate real-world data sets very quickly and easily, or test ideas on previously collected data.

The contents of the following chapter comprise a manuscript that has been submitted for peer-review, but not yet accepted.

Jensen, G. W., van der Smagt, P., Luksch, H., Straka, H., and Kohl, T. (2020b). Tentative title: Chronic multi-electrode electromyography in snakes

This author's contributions were as follows:
- Conceptualization: together with HS, PvdS, and TK
- Methodology: together with TK
- Validation
- Formal analysis: together with TK
- Investigation: together with TK
- Data curation
- Writing - original draft: together with TK
- Writing - review editing: together with HS, PvdS, and TK
- Visualization: together with TK

Chapter 2

Chronic Multi-Electrode Electromyography in Snakes

Surface electromyographic recordings (sEMG) in snakes are challenging because of the tight body coverage with scaled skin. This coating forms a mechanical barrier that prohibits an easy and low-impedance access to epaxial muscles. Furthermore, the flexible body and undulatory motion of snakes may cause unintentional removal of surface electrodes by force or friction and thus impede chronic EMG recordings. We present a method for performing EMG on a snake that produces signals analogous to surface EMG signals, or likewise to bipolar inter-muscular signals. Our method involves subdermal implantation of recording electrodes without penetration into the muscle. This method allows for collection of high signal to noise surface EMG signals with minimal discomfort, less likelihood of wire loss, and at multiple placement sites along the body. The latter allows muscle coordination information to be collected.

2.1 Introduction

Electromyography in reptiles, especially snakes, is a complicated task. Intramuscular electrode implantation is invasive and limited to the recording of activity of single muscle fibers, when using the prevalent monopolar regime. In contrast, a bipolar configuration allows for the collection of signals from entire groups of muscles when performed with sufficient inter-electrode distances. Alternatively, multi-unit activity from muscle fibers can be recorded over a wider area with non-invasive surface electrodes, i.e. sEMG. Both of these approaches are unsatisfying and usually lead to complications and subsequent signal loss, when snakes remove electrodes and recording devices attached to their skin by rubbing either body segments against objects or other structures. Besides affecting recording quality, this reaction can remove scales or damage the skin of the snake more grievously. Nonetheless, intramuscular EMG has been used previously to shed light on a variety of snake behaviors from locomotion (Jayne (1988); Newman and Jayne (2018)) to feeding and

drinking (Cundall and Gans (1979); Cundall (1983); Jena et al. (1995)) as well as on more specific behaviors such as strikes (Young (2010)), constriction (Moon (2000)), or venom spitting (Young et al. (2004, 2009)). There has even been a study on how the epaxial muscles of the snake are activated during reaching tasks (Jorgensen and Jayne (2017)).

In all these studies, electrodes were inserted into locally restricted body segments for less than a day as the position of the electrode had to be physically verified. To overcome the technical limitations of muscle group EMG recordings in snakes and to allow for multi-site muscle activity analysis, we have developed a new technique for collecting multi-channel EMG data from multiple body segments of snakes during the execution of natural behaviors. This technique allows for stable EMG recordings over several days with a high signal to noise ratio and only small movement artifacts. Both individual spikes as well as the local group dynamics, normally associated with sEMG data, are robustly and consistently visible. Furthermore, this technique is suitable for recording of high-quality data over several days and thus can be used for chronic recording of EMG data in snakes.

2.2 Materials and Methods

We break the method into its constituent parts so that we are able to fully discuss the parts in detail without losing their high-level overview. This is important as some parts must be done in a very specific manner in order to ensure reproduction of this method.

2.2.1 Experimental Animals

In this study 5 semi-adult (snout-vent length (SVL), range: 85–106 cm; body weight range: 79–174 g) amazon tree boas (*Corallus hortulanus*) were used. Snakes were bred at the Chair of Zoology (Technical University of Munich) and maintained on a 12h:12h light:dark regime, 22–33°C temperature range, and a diet of pre-killed rodents with water *ad libitum*. Permission for the experiments was granted by the respective governmental institution for animal welfare (Regierung von Oberbayern, Gz.: ROB-55.1-2532.Vet_02-19-115).

2.2.2 Presurgical Preparations

EMG electrodes and implantation needles were prepared before (1 hour) application of the anesthetic drugs to minimize the time necessary for the actual implantation. For this procedure, thin flexible cables were used in order to avoid an impairment of the natural movement capabilities of the snakes and to support the large number of electrodes used.

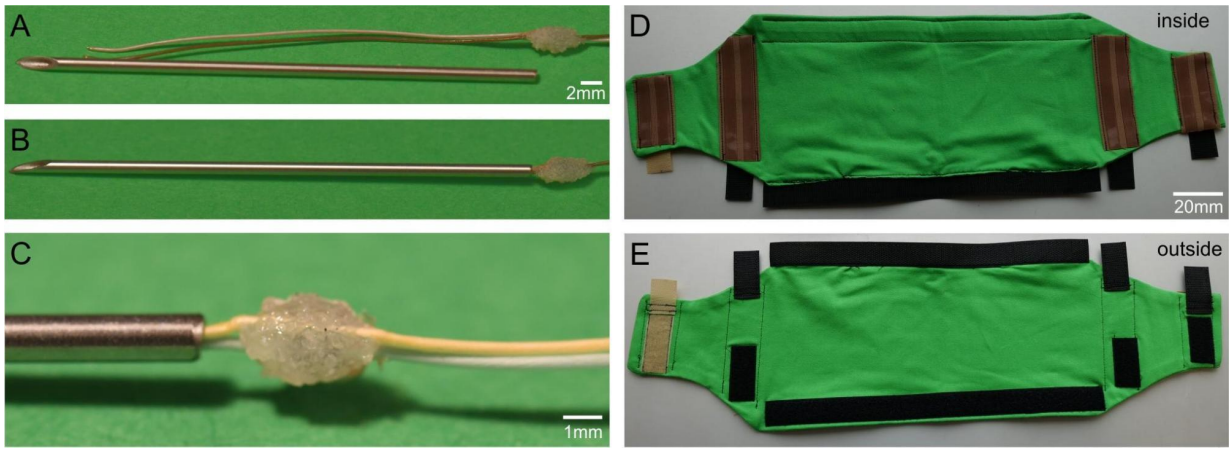

Figure 2.1: Custom-built items required for chronic implantation of multiple EMG-electrodes (**A**) Shortened injection needle and EMG-electrodes with an attached cyanoacrylate sphere that bonds two cables together to form a bipolar electrode. (**B**) Needle with cables inserted up until the cyanoacrylate sphere. Position of the sphere and needle length must be adjusted such that the electrode tips remain inside the needle. (**C**) Detailed view of the needle and cyanoacrylate sphere. The sphere diameter needs to be bigger than the needle opening to ensure that EMG-electrodes remain inside the needle. (**D**) Outside view of 'snake sleeping bag' required to prevent accidental removal of cables by the snake during recovery. Brown silicon stripes increased friction and helped to prevent the snake from exiting the bag. (**E**) Outside view of the same 'snake sleeping bag' as in D. Black and beige hook and loop fasteners allow for easy and fast closing/opening of the bag.

The absence of any impact of the implanted recording electrodes on natural motion dynamics and pattern was verified by a qualitative estimation of the locomotion capacity before and after the implantation. For connecting the electrodes, Omnetics Neuro NanoStrip connectors (A79021-001, Omnetics, Minneapolis MN, USA) that consisted of a miniaturized connector (7.4 mm x 4.4 mm x 1.8 mm), pre-wired with 18 cables (length: 46 cm; ⌀ 0.4 mm) were used. Each cable was electrically shielded with an individually colored layer of biologically compatible PTFE (Polytetrafluoroethylene) coating and thus was protected from short-circuits with other wires. The total weight of the wires including the connector was 2.8 g which equals 1.6–3.5 % of the snakes' body weight and thus was easily supported even by the smallest employed snakes. The cables were used in pairs, such that the cut ends formed a bipolar EMG electrode (Figure 2.1A,B). Using a connector with 18 cables generated 8 bipolar electrodes with the two remaining electrodes being used as ground wires, such that one electrode remained as backup in case the first ground electrode is damaged or removed during the recordings.

In order to keep the EMG electrodes in a close and constant relative position to each other as well as to prevent undesired, accidental removal, the cables were fixed to each other

using a small drop of cyanoacrylate glue (Figure 2.1C). As an actual spherical object is required to prevent removal (discussed below), small granules of sodium bicarbonate were used to speed up the drying process of the glue as well as to form a spherical structure. The distance between the location of the generated sphere and the tip of the EMG-electrodes determined the cable section that was subdermally implanted and was ensured to be consistent across all cables. In our experiments a distance of 40 mm has been proven suitable as it enables robust fixation of the cables without affecting natural movement capabilities. The position for the spheres on the cables is marked while holding the two cables together. At the same time a small drop of glue was applied to both of the cables at the marked position. Both cables' relative length was ensured to remain invariant relative to each other, as this would cause problems with cable management later in the experiments. After application, the small drop of glue hanged from both cables in a half spherical form, a pinch of sodium bicarbonate was sprinkled from above onto the glue to facilitate solidification and drying of the glue. This also allowed the downwards hanging glue to be pulled upwards into the aforementioned half-spherical form, because of the combination of surface tension and instantaneous fixation. Continual sprinkling of sodium bicarbonate from above created a half-spherical object on the top of the cable. Rotation of the cable and repeating the procedure ensured a small but strong hold that finally was spherical in form. Care was taken to avoid that the created sphere did not become too large since a large sphere causes a configuration where a space between the snake's body and the cable is formed. Another object could position itself between the cable and the snake and exert sufficient force to remove the cable. A sphere diameter of $\sim$2–3 mm was adequate for stable cable implantation. Any rough edges were removed from the sphere by careful sanding with high-grit sandpaper. The soldered connector for the cables was oriented in relation to the snake such that all cables, were directed towards the middle or back end of the snake. This helped to prevent entanglement and minimized cable tension caused by animal movements as the plugs will have a smaller dynamic range in this position as opposed to being located more towards the rostral end of the animal. To prevent bundles of excess cable caudally, the length of the cables was trimmed according to the distance between electrode insertion points: if the electrodes were directed from rostral to caudal in a distance of 6 cm from each other with a bipolar electrode on the left and right side of the vertebral column, then cables 1–4 remained at a length of 46 cm, cables 5–8 were trimmed to 40 cm, and cables 9–12 were trimmed to 34 cm, etc.

Insertion of the cable was performed with a hypodermic needle. The diameter of the

needle was just wide enough to accommodate the two cables that form a bipolar electrode pair. The plastic Luer-lock connector was cut off with a sanding disk attached to a rotary tool such that the needle could be used in the fashion of a hollow sewing needle. Thereby rough edges were sanded off and a closure of the internal canal was prevented.

2.2.3 Anesthesia

Prior to electrode implantation, snakes were placed in an induction chamber and pre-anesthetized with 2 ml isoflurane (Isothesia, Henry Schein Vet, Hamburg, Germany). As soon as the tail-pinch reflex ceased, snakes were intubated with a cat catheter (diameter: 1.2 mm) which was connected to an isoflurane vaporizer (Isotec-3, Völker GmbH, Kaltenkirchen, Germany). The isoflurane concentration provided by the vaporizer was set to 2.0–2.5%, to ensure surgical anesthesia for the entire duration of the electrode implantation. Additionally, Carprofen (Carprosol, cp-pharma, Burgdorf, Germany) was administered (2 mg/kg body weight, i.m.) one hour before the electrode implantation and once every following day during the EMG recording.

2.2.4 Electrode Implantation

For electrode implantation, the sharp end of the needle was used to penetrate the skin of the snake and was subdermally guided over a distance of 4.5 cm (fig 2.2). Care must be taken to prevent the penetration of muscles or inserting the needle even deeper into the body cavity. The needle was then pushed from caudal to rostral in parallel to the long axis of the snake's body. After insertion of the needle for 4.5 cm the tip was pushed outwards again to exit the skin. Thereby the needle enters and exits the skin simultaneously at two points to form a subdermal tunnel. Using a stereo microscope, the bipolar electrodes were inserted through the cut end of the needle until the sphere was flush with the end of the needle. At this point the sharp end of the needle was grabbed with a small set of pliers and the needle was fully pulled through the rostral penetration site. The cables remained underneath the skin as the sphere was unable to traverse through the caudal penetration site formed by the needle. The electrodes were thus precisely positioned underneath the skin with a distance of 4 cm from the initial penetration site and followed the direction provided by the penetrating needle. Overall, this process was performed 8 times for each of the bipolar electrodes and two further times for each of the single ground electrodes resulting in a total of 18 implanted cables.

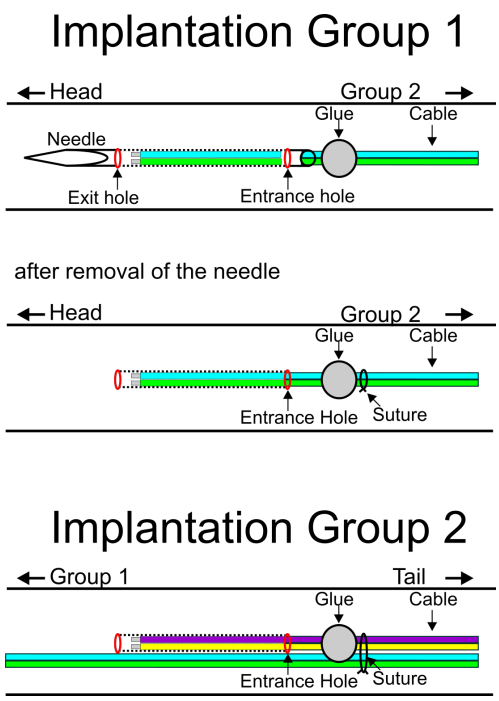

Figure 2.2: A diagram showing the process of electrode implantation for a specific site in an implantation group. An implantation group consists of two implantation sites, one on each side of a vertebral position. Each site consists of a bipolar electrode that is inserted sub-dermal and left in place. The lower portion of the diagram shows how a second group position would look after electrode implantation. This position should bundle the cables from the previous group on its side of the spinal column to better fix the wires to the snake's body.

2.2.5 Cable Fixation

In order to prevent cable removal, a suture (Daclon Nylon, Monofilament Nonabsorbable, USP 2/0, SMI AG, St. Vith, Belgium) binding skin and cables was placed at the side of the glue sphere opposite to the cable's entry hole to tightly hold the two cables in place. Importantly, it is recommended to use a non-absorbable nylon monofilament, as it has a high tensile strength and is easy to manipulate with only minimal tissue reaction. The suture needle was inserted laterally from the center of the cyanoacrylate sphere such that it appears that the suture will bisect the sphere. Before the initial knot of the suture was tightened, the suture thread was positioned to the side of the sphere, such that the sphere was centered between the electrode penetration site and the suture loop. The suture thereby applied a slight pressure against the sphere, which helped to keep the open end of the cable underneath the skin and minimized the possibility of cable removal. This could happen when an open space forms between the snake and the end of the cable separated

by the sphere. Further intermediate sutures were placed at locations in between adjacent implanted bipolar electrodes to bundle cables from several insertion points together. Care was taken to create enough slack, such that the cables did not prevent a restriction of natural movement capabilities when the snake formed pronounced body loops. At the end of the implantation, extended cables proximal to the connectors were coiled and carefully wrapped in parafilm.

2.2.6 Recovery from the Implantation

Following implantation, isoflurane concentration was set to 0%, which caused a quick and complete recovery of the snake from the anesthesia within a few minutes. It was very important that during extended recovery and between experimental trials on successive days the snake's movements remained restricted to prevent application of undesired forces onto the implanted cables. This measure largely prevented accidental removal of cables and consequential damage to the skin. In chronic experiments that lasted for several days, snakes were kept overnight in quarantine cages. If the cables were not covered when the animal was at rest overnight, cables might have become entangled in installations within the cage, e.g. branches. A major advancement for the possibility to perform chronic measurements over multiple days was the reliable and faithful securing of the recording electrodes and cables at all times. This was particularly challenging during the resting time of the snake at night in the home cage when the animal was largely unobserved. Instrumental for successfully maintaining all electrodes in place and functionally was the invention of an individually adjusted 'snake sleeping bag', which prevented any impairment and deterioration of the recording condition over the experimental period of up to 4 days.

This item was made out of fabric and securely covered the snakes where the cables were inserted. The bag prevented the animal from exiting the enclosure, but still allowed the animal to perform fair locomotor movements. The use of the bag is snake species-dependent. For arboreal species with a more elongated and slender body such as the amazon tree boas (*Corallus hortulanus*) used in our study, the use of the bag was highly beneficial as the snakes generally used their prehensile tail to wrap around objects, as well as around their own body. For heavy bodied, e.g. western-diamondback rattlesnakes (*Crotalus atrox*), such a bag wouldn't be strictly required, as the diameter of the animal is larger and this species usually shows a different behavior during recovery and resting. Even though these snakes also curl themselves up, this behavior does usually not require substrates such as branches and the curvature is in much simpler curves than those of tree

boas. The sleeping bag was constructed from an innately stretchy jersey fabric. Important for the stable positioning of the bag was the fact that the snake extends out of the fastened shut bag on both sides. If only the head were to come out of the bag, then the snake could still insert the tail through any loops that would exist with the inserted cables, potentially removing the latter.

At the points where the head and tail exit from the bag, hook and loop fasteners were attached on the outside of the bag. On the inside of the bag in relation to the hook and loop fasteners were silicon stripes. These stripes helped to hold the bag in place such that the snake is unable to slither out. The middle section of the bag consisted of a large compartment that is closed by a long strip of hook and loop fasteners running parallel to the extent of the compartment. The width of this compartment was adjusted to the size of the snake such that the snake was not able to fully extend its individual body segments. This prevented the snake from forming several S-shaped curves at body midsection and to pull the tail in through the bottom of the bag. As the diameter of the part of the body directly behind the head is smaller than that of the midsection of the snake, a well-fastened hook and loop closing mechanism prevented the animal from slithering out of the bag during forward movements. The head of the snake being larger than the section of body behind the head also prevented the snake from pulling the head back into the closed bag. Besides ensuring a strong and uniform closing mechanism, hook and loop fasteners facilitated a quick and easy opening and closing of the bag to place and remove a snake. The size of the bag was tailored to the size of the snake. The bag shown in figure 2.1D was designed for boid snakes with a body length 0.9 m to 1.4 m (SVL).

2.3 Data Collection

In this pilot study, 8 bipolar electrodes and two additional ground electrodes were prepared and implanted as described above to demonstrate the unaltered quality of the EMG data recording over multiple days. The bipolar electrodes were inserted in a pairwise fashion on the left and right side of the spinal column approximately one third of the distance to the ventral scales. To identify each electrode pair, electrodes were referred to a particular 'position', as shown in figure 2.3. The insertion points for the four rostro-caudal positions were determined by the following distances along the spinal column starting from directly behind the skull: 6 cm, 17 cm, 28 cm, and 39 cm. The two ground monopolar electrodes were inserted at approximately 45 cm behind the skull on opposing sides of the spinal

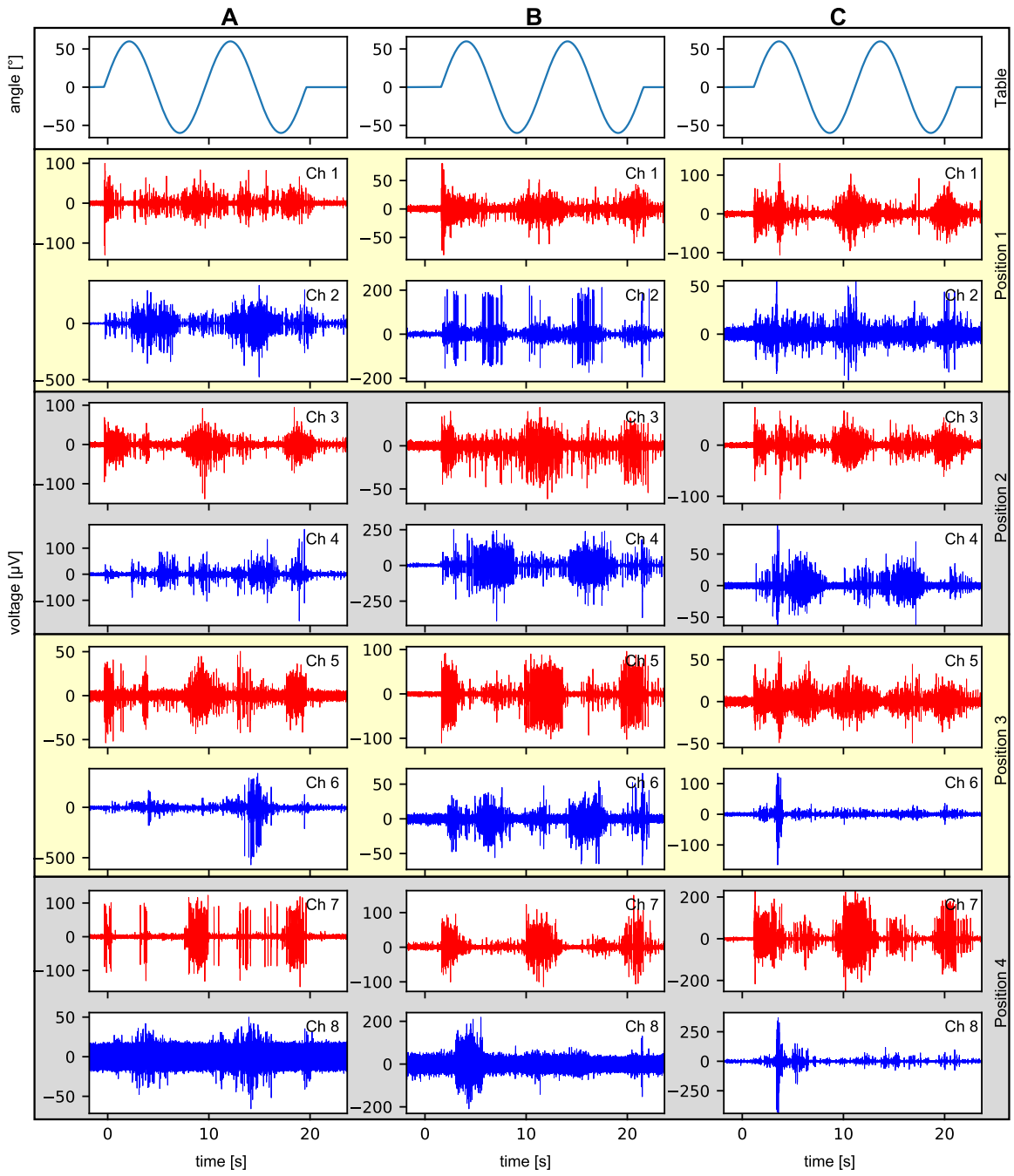

Figure 2.3: Representative example of multi-electrode EMG-recordings during turntable rotation. The data is pre-processed with a 50 Hz notch filter, as well as a Butterworth band-pass filter with low end of 20 Hz and high end of 850 Hz. Electrodes implanted on the left side of the snakes are colored red, while electrodes implanted on the right side of the snakes are colored blue. The first row shows the angle of the turntable relative to its starting location with positive angle equivalent to a clockwise movement. Yellow and gray backgrounds labeled 'position #' refer to the recording positions where electrodes were placed on the snake's body. (**A**) 8-channel EMG collected one day after implantation. (**B**) 8-channel EMG recorded from the same snake 4 days after implantation. (**C**) 8-Channel EMG recorded 3 days after implantation from a snake different than figures A and B.

column.

After implantation, each snake was allowed to recover overnight, and EMG data were collected over a period of 4 days. Recorded EMG-signals were amplified 192 times and digitized (20 kHz) by a 16-channel amplifier board with bipolar (differential) inputs (RHD2216, intan Technologies, Los Angeles, California). Digitized EMG-signals were forwarded to a USB-interface board (RHD2000, intan Technologies, Los Angeles, California) and stored on a computer using the USB interface board software provided by intan Technologies. A 50 Hz notch filter was applied to the recorded signal by the recording software. Thereafter, the collected signals were further processed with a 4th order Butterworth band-pass filter with low end of 20 Hz and high end of 850 Hz and sub-sampling of the data to 4 kHz to ease plotting of the data, though the 20 kHz data were stored for further analysis.

A custom-built turntable was used to provoke stereotypic muscle activity for the assessment of EMG quality. Accordingly, the snake was placed on a branch that was positioned in the center of the turntable. The turntable had a dimension of 30 x 30 cm and was driven by a brushless DC motor (Model:3268G024BX4 CS, Faulhaber, Schönaich, Germany). A Matlab script (Matlab ver. R2016a, Mathworks, Natick, Massachusetts, USA) was used to control turntable movements. The standard stimulus consisted of a sinusoidal motion with an angular rotation of $\pm$ 60° and a frequency of 0.1 Hz (period of 10 s). Data was recorded covering two periods with a lead and a trail buffer period resulting in a total recording time of approximately 25 s, for a single experimental trial. An infrared stimulus (IR-Emitter, Steady State IR Source, Model EK-5270, Laser Components GmbH, Olching, Germany) was presented in front of the snake to attract the attention of this infrared-sensitive snake species.

Since the snake was focused on the fixed position of the IR-Emitter, the head position was relatively stable in space during turntable rotation. This was achieved by active compensatory movements of the body involving the most rostral slings. Thus, the turntable motion caused the snake to decrease or increase the diameter of its S-shaped body loops which resulted in a stereotyped motor behavior, ideally suited to assess the quality of the EMG recordings. At the end of each experiment over a period of 4 days, the snakes were decapitated under deep isoflurane anesthesia (5%) using an animal decapitator (Small Animal Decapitator, Stoelting Co., Wood Dale, IL, USA).

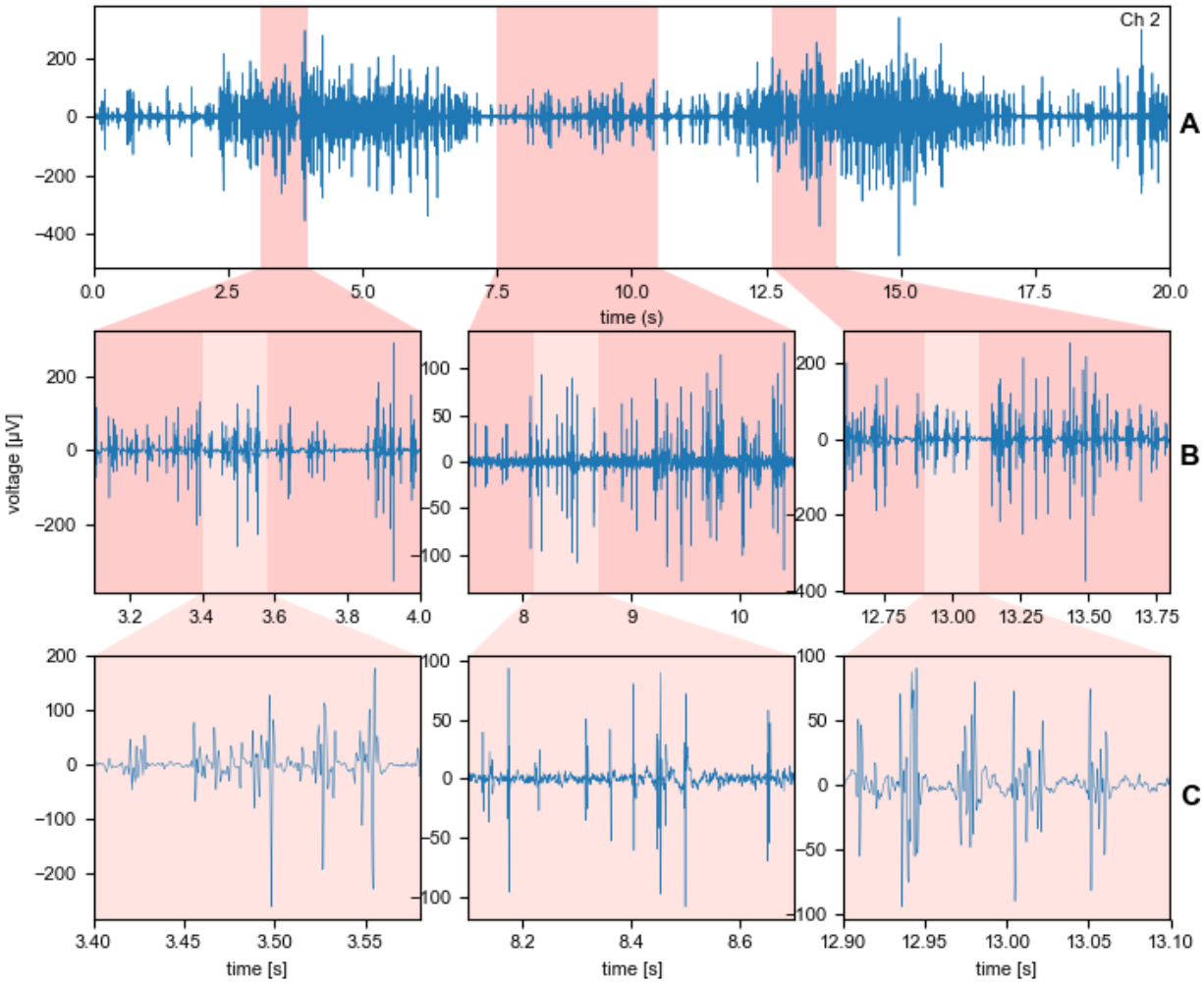

Figure 2.4: Muscle activity recorded one day after implantation in finer temporal detail. (**A**) The data from Figure 2A channel 2 showing grouped muscle activity during turntable movement. (**B**) 3 selected sections of the muscle activity from (A) at a finer temporal resolution (**C**) Light red insets in (B) with a yet greater temporal resolution.

2.4 Results and Discussion

All snakes used in this pilot study recovered completely from anesthesia and did not show any signs of pain or altered locomotor behavior in comparison to experiments on snakes, which were not equipped with implanted electrodes. At the implantation sites no swelling, bleeding, or signs of wound infection occurred. Thus, subdermal implantation of multiple electrodes with the newly established technique therefore has to be considered as a minimally invasive surgical intervention, which does not affect the natural locomotor behavior of the snake. Figure 2.3 shows data collected from three separate days, i.e. the data in figure 2.3A was recorded on day 1 after implantation and the data in figure 2.3B was recorded on day 4. Since it was impossible to cause the snake to assume the same body configuration, when the snake was placed on the branch during each recording session, the recorded EMG varied across subsequent days of data collection due to the individual formation of the loops. Therefore, the recorded muscle activity pattern shown in figure 2.3A does not completely match the activity pattern recorded three days later (Fig. 2.3B) when the same recording channels were compared. Channel seven in A and channels three and six in B show a higher noise than the other channels at first glance. This is only because each graph does not share the same y-axis range. These three channels, for example, only have a range of 50 μV while others can be as large as 1000 μV or larger. This is done to showcase the quality of the signal even at low voltages. The data shown in figure 2.3C shows data from a different snake. The data shown was collected 3 days after electrode implantation.

Even with these differences, recorded EMG signals of the same channels are very similar qualitatively across the two days. In these figures, the recorded muscle activity exhibits a high signal to noise ratio that varies across channels, but nevertheless allows for a detailed data analysis were this technique to be used in the future to study specific snake movements. Although this study was designed as a proof-of-concept, a stereotyped motor behavior is already visible in the presented qualitative data set. The turntable movement provoked a compensatory change of body loop (S-shape) formation, which is caused by alternating muscle activation (Fig. 2.3). The subdermal bipolar electrodes primarily recorded summed muscle activity. However, single-unit spike potentials were recorded as well. These could be considered as activity recorded from single-muscle fibers.

2.5 Conclusion

Until now, a robust technique to reliably record muscle group activity in snakes across multiple days was lacking. Our novel electrode implantation cable insertion technique proved to be highly successful and excellently suited for collecting high-quality data and to allow for the chronic collection of group EMG activation information. Most instrumental for chronic recordings, however, was the use of the 'snake sleeping bag' in order to prevent the loss of wires and to ensure safe resting of the animal overnight. The bag keeps the cables unimpaired while the animal recovers from anesthesia and allows multiple recording sessions over several days with the same animal and the same recording configuration. In addition, our method has no visible detriments to the health or vitality of the animal and can therefore be used over several days. While this technique has less accuracy for the determination of muscle specificity in comparison to intramuscular electromyography, it is more than sufficient to provide vital information on muscle activity that can be used to determine muscle coordination in future studies on snake locomotor or strike movements.

Part II

Diving into the Data

This author's contributions to the contents of the following chapter were as follows:

- Conceptualization: together with HS, PvdS, and TK
- Methodology: together with TK
- Validation
- Formal analysis
- Investigation: together with TK
- Data curation
- Writing
- Visualization

Collaborators:
– TK: Dr. Tobias Kohl
– PvdS: Prof. Dr. Patrick van der Smagt
– HS: Prof. Dr. Hans Straka

Chapter 3

Compensatory Kinematics in Response to Perturbing Stimulus

A motion capture tracking system for capturing high-speed 3D movement was described in Chapter 1. In Chapter 2, a novel method for electromyography collection was described and exemplary data that proved the quality of the techniques were shown. This chapter discusses data that leverages these two techniques, and provides a first analysis of the general trends of the data. Discussion in this chapter will focus, specifically, on the data where cantilevered compensatory movements in response to a turntable's sinusoidal movement were performed.

3.1 Introduction

Locomotion of snakes has been heavily researched (Gray (1946); Jayne (1986); Hu et al. (2009); Jayne (1988); Newman and Jayne (2018); Lissmann (1950); Moon and Gans (1998)) and now the muscular mechanisms for locomotion are well understood. Investigation into the ability of snakes to cross gaps and cantilever themselves has also been done (Lillywhite et al. (2000); Jorgensen and Jayne (2017)) so that now there is a better understanding of how the epaxial muscles contribute to these behaviors. All of this research, however, has leveraged a static study condition.

There have been no studies to date that look at the compensatory abilities of snakes to a non-stationary environment. An arboreal snake is subject to a variety of different perturbatory stimuli as the substrate on which it anchors itself is not static. A strong wind moves a tree branch quite easily, and thus the ability of the snake to stay fixed as well as hunt prey cannot be based on the assumption that only the prey is moving.

The snake is able to respond to these perturbations from a cantilevered position. Physics explains that an energy expenditure, or sufficient mass, is required to act as a counterweight to keep a position stable while cantilevered. How are boid snakes able to keep this cantilevered position and compensate for perturbation to their position? Fur-

thermore, since these types of perturbations would be common occurrence, how does the snake do this without large energy expenditure?

In this chapter, the behavioral strategies of snakes in response to a disruptive stimulus applied to the anchoring object of the snake, in addition to the muscular activity associated with these strategies, are investigated for the first time. The data is described in a qualitative and comparative manner and suggests several lines for future research.

3.2 Materials and Methods

The electromyography (EMG) method used in this study was fully described in section 2.3 of chapter 2. The video and motion capture system from chapter 1 was used to capture video during the study as well as for triangulating the markers on the snake afterwards. The markers for the motion capture system were placed such that they were directly over the open ends of both bipolar electrodes for that position. Details regarding approval of the study and the care of animals can be found in section 2.2.1 of chapter 2.

3.3 Data Collection

A study was conducted to test the EMG methodology described in chapter 2. It consisted of five snakes (CH34, CH35, CH36, CH37, and CH38) and two experimental conditions (with and without EMG implanted) with 3 modalities of movement recorded, i.e. locomotion on a flat surface, compensatory movement on a turntable, and strike movement. In this chapter, only the turntable data will be discussed in detail. For a first-look analysis of the strike data from this study, see chapter 4.

The first experimental condition was a control experiment where data on the 3 movement types were recorded without EMG implantation. This meant that only markers were attached to the skin of the snake and tracking was performed using the system from chapter 1. This data allowed for the collection of metadata in the case of the striking movement, but also recordings which were then visually compared to later recordings, along with personal observations, to determine if the behavior of the animal was changed by the implantation of the bipolar electrodes. The data collection for the group of snakes was done in a piecemeal manner, i.e. the locomotion was collected, then after a rest period (1 h) the turntable data was collected, and then after another rest period the strike data was collected. A 7 day rest period was provided before the start of the second experimental condition, the EMG implantation.

As the EMG method had only previously been tested using sacrificed snakes, it was initially verified using a single snake (CH34) to allow for procedural changes. The initial implantation of the bipolar electrodes was successful, as was the first overnight spent in the 'sleeping bag' (section 2.2.6). Several turntable angles and speeds were tested on the first day after implantation. This facilitated finding an angle and speed that allowed for a great amount of vestibular stimulation, but still allowed the snake to compensate for the perturbing movements. For these reasons, the angle of $\pm 60^{\circ}$ was used for all following experiments. Due to the trial-and-error process, the perturbation method was inconsistent for the majority of the trials of this day; therefore, they are excluded from the results to prevent inclusion of data that may compromise the data collected with a consistent method. Day 2 also proved that the method performed well and a set of consistent turntable data for the snake was collected.

In order to test the robustness of the EMG implantation, as well as the 'sleeping bag', over a longer period of time, no data collection was performed on day 3. On day 4, it was discovered that the snake had managed to extricate a large portion of its body out of the 'sleeping bag'. This had allowed the snake to remove a number of EMG cables from underneath its skin. The assumption for this incidence was that the ends of the 'sleeping bag' were not firmly and properly fastened at the end of day 2. As a number of bipolar electrodes were not usable, further data collection with this snake was halted.

Using the information gained from the first snake, a valuable piece of which being the duration of the data collection for a single snake over one day, the second data collection consisted of two snakes (CH35 and CH36). Again, a control set of data and an implantation set of data were collected, both with 3D marker tracking. This data was collected in a manner consistent with the second day of data collection from snake 1 (CH34), and data were successfully collected on day 1. At the end of day 1 the 'sleeping bags' for each snake were fastened and reaffirmed to be situated properly, as day 2 would not be a data collection day because required support personnel were not available. As was done with snake 1 (CH34), snakes 2 and 3 (CH35 and CH36, respectively) were checked periodically during day 2 and were found to be still in their bags as well as in a calm disposition. On the following day, the snakes were found to be still contained safely inside their respective 'sleeping bag', and the data collections for day 3, as well as day 4, were successful. These are the first data collected with no wire loss 4 days after bipolar electrode implantation. A similar procedure was followed for the final two snakes (CH37 and CH38), with the only difference being that data was collected on all 4 days following the implantation.

3.4 Results and Discussion

3.4.1 Data Collection

In general, no overt changes were seen to the behavior of the animals in both the recorded data and personal observations when comparing the control recordings to the implantation recordings. Examples of overt changes would have been decreased flexibility, change in level of aggression, increased flee response, etc. During the data collection of snake 1 (CH34), the locomotion recordings for the snake were quickly proven to be detrimental to the success of the other two types of recordings. Two main problems forced the abandonment of the collection of this data for subsequent snakes. The EMG cables used were not long enough to allow for the free movement of the snake without tension being applied to the cables. The length of these cables necessitated that the EMG amplifier, seated on a stand, was positioned close to the snake. For turntable and striking motions this was a non-issue, as there was ample slack in the cable to accommodate snake movement. However, for locomotion, the stand created an obstacle that could get tangled in the cables, which could potentially cause harm to the snake. The ideal arrangement would have been to have longer cables and an apparatus that holds these cables in the air away from the main body of the snake, but not lying on the experimental floor where the snake could interfere with them.

The second obstacle for collecting the locomotion data was that the experimental setup was not large enough to allow the snake free-ranging movement without external corrective intervention. While the open space of the experimental setup was approximately 1 m^2, it was too small to accommodate more than a couple of undulatory movements given the prior mentioned problem of the EMG amplifier stand. Future studies of locomotion using this method should take this into consideration.

In terms of animal movement recordings, there were 189 usable turntable recordings, see figure 3.1. In this figure the composition of good and bad trials are shown, i.e. usable and non-usable. Bad trials fit into one of three categories: 1) an error occurred in the collection of camera video, 2) either a strike was performed by the snake or there was an additional perturbation stimulus applied to the snake, and 3) the EMG was bad or the trial was removed from inclusion because the data collection method differed (i.e. day 1 for snake CH34). Additional perturbational stimuli could come from snake handler interaction during recording or cables getting snagged and thus slightly pulling on the skin of the animal. The exclusion of trials, referred to as skipping, could occur because of a

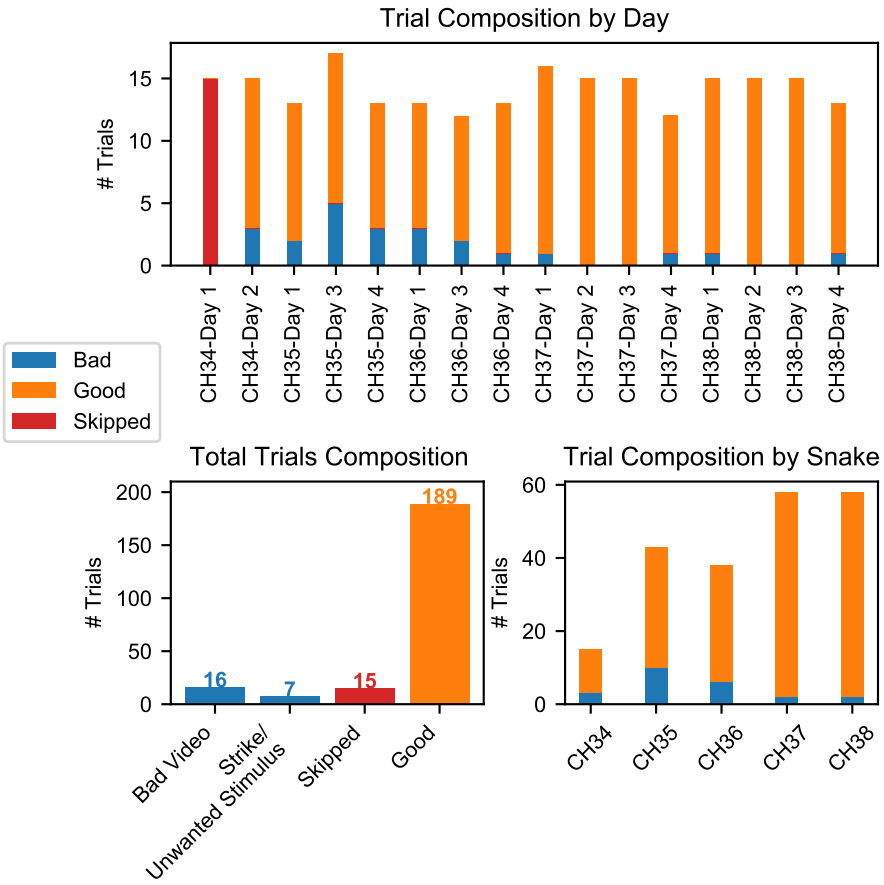

Figure 3.1: Statistics for the number of usable trials for the data collected using a turntable as a perturbatory stimulus. The good and bad, i.e. usable and non-usable, trials are shown grouped by day, by snake, and in total for all snakes.

problem with the collected EMG signal, or that the method of collection differed across trials and thus the trials were not immediately comparable to the others in the set.

In total, the data collected from the snakes makes up ∼7.6 terabytes (TBs) of raw data. The majority of this was from the turntable recordings as they had a recording time of 24 seconds compared to the recording time for the strikes of 8 seconds, with roughly similar numbers of total trial captures. The fully processed data, i.e. the triangulated data, metadata, and processed EMG data, only comprised ∼270 gigabytes (GBs) of data, or a roughly 28 times reduction in the data.

While this amount of data may seem excessive, it was necessary for proper data fusion. As mentioned in chapter 1, using a commercial system would mean that the amount of stored raw data needed would be closer to the order of the processed data from SnakeStrike.

However, determining the phases of the snake strike or seeing how non-tracked portions of the snake responded to perturbation stimuli would not be possible using a commercial system, as the original images are not stored. It is these original images that allow the collection of metadata for analyses such as: identifying whether an error in the capture was caused by an error in the system, identifying whether extra external forces were applied to the snake during the movement, or even using these recordings to create and test new hypotheses. If only the processed 3D points are available, the richness of the fusion of motion capture and EMG is lost.

3.4.2 Behavioral Movement

The fixation of the head of the amazon tree boa (*Corallus hortulanus*) while the S-shaped curves of the snake compensate for perturbations to their anchor point was first described in section 2.3 of chapter 2. An external infrared (IR) stimulus was used to provoke the snake to compensate for the deflection of the body caused by the turntable and achieve a fixed head position. When no stimulus was present, the snake would often choose to not reorient its body curves in relation to the stimulus and would allow its whole body to be moved in space with the turntable movement.

Figure 3.2 shows a representative example of the head fixation during turntable movement. The outline of the snake to the right is mapped approximately to the same view of the triangulated data to the left. A numbering system is used to demarcate the markers in the text, i.e. position 1–5 (rostral to caudal), but in the figures the colors blue, orange, green, red, and purple represent positions 1 through 5, respectively.

The triangulation shows that the head was not perfectly fixed in space. There was, in fact, some movement, but in relation to the other parts of the body this movement was very small. Incidentally, this amount of movement was hardly noticeable in the raw video using the naked eye, even when viewed at slow speed. In the example shown in figure 3.2A, positions 4 and 5 were adjacent to the snake fixation points on the branch and position number 4 was approximately above the center of the turntable. Thus, positions 4 and 5 were the least able to respond to the perturbations of the table. This explains why the curves of positions 4 and 5 seemed to parallel each other and follow the motion of the turntable with very little variation outside of the turntable-defined trajectory. Furthermore, position number 5 had the most movement in relation to the other positions on the snake, as it was not directly over the center, and it was the closest position ($\sim$2 cm) to the snake's anchor point.

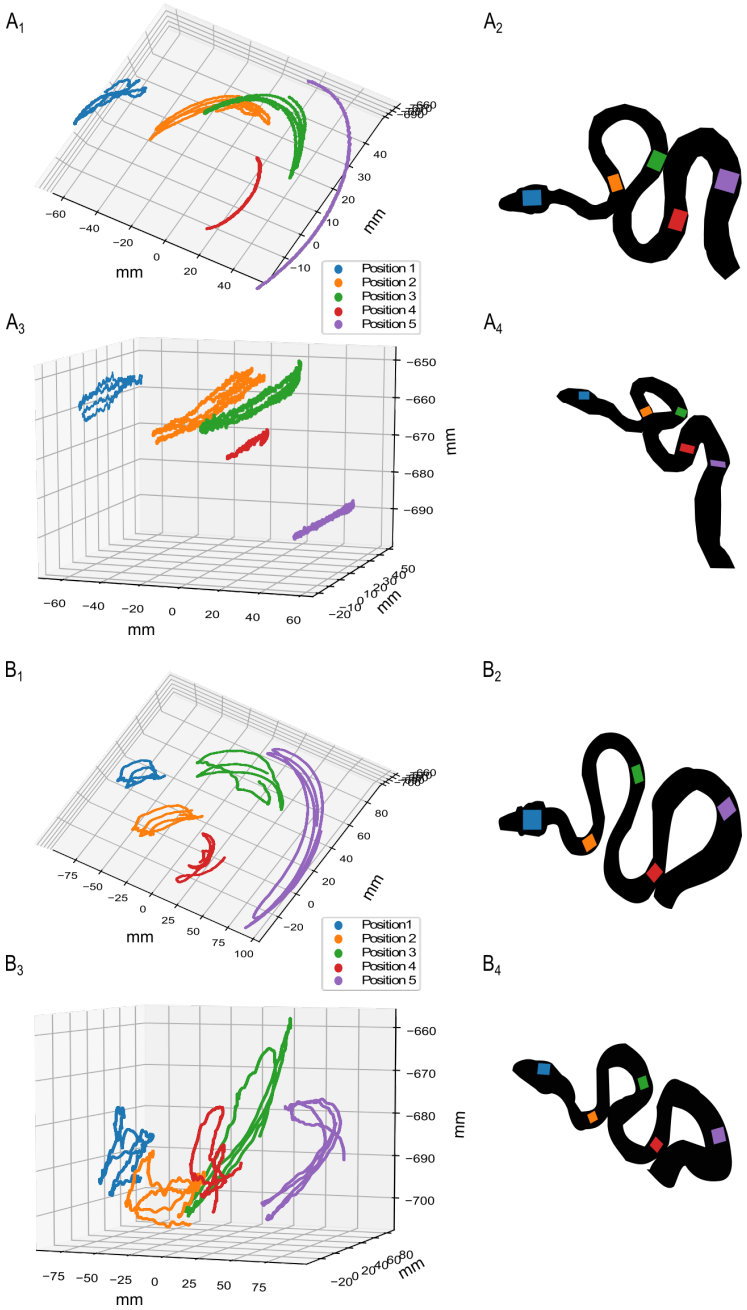

Figure 3.2: Two different captures from different snakes but in similar body positions showing the corresponding positions on the body of the snake in relation to the 3D tracking data. Pair A_1 and A_2, and pair A_3 and A_4 show approximately the same view of the same trial. The positions shown in views A_2 and A_4 correspond to the starting position of the turntable but from a different camera angle, thus they are approximately in the middle of the corresponding colored curve in A_1 and A_3. The data in B is similarly configured to the data shown in A but shows a different snake and trial. The table turned $\pm 60°$, for two periods at a rate of 0.1 Hz. The snake was situated on a branch held up by a stand that was placed on the turntable. The body position of the snake relative to the table was roughly centered underneath marker position 4 on the snake for both A and B captures. (Corresponding EMG data in fig 3.4)

The body configuration of each snake, individually and across trials, varied. However, two specific coping strategies were seen across snakes and across trials, planar loop closure and planar orientation shift. For example, if initially there was enough space between S-shaped curves to accommodate the movement, the snake would remain relatively flat in the same plane (strategy 1). However, if less space was available, the snake would change the orientation of some of its S-shaped loops in space to give it more movement so that it could keep its head fixed in space. If the angle was too severe to be countered by changing the inside angle of the S-shaped loops, another strategy that the snakes presented was to change the plane in which the body was residing (strategy 2). An example of this is shown in figure 3.3 A,B in a minimal fashion at $+60°$ and to larger effect at $-60°$. The snake used the same coping strategy for both periods of the turntable movement, as can be seen by comparing the composition of the snake from similar turntable positions. The turntable's first motion was to the snake's right, i.e. clockwise, and continues for $60°$. In total the turntable movement was $\pm 60°$ for two periods at a speed of 0.1 Hz (10 s per period).

Using strategy 1, if the snake was able to keep itself in the plane in which it originally started, the S-curves with apex, i.e. the outermost point of the S-shaped curve, in the direction of turntable movement were the first to decrease their opening angle. If more than one S-shaped curve matched this description, there didn't appear to be a rule as to which moved first or whether they simultaneously moved; it was a mixture. Until no more movement can be gained by closing the curve angle opening for apexes in the direction of movement, the curves with apex in the opposite direction appeared to hold their angle. After that point, curves at or near positions 3 and 4 were typically the first to increase their open angle (this included position 5, so long as position 5 was at the apex of a curve and was sufficiently far away from the anchor point of the snake to the branch). The S-shaped curve closest to the head was usually the last to be modified, unless all other body loops are already closed. Upon reversal of the turntable direction, the order in which the curves were modified was reversed. However, this reversal was not a perfect mirroring of what had transpired in the other direction.

In the second coping strategy, S-shaped curve apexes that were in the direction of the turntable movement increased in absolute height during turntable movement. This effect was more pronounced the more caudal the apex. Thus, the snake kept its body in a rough plane, but changed the plane orientation in space. The S-curve apexes in the opposite direction to turntable movement decreased in height accordingly. Since movement in the reverse direction was not a perfect reversal of the movement, this lead to some small

perturbations in the form across periods. In some trials the maximum turntable angle ($\pm 60°$) was too great for the body position and the snake drastically reconfigured their body, or ceased head fixing behavior and fixed its body position.

Often, if the snake was in a more extended S-shape configuration it slowly pulled the anterior portion of its body back into a more compact position. This continued until the S-shaped loops came into contact with other parts of the body, or the curves were able to slip under or over more posterior loops. The preferred compact hanging style of the amazon tree boa is similar to that shown in the introduction in figure I-1 where the anterior loops were positioned slightly underneath the more immediate posterior loop. This behavior could be classified as a more general form of coping strategy 1. It was not included in the description of strategy 1 because the variability in potential configuration was too high. Future studies that use more markers to distinguish a finer granularity of anterior body position should consider including this behavior under strategy 1. When body segments associated with curves were not able to slide over each other to further facilitate decreasing of the curve angles needed to compensate for the perturbatory movement, the behavior of strategy 2 resulted.

Tracking of markers during turntable movement and the subsequent changes to snake body configuration was not always a simple task. When the snake reverted to the aforementioned under-hanging position for either all of the anterior portion or at least portions, the markers had the potential to become occluded. This lead to missing timesteps in the data record. Occlusion is a common problem in motion capture. Sophisticated strategies for applying motion trajectories to points can be applied for helping disambiguate points that overlap each other, but they are no guarantee that fully occluded points can still be tracked (Betke and Wu (2017)). To minimize this occurrence, it was important to have a wide range of camera angles. Often this occlusion only occurred when the snake was at the more extreme ends of the turntable rotation, so little data was lost.

3.4.3 Muscular Activation

How quickly does the snake respond to a perturbation stimulus and how is the movement strategy of the motor system implemented? The last section showed the effect caused by the underlying activation of muscles. Here, several examples of different snake activation profiles that match those behavioral movements are shown. While a full analysis is left for future work, apparent trends in the data that will serve as starting points for future models are shown.

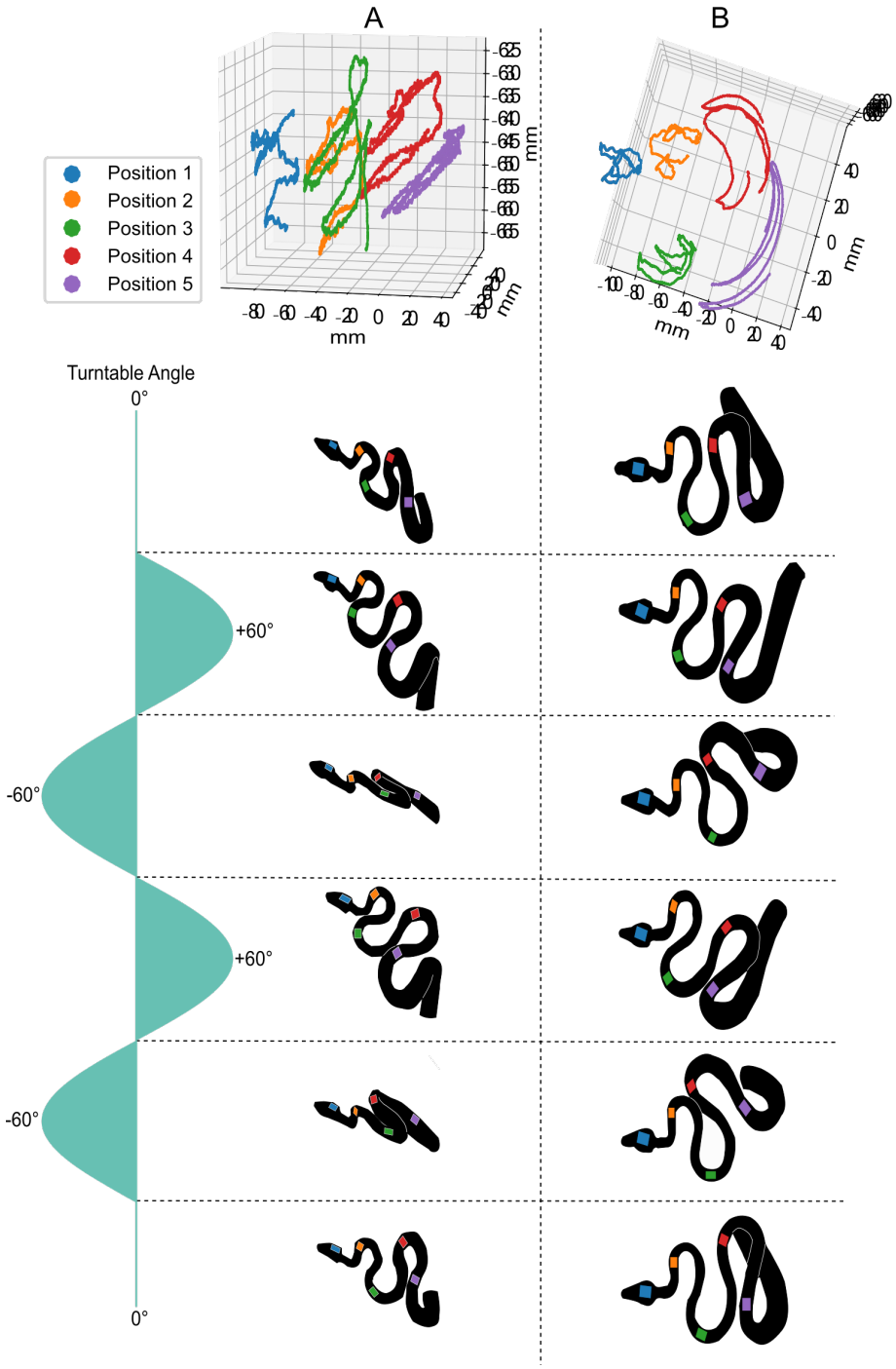

Figure 3.3: Two views of 3D tracking data from the amazon tree boa on a turntable and their corresponding positions on the snake. A and B at the top show all tracking positions throughout the course of the turntable movement. Underneath each of these plots a series of snake captures are shown from an approximately corresponding camera view. Camera captures are shown at starting position, maximal angle in each direction, and end position. The table turned ±60° (positive is clockwise), for two periods at a rate of 0.1 Hz. The snake was situated on a branch held up by a stand that was placed on the turntable. The body of the snake was roughly situated such that position 5 was centered above the turntable.

Unlike what we've been able to show comparing the tracking of points across different snakes in the previous section, comparing the EMG of the snakes is quite difficult. While the body configuration the snake takes may be similar to another snake, the positioning of the bipolar electrodes would need to be in the same positions relative to the curves of each snake's body composition. As the musculature of the snake is a near-continuum, the S-shaped loops across two body configurations may be very similar, but the actual position of the bipolar electrodes in each body configuration may be different. For example, if one snake has the same rough body configuration as another snake, but its loops start 2 cm more posterior than the other, the positioning of the bipolar electrodes will be shifted accordingly. If the bipolar electrodes in one snake were at the apex of the S-shaped curves for that snakes body positioning, then the bipolar electrodes for the other snake could be between the apex of two opposing curves. The information provided could be very different and might make direct comparisons difficult.

Activation in Relation to Body Position

In figure 3.4, two trials are shown. In 3.4A the EMG data that matches the behavioral data from figure $3.2A_{1,2,3,4}$, further referred to as snake trial 1 is seen. The data in figure 3.4B comes from the behavioral data shown in figure $3.2B_{1,2,3,4}$, further referred to as snake trial 2. The data was plotted using the same scale for easy comparison. Each plot presents the data from one bipolar electrode; the color of the plot shows whether the bipolar electrode was on the inside (red) or outside (blue) of the S-shaped curve where the bipolar electrodes are positioned. Each bipolar electrode position pair was marked visually by a marker. To aid comparison with the behavioral data the corresponding color is located on the right side surrounding the position name. These two snake trials were chosen as they consisted of trials with different individuals and the body configuration that the snakes assumed in these trials were very similar. Furthermore, the location of the bipolar electrodes for each snake were in similar places on the S-shaped curves of the snakes. Finding similar body and bipolar electrode positions across snakes was a difficult task, quite often similar body positions were found, but the bipolar electrodes were in completely different parts of the body curve.

Upon first examination of the plots, it was immediately apparent that there are differences between the two trials. This was not surprising as figure 3.2 showed considerably more variance in the tracking data associated with snake trial 2 than that with snake trial 1. Furthermore, there were differences in the activity of the two snakes prior to the start

of the turntable. In snake trial 2, there was activity prior to the start of the turntable movement. This activity was caused by the introduction of an IR stimulus to keep the focus of the snake for facilitating head stabilization. This specific snake was more quickly interested in this stimulus and had started to move its body slightly forward towards the stimulus when the motion of the turntable had begun. However, close examination still showed a lot of overlap between bipolar electrodes of corresponding position in both snakes.

One would expect that when the table is moving in the direction of the opening of the S-shaped loop they would see that the outside has stronger firing than the inside, but the reality is more complicated. The firing seemed to be dependent on whether the opening angle was also increasing. This is visible in the outside curve of position 2 of trial 1, figure 3.4A, and a similar, though weaker stimulus was seen in the corresponding plot of strike trial 2, figure 3.4B. The activation of the inside curves showed different activity as the inside curve of position 2 of trial 1 showed paired activity between inside and outside, while the corresponding position in trial 2 showed alternating activity, i.e. the expected activity. This activity between the two trials seemed to also occur in position 4. The paired activity seemed to be correlated with the fixation of a body curve to change the inside angle of the curve. The differences in relative firing magnitude also seemed to reflect the amount a curve was moving. In trial 2, the firing in position 4 was most likely weaker as that loop was not opened as much as the loop associated with position 2. This was further supported by the initial activity in the inside of the loop during the turntable's positive angle movement for snake trial 2, where the posterior loop was held fixed by the inside muscle activity and the loop near position 2 adjusted to compensate for the movement. This exact activity was not replicated in snake trial 1, possibly because the loop near position 4 had partial support of the branch, though it still modeled the expected behavior with low activity.

As previously mentioned, position 2 for snake trial 1 showed firing that seemed to match up for both the inside and the outside of the curve. This could be the result of the diameter of the curve not changing much. The snake in trial 2 assumed a much more open body position compared to trial 1 and this increased the movement between positions quite dramatically. In the direction of movement one would expect to see large activation for the inside of position 2, i.e. rising sinusoidal (positive increase in table angle and clockwise movement), and the corresponding activation was seen. Examination of the video showed the opening of the angle of the S-shaped loop was not a constant process, it was modulated by the snake in combination with the other body angles. It was a stop-start-stop-start-etc.

process of increasing the angle or holding the angle to keep the head in the desired position and orientation.

Stabilizing Activation

The activation of position 5 and sometimes position 4 was quite similar across snakes and across trials. In figure 3.4A, given that position 5 was fully supported by the crook of the tree branch, and position 4 was also partially supported, why was the major muscle activity visible in position 5 and not position 4? Visually, it could be seen that the loop of position 4 was closed by self touch, so there wasn't any positioning gain to be had. The spacing of position 4 and position 5 changed, at the largest extreme, less than 2.43 mm of absolute distance from each other. This meant that the body segment connecting position 4 and position 5 hardly moved throughout the entire turntable movement. This was similar to the amount of baseline system error seen in section 1.3.1 of chapter 1, and thus implied that they could move, relative to each other, even less than what was calculated. This could mean that position 5 was functioning as a stabilizer to counteract the physical movement of the anterior portion of the snake with the anchoring to the branch. In the second trial an absolute movement of 15.76 mm between positions 4 and 5 was seen as the snake made a large majority of its body configuration changes at the loop near position 5.

The muscle activity near where the snake anchors itself varied in expression depending on how the positions near the anchor were supported. Preliminary analysis seemed to show that positions anterior to the anchor point function similarly to the other positions in the anterior portion of the snake where there was no extra structural support other than the body of the snake itself. When the measurement position was at the anchor point, or posterior to where the anchor point supports the snake's body, then the muscle appeared to act in a stabilizing manner. At the start of movement, muscles at these positions had significant activation that seemed to seek to counteract the forces being applied to the snake.

This hypothesis was further investigated by finding examples from different snakes over different days and visually inspecting the activity of the muscles for positions 4 and 5 in the following situations: position 4 was the anchor point, position 4 was a secondary anchor point (position 5 was the anchor point and the snake forms a loop to allow position 4 to lay on top of position 5 but still have solid support), position 4 was partly supported by the branch (but not a solid anchor point), position 4 was not supported at all by the branch while position 5 was the anchor point, positions 4 and 5 were anterior to the anchor point,

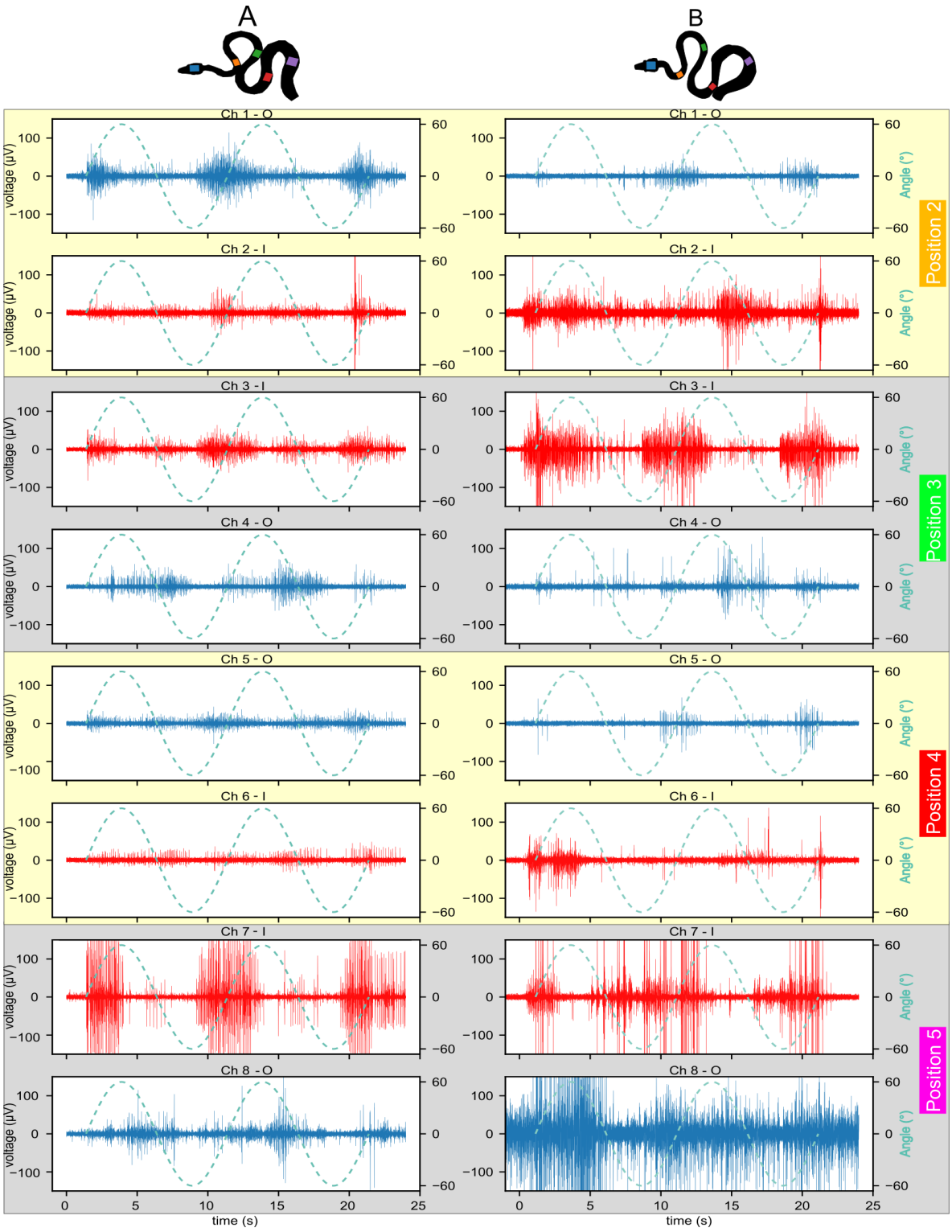

Figure 3.4: EMG collected from two different snakes. Blue represents that the bipolar electrode was on the outside of a S-shaped curve, while red represents that is was on the inside. The dotted line represents the angle of the turntable during its sinusoidal movement and positive values are in the clockwise direction. (**A**) This column of plots shows the EMG that corresponds with the tracking images from figure 3.2 A. (**B**) This column of plots shows the EMG that corresponds with the tracking images shown in figure 3.2 B.

and the anchor point was between positions 4 and 5.

The first two situations showed that the EMG of position 4 and 5 looked very similar. These positions are referred to as non-movement positions. The other four situations consisted of movement positions, either full or partial. In the 'partial movement' situations, i.e. where position 4 was partially supported by the branch and the anchor point was between position 4 and 5, strong activity from position 5 was seen, but very weak activity from position 4, that approximately matched the activity of position 5, was visible. In the situations referred to as 'full movement', very large activation in position 5 was seen, but there was a relatively activation in position 4. The activity in the latter situation for position 4 was greater than in the former, partially supported by the branch, situation. This was expected as that part of the body needed to have stronger activation to move or keep itself fixed than if it were partially supported.

While examples for all six of the situations were able to be found in the data, some many times over, the amount of data was still not satisfactory to confirm the stabilization hypothesis in turntable movement. Future experiments should consider placing more bipolar electrodes posterior to the anchor point and varying the positioning of the snakes on the supporting branch. This is easier said than done, however, as any attempted re-positioning of the snake could lead them to prefer an escape behavior rather than a tail grasp and hold behavior. A balance between variety and quality should be sought.

Frequency and Power

While EMG information has been included in snake studies for a long time, there has never been a deeper analysis of the properties of the muscle signal. In fields such as biomechanics, the frequencies present in the muscle activation reveal vital information regarding muscle recruitment as well as diseased states or muscle fatigue (Agarwal and Gottlieb (1975); Inbar and Noujaim (1984); Sadoyama and Miyano (1981); Berzuini et al. (1982)). When capturing human EMG there are recommendations for where and how to place bipolar electrodes and how to process the data. For example, when processing human EMG a band pass filter of 20 to 500 Hz is standard as the frequency and power, even of fast acting fibers, in humans rarely exceeds 500 Hz (Merletti (1999)).

In figure 3.5, both the normalized frequency spectrum and power spectral density (PSD) of all snake turntable captures that were not discarded is shown. Figure 3.5A shows the PSD organized according to where the bipolar electrode was positioned in relation to the S-shaped curve on which it was located. The PSD was computed using Welch's method

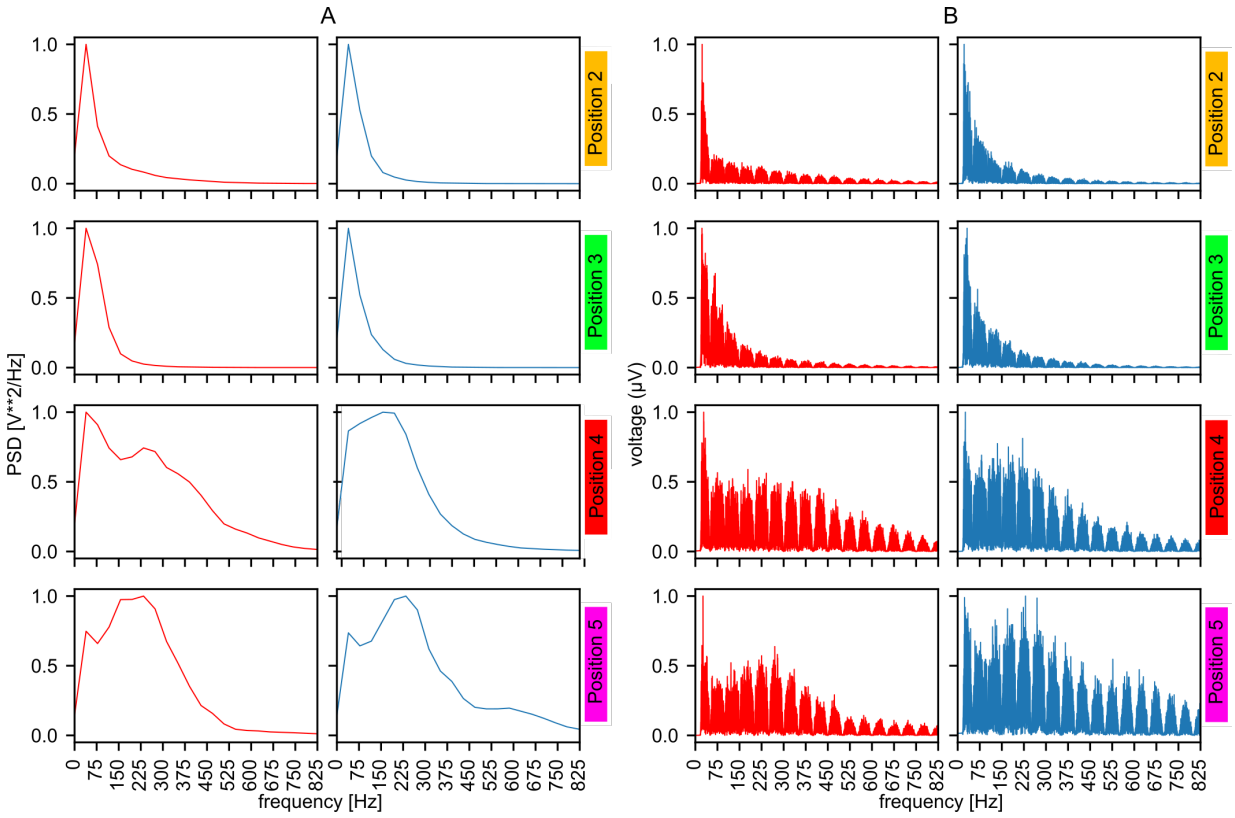

Figure 3.5: (A) Normalized power spectral density of all non-excluded turntable captures. The red plot indicates the position of the bipolar electrode was on the inside of a curve;blue represents the outside. (B) The frequency spectrum of the muscle activation of all turntable captures normalized and ordered according to whether the bipolar electrode was on the inside of an S-shaped loop (red) or if it was on the outside (blue). The raw signal included strong signals at 96 Hz, 100 Hz, and 110 Hz. These frequencies were judged to be noise and removed from the data using a notch filter. The signal was further processed with a band-pass filter between 20 and 850 Hz, and cropped to include only the muscle activation during turntable movement.

with a window size of 512. In these plots red indicates interior to the curve while blue represents exterior. Figure 3.5B shows the same data as 3.5A but processed with the discrete Fourier transform. The raw signal was processed with a band-pass filter between 20–850 Hz. Strong signals were initially found at 96 Hz, 100 Hz, and 110 Hz. These signals were classified as noise and removed as well as their harmonics, this accounts for the serrated look of figure 3.5B. The data was also cropped so that only the signal during table movement was analyzed.

The frequency spectrum for positions 4 and 5 was considerably wider than that for positions 2 and 3, i.e. approximately 75–300 Hz vs 20–100 Hz, respectively. Furthermore, there was a considerable shift of power to a higher frequency for these posterior positions.

This aligned with what is here hypothesized to be stabilization behavior in these positions during movement. There also appeared to be a small amount of lower frequency signal spikes in the output of these positions as well. This further supports the idea that the positions located close to the anchor seemed to have a different purpose than the positions located well anterior to the anchor point. As the different locations of positions 4 and 5 cannot be separated from each other at time, it is not clear how the frequency ranges of these small differences compare. Nevertheless, the frequency of this shift to the right of positions 4 and 5 was a high frequency, by human standards, for this slow-paced movement. The PSD also shows that there was significant power in frequencies higher than 500 Hz, so if the recommendations for the processing of EMG collected from human muscles were followed a significant portion of the signal would be lost. Future experiments should take this information into account when considering how to process EMG data.

3.5 Conclusion

This chapter has presented the first dataset collected where a snake was in a non-stationary environment. The behavioral strategies of the snake have been described in detail and the underlying muscular activations that produce this behavior have been described for the first time. It is shown that the head fixation activity is dependent on a stimulus to interest the snake as well as enough maneuverability in the body curves of the snake to handle the perturbing stimulus. Investigation into the EMG of the caudally located bipolar electrodes shows that these muscles have different activation profiles depending on where the snake is anchored to the branch. Furthermore, there does not appear to be a single strategy for neutralizing the perturbing movement, but rather the position and possible range of movement dictate the strategy. The stabilizing activity of the caudal bipolar electrode locations, hypothesized here, requires more data to prove or disprove. Placing more bipolar electrodes in the anchoring area of the snake and moving the snake body position that comes in contact with the anchor should provide the information needed to verify this hypothesis. Additionally, it is recommended that future studies of EMG in snakes publish frequency and power information to compare with the data shown here.

This author's contributions to the contents of the following chapter were as follows:

- Conceptualization: together with HS, PvdS, and TK
- Methodology: together with TK
- Validation
- Formal analysis
- Investigation: together with TK
- Data curation
- Writing
- Visualization

Collaborators:
– TK: Dr. Tobias Kohl
– PvdS: Prof. Dr. Patrick van der Smagt
– HS: Prof. Dr. Hans Straka

Chapter 4

Strike Kinematics in Response to Artificial Prey Stimulus

While slow movements and a consistent stimulus can provide information regarding muscle activity at rest and during perturbation, what is really fascinating are the fast and dynamic movements of the animal. These movements are especially interesting for arboreal species of snakes, as the snakes make their strikes from a cantilevered position. Physically, a cantilevered position requires energy expenditure, or a large mass to act as counterweight, to keep a lever arm cantilevered. How are arboreal snakes able to perform this maneuver often and, presumably, without large energy expenditures? While the data needed to answer that question does not yet exist, this chapter discusses results from a pilot study that dramatically increases the available data on muscular activation during snake strikes. These data represent the first arboreal strike data comprised of video and electromyography (EMG) data from a non-viperid snake, as well as the first that focus on muscle coordination over the entire anterior portion of the snake. These data confirm some experimental findings in snakes, but are contrary to others.

4.1 Introduction

There has been significant work focused on snake strikes (Penning et al. (2016); Herrel et al. (2011); Gans (1986); Kardong and Bels (1998); Kardong and Smit (2002); Cundall and Greene (2000); Cundall and Gans (1979); Cundall and Deufel (1999); de Cock Buning (2015); LaDuc (2002); Young (2010); Ryerson and Tan (2017)). Unfortunately, all studies, except for Young (2010), have used video data without the help of electromyography. Furthermore, in most cases these video data were not triangulated, or used slow camera speeds and had to be heavily interpolated. While video data is useful for measuring performance of the strike, it doesn't allow deeper causal analysis of the movement.

Until now, the only work that has paired video capture and multi-electrode EMG in order to capture details of a snake strike was performed by Young (2010). In Young's work,

four electrodes were placed in the *Musculus semispinalis-spinalis* (SSP) muscle of the snake somewhere around the first curve behind the head of the snake. For electrode placement, an exact distance behind the cranium was not given. Though, from images provided it can be assumed this was somewhere less than 15 cm behind the head of the snake. While three different implantation location strategies were utilized, the majority of the results focus on the data from a pattern of implantation where two electrodes were inserted on each side of the snake and into the same muscle with one of the electrodes being more rostral than the other. Young found the following patterns in his data: the outside of the S-shaped curve had activity prior to the inside; in relation to the curve, muscle activity started caudally before the muscles located more rostral had activity; and the muscle in the rostral portion of the curve had a longer activation time than that in the more caudal position. Furthermore, the muscle activity seemed to occur prior to the visual launch of the snake strike, whereupon it ceased activity until slightly after contact with the target was established and was subsequently active again. Furthermore, in all observed strikes of the puff adder (*Bitis arietans*) the body loops extended from rostral to caudal.

Young found that the mean velocity of the puff adder was 2.6 m/s with peak velocities of 5.8 m/s and mean accelerations of $\sim$72 m/s^2. The puff adders used were 72–151 cm in length with masses that could reach up to 5 kg. The question that Young posited concerned how the puff adder was able to accelerate so much mass, and so quickly. Young (2010) hypothesized that this speed in combination with the unusual pre-firing of muscles prior to strike described a high-power output muscle system, here referred to as the elastic energy storing hypothesis. He based this idea on the work of Deban et al. (2007) where a high-power tongue mechanism of the plethodontid salamanders was described. The EMG trace of this tongue mechanism was similar to the EMG seen in the puff adder strikes, i.e. a pre-loading of the strike followed by no activity during the physical movement of the snake. This pre-loading put tension on tendons and was followed by an elastic recoil of the tendon that allowed for achieving high rates of acceleration.

This chapter presents the first non-viperid strike data to combine video and EMG. Furthermore, the EMG electrodes were positioned so that a large part of the anterior portion of the snake was covered. This allows for unprecedented insight into the muscular activations responsible for amazon tree boa strikes, and creates a strong base of data for comparison to other species. In addition, this data provides a strong data counterpoint for the application of the elastic energy storing hypothesis to the arboreal snakes of this study.

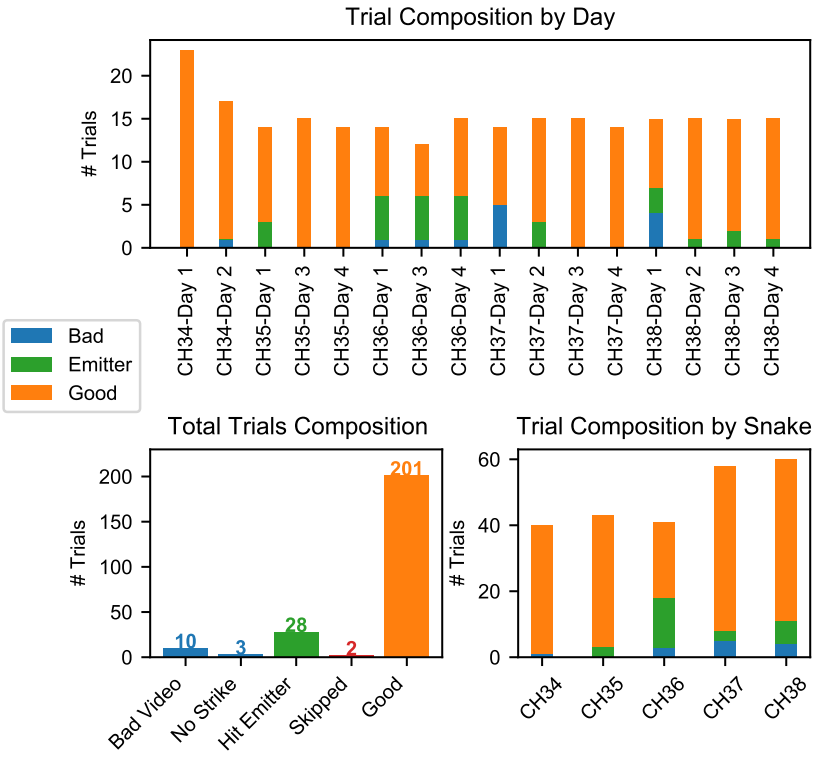

Figure 4.1: This figure shows the composition of all video recordings of strike activity. (A) The usability of the strikes recorded for each snake and each day is shown. (B) The totals for all snakes combined. (C) The totals for all snakes separately.

4.2 Materials and Methods

The method of EMG used in this chapter was described in chapter 2, section 2.3. The video capture and subsequent 3D triangulation was done using the system described in chapter 1. The bipolar electrode placement, as well as marker placement, was the exact same as in chapter 3. Details for the care of animals and approval of the study can be found in section 2.2.1 of chapter 2.

4.3 Data Collection

The data described here were from the strike phase of a pilot study data collection. A more in depth description of the format of the study can be found in section 3.3 of chapter 3. For the strike portion of the daily schedule of data collection, the snake was placed in the

same setup as the turntable. The same branch was used with the same snake between the turntable and the strike recordings. In order to provoke a strike, the same infrared (IR) emitter was utilized as that used in the turntable recordings to maintain the snake's interest while the turntable was moving. A researcher moved the IR emitter in front of the snake changing its relative position to the snake as well as the movement speed. This method worked very well to initiate a strike from the snake. A trial consisted of a single strike. As the amazon tree boa (*Corallus hortulanus*) is a very aggressive species (Esbérard and Vrcibradic (2007)), it was quite easy to procure a large number of quality strike recordings within 45 minutes to an hour of time. Figure 4.1 shows good and bad trials collected during the pilot study. Trials were marked as bad and not used for further analysis when the snake made contact with the emitter or there was a problem with the recording. This resulted in 201 successful strikes and 43 non-used strikes. Of the 43 non-used strikes, 28 were instances where the snake made contact with the emitter, 3 didn't record strikes, 10 had issues with the recording of the video, and 2 were instances where the EMG recording had issues.

4.4 Results and Discussion

4.4.1 Data Collection Methodology

The same branch was used with the same snake between the turntable and the strike recordings. The reasoning for this was that when collecting data from multiple snakes, it was less stressful for the snakes to stay attached to the branch on which they were currently positioned and to move the branch out of the setup into an appropriate area for the snake to recover, than to try to remove the snake from the branch. In hindsight, this may have limited the number of original body positions in which the snakes configured themselves.

4.4.2 Strike Performance

As mentioned in the introduction, there are currently a number of factors used to determine strike performance, i.e. speed, duration, etc. Table 4.1 presents some of these indicators for the amazon tree boa (*Corallus hortulanus*). The first row of values comes from the X-ray study discussed in chapter 1.3.2. The other two rows consist of the data from the pilot study's control and implantation collections.

Across the three types of data collection similar performance statistics were seen. However, comparing the data from each of the three studies in a pairwise manner using a two

Study	Avg. Dist (m)	Avg Speed (m/s)	Avg Max Velocity (m/s)	Avg Dist to Stim (m)	Max Velocity (m/s)
Ch 1 *X*-Ray	0.1522	1.1208	1.6376		2.3136
Pilot	0.1885±0.0063	1.0110±0.0395	1.4655±0.0514	0.2436±0.0128	1.8751
Pilot Control	0.2296±0.0062	1.2688±0.0378	1.8194±0.0462	0.2996±0.0173	2.1155

Table 4.1: Meta-data from the pilot study compared to meta-data collected in the X-Ray study of Chapter 1.3.2.

Study	Comparison to Pilot			Comparison to Pilot Control		
	Avg. Dist	Avg Speed	Avg Max Velocity	Avg. Dist	Avg Speed	Avg Max Velocity
Ch 1 *X*-Ray	✗	✓	✓	✗	✗	✗
Pilot	-	-	-	✗	✗	✗
Pilot Control	✗	✗	✗	-	-	-

Table 4.2: The results of using the Kolmogorov–Smirnov two sample test to see if the data across studies were significantly different. The pilot data was significantly different from the control data where EMG electrodes were not implanted, but similar to the X-ray metadata where EMG electrodes were also not implanted. Significance determined with a p-value of 0.01.

sample Kolmogorov-Smirnov test with p-value of 0.01 showed that there were statistical differences. The overview of which study indicators were statistically different is shown in table 4.2 with an ✗, and non-statistically different is shown by a ✓. While the metadata from the implanted pilot study was statistically different from the control for that study, it was interesting that the metadata from the *X*-ray study was statistically similar to the implanted pilot metadata even though no electrodes were implanted in the *X*-ray study. This seemed to suggest that performance indicators are not a good measure of behavioral difference for arboreal species, and puts more importance on the observations of researchers until a suitable metric for behavioral difference can be found. For arboreal snakes, controlling for where the snake attaches to the anchoring branch may be vital as this affects the distance of the strike. Accordingly, strikes with a higher average maximum velocity have a longer strike distance to reach that speed. This does not mean, however, performance metrics should be completely abandoned, as they provide a useful measure for comparing and contrasting activity amongst different species of snakes.

In comparison to other species, the maximum velocities for the amazon tree boa were at the lower end of the spectrum. For example, the puff adder (*Bitis arietans*) has an

average velocity of 2.6 m/s with peak velocities of 5.8 m/s covering a distance of ∼21 cm during a time span of ∼87 ms (Young (2010)). Other snakes such as *Crotalus atrox*, *Agkistrodon piscivorus*, and *Pantherophis obsoletus* have faster velocities over shorter distances compared to the puff adder (Penning et al. (2016)). In the only other strike data of an arboreal species of snake, Herrel et al. (2011) showed that the arboreal pit viper (*Cryptelytrops albolabris* — formerly *Trimerusurus albolabris*) had average speeds of ∼1.45 m/s for males and ∼1.6 m/s for females with an average strike distance of ∼12 cm. Using the provided acceleration information from this study it can be calculated that peak velocities of 5.8 m/s and higher are possible in this species of snakes. Nevertheless, the strike velocity data shown here for the amazon tree boa was slower than all aforementioned species of snake. The average strike speed velocity was similar to the arboreal pit viper, but the maximum velocity was slower. This suggests that the viperids may have a different strike mechanism than the boidae.

4.4.3 Behavioral Movement

As discussed previously in the introduction (figure I-2), the strike of a snake can take two forms according to Kardong and Bels (1998), i.e. the gate model and the tractor-tread model. The primary form that was utilized by the amazon tree boa was that of the gate model. This was shown through visual analysis of the video recordings, but also in the 3D tracking data. In figure 4.2, the trajectories for markers not located on the head of the snake stayed either fixed, or they tended to converge onto the trajectory of the head marker (position 2 and 3 of 4.2B). If this motion was primarily caused by the tractor-tread model, one would expect to see very different behavior as the markers should follow the path of the head marker, not converge to, or even, in the case of the second position marker overshoot the path of the first position marker. Though it was clear that the large majority of the strikes follow the gate model, there were instances in these data where the tractor-tread model was used for a short period of time. These instances mainly involved the snake moving forward towards the stimulus, or adjusting the anterior portion of its body to better position itself in relation to the stimulus.

Another aspect of the snake's strike, that was visible in figure 4.2A, was that the strike vector of the head was not always a straight line. It could be, as was the case in figure 4.2B, but the form of the snake's body as well as the direction it would like to strike seemed to affect the strike vector. For example, if the S-shaped curves of the snake were fairly uniform in their distribution on each side of the snake, then the strike vector of the snake appeared

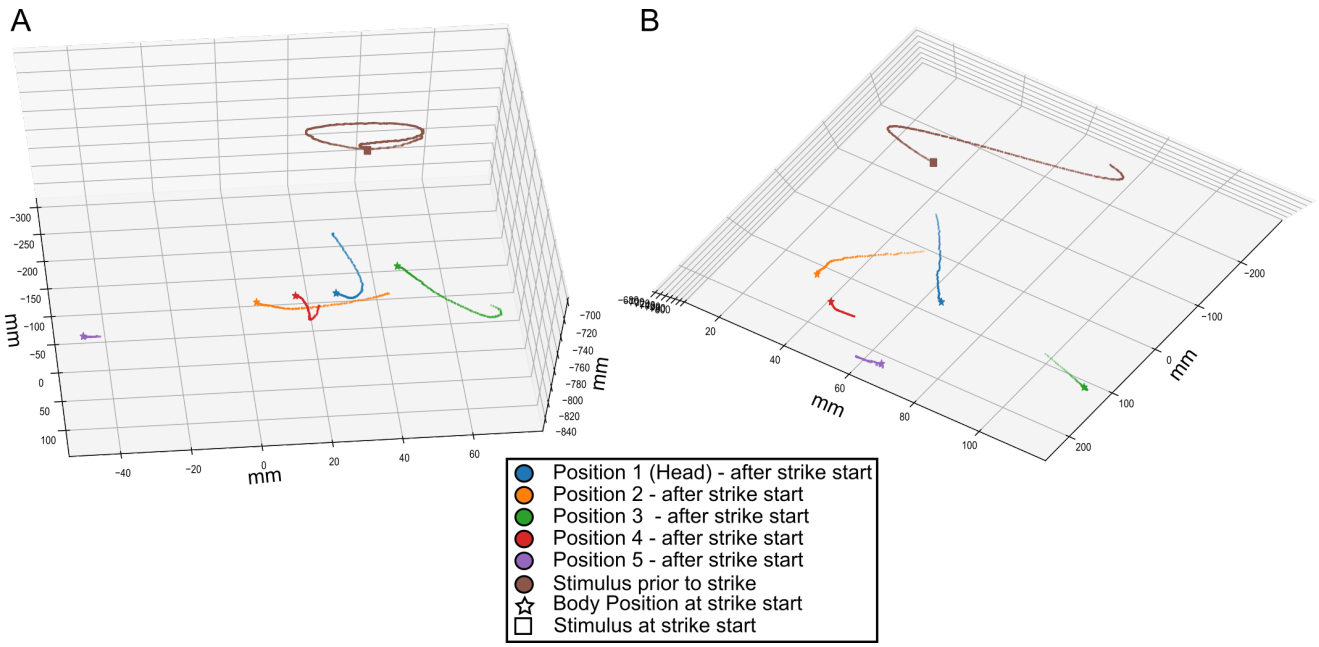

Figure 4.2: These two plots show the tracking of markers from the start of the strike until just before the point of maximal extension. The colors blue, orange, green, red, and purple correspond with the marker positions from head to tail of the snake, and the starting position of the marker is marked by a star. The brown line shows the movement of the stimulus prior to strike with the start of the strike marked with a square. (**A**) Example of a snake strike where the head vector of the snake was not a straight-line. (**B**) Example of a straight strike vector during strike and the characteristic movements of position 3 and 4 towards the path of the head.

to be more straight. However, if there was an imbalance, the strike vector tended to have a skew. Perhaps this is an explanation for the behavior seen by Frazzetta (1966), where the snake appears to change strike vector towards the end of the strike, but has not been duplicated in any other studies. Depending on the camera angle, and without the aid of triangulation of markers, the snake could appear to be changing direction towards the end of the strike when in reality it was following a skewed vector the entire time. Additionally, the other factor that can skew the end of a strike is gravity. The farther a snake strikes, the more the snake has to fight against the downward pull of gravity to keep its vector on target. It has been observed throughout the course of the strike data collection that the amazon tree boa preferred to strike in a slightly downward angle, thus potentially seeking to decrease the immediate effect of gravity. Whether or not the snake takes gravity into account in its strike vector initial path, in that it aims initially higher, will have to be tested in a future study.

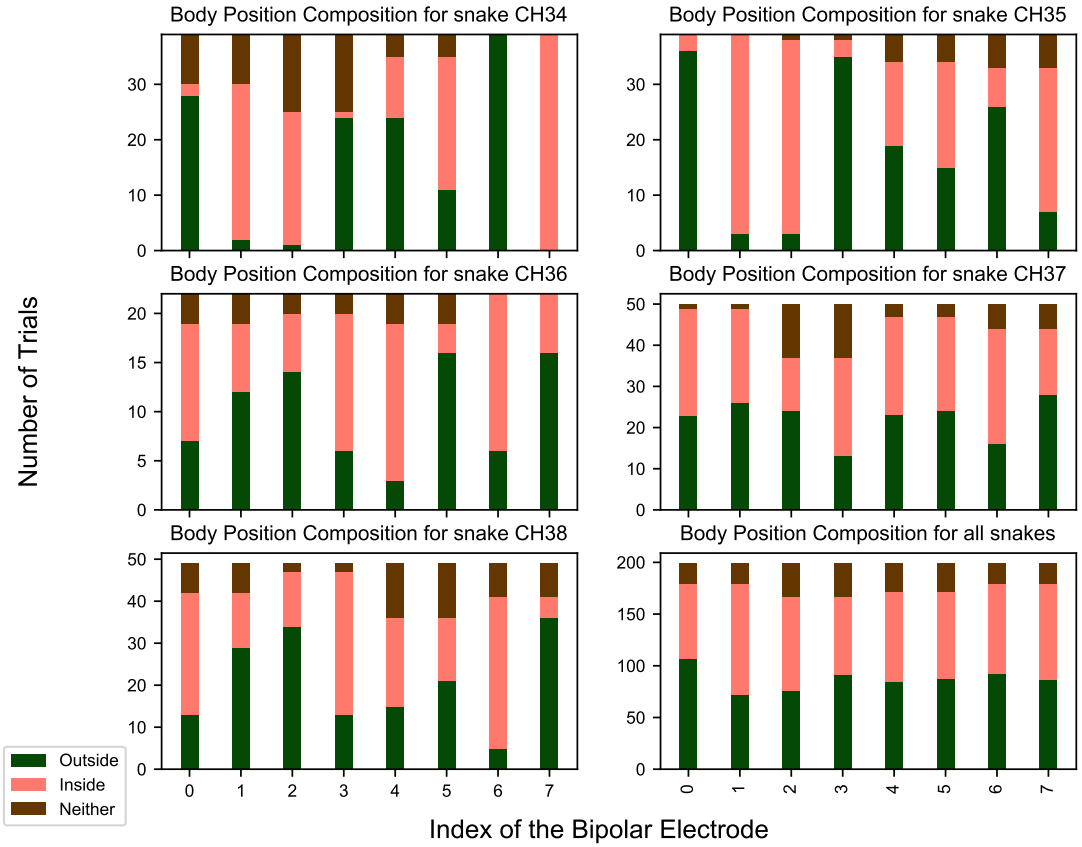

Figure 4.3: Snake preference for positioning and forming of S-shaped curves. Plots marked with 'CH##' show the aggregate data for that specific snake. It appears that snakes may have personal preferences as to how they configure themselves into s-shapes, but across snakes there was clearly no common preference of how to configure their body.

Body Position Preferences

Since the strike vector was so heavily affected by the position of the snake, the next question was whether there was a common body position shared by all amazon tree boa individuals. The data that were collected from the pilot study, showed that this was not the case. While it may be the case that specific individuals had preferences for how they configured their body, there does not appear to a be common positioning across the whole.

Figure 4.3 shows each electrode position on the snake and whether that position was on the inside or outside of a curve, or if it was in-between. While the data for each electrode was biased to the fact that the snakes were rarely re-positioned on the branch during a day's data capture, the aggregate of all trials for the snake, as well as the aggregate of

all trials for all snakes, should show a trend if one exists. What was shown was that for all snakes, across all trials, there was a fairly uniform distribution concerning whether or not a specific electrode would be on the inside or the outside of an S-shaped curve. For example, snake CH34 never had its electrode number 8 in an outside position. In the aggregate data, however, the distribution of inside and outside positioning was fairly split with a small amount going to the neither, i.e the in-between curves, category. The small amount of in-between curve instances could make it appear that the size of the S-shaped loops must stay relatively constant, otherwise one would expect to see equal amounts in each category. However, the categorization of the positions had a bias towards inside and outside as the amount of body length that constituted the in-between curve category was smaller than for the curve category.

Strike Vectors

There are many mysteries concerning the final destination of the snake strike. Does the snake strike in a straight vector, or can it change the direction of its strike mid-strike? If the strike is a single ballistic movement, at what is it aimed? Does it predict where the stimulus is going and strike there as is the case with tentacled species of snakes that exploit the stereotyped C-Start of fish (Catania (2009); Catania et al. (2010); Catania (2010))? Or does it simply strike where the stimulus is at the start of the strike?

While it has been shown for rattlesnakes that they strike towards the back end of a prey as it is moving laterally to the snake (Clark et al. (2012)), no similar data exists for arboreal snakes. It is known that this species of snake feeds on birds, bats, frogs, or other vertebrates. For flying prey, the challenge of determining a strike vector is considerably more difficult than for terrestrial prey. While it has not been documented that *Corallus hortulanus* strike at flying prey, it has been documented in other boid species, as well as the similar arboreal species of colubrid. These snakes are known to wait in ambush at the mouths of caves where bats fly in and out (Esbérard and Vrcibradic (2007)).

While 3D tracking can show us the course of the snake strike, it cannot show us the intention of the snake. This is further complicated in a 3D environment. As our artificial prey stimulus was intended to evoke the predatory response, but not include contact, the stimulus was kept out of reach of the snake most of the time. Furthermore, the movement of the stimulus was very non-prey-like as it was presented using an IR emitter attached to the end of a stick. This stick was actively controlled by a researcher to evoke a strike, but also prevent contact. Contact was avoided to prevent modification of the path and other

metadata of the strike.

It was difficult to ascertain whether the snake accounted for the trajectory of its prey when it aimed, or even if it aimed for a specific 3D position at the start of the strike at all. If the snake did aim for a specific 3D position for the strike, the variability of the snake's execution further obfuscated the determination of the goal position. As the strike vector of the snake was not necessarily a straight line, as shown in figure 4.2A, three different straight vectors were created from the strike path: the start of the strike, the part of the strike leading up to the point of maximum velocity, and the end of the strike. Each of these lines was fit to 30 timesteps of the strike at their respective position in the strike. These lines were then extended for subsequent timesteps to show where that trajectory would have continued to had it been straight. There was a very large variance in the data, i.e. approximately 400 ms. The mean values for each of the three vectors were approximately 40 ms behind the position of the stimulus at the start of the strike. This showed that the closest point of each of these vectors with the path of the stimulus was 40 ms prior to where the stimulus was at the start of the strike. However, the variance of the data showed that the value could have just as easily been 40 ms after the start of the strike and within 3 standard deviations a lot of time was covered, i.e. approximately 400 ms. What this means is that there doesn't appear to be evidence for the idea that the snake was anticipating where the prey was heading, or at the very least a better metric needed to be devised for measuring the true direction of the strike vector. A study where the path of the stimulus followed a much more uniform and expected path might be able to answer this question in a more satisfactory manner.

4.4.4 Muscular Activation

Determining the start of muscle activity is not a straight-forward task. Raw EMG was processed as before using a Butterworth band-pass filter with low end at 20 Hz and high-end at 850 Hz. Additionally, in order to create an envelope of activity, the EMG data was rectified and low-pass filtered at 40 Hz. Strikes captured were 8 seconds in length, so any pre-strike-start EMG activity that may have been recorded was cropped. A variety of different metrics were tested to determine when the strike had started based on the activity level of the EMG and how far it was from the mean of the baseline activity. It was observed that 1.5 standard deviations above the mean worked well for a large portion of the data, but had quite a few wrong attributions. To mitigate this problem, a sliding window approach of 35 ms was used. Once all timesteps in the window were above the

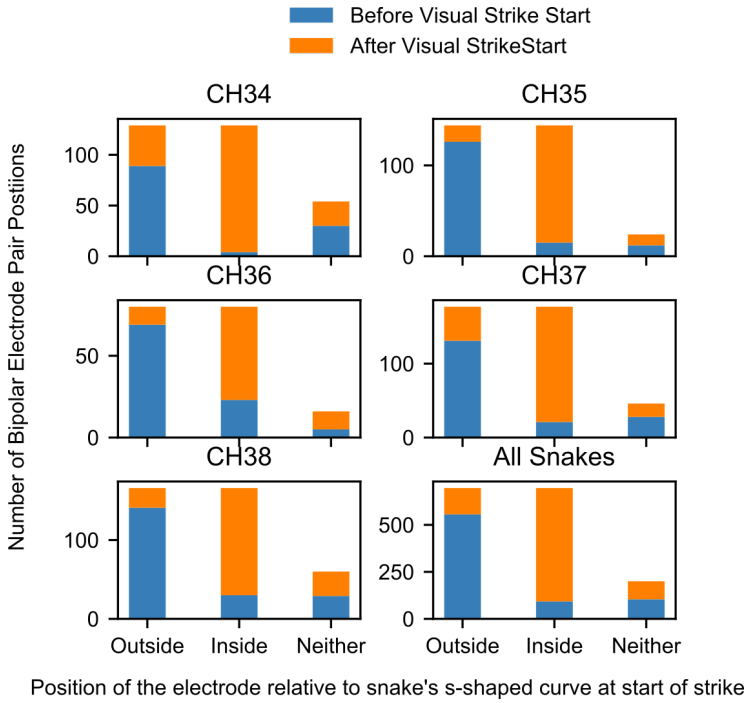

Figure 4.4: Which part of the S-shaped curve has muscle activation first during a striking motion? The start of muscle activation during a strike on the outside of the loop has been previously described by Young (2010). This data shows that while it was often the case that the outside fires first, it was not always the case. The category neither was used when the position of the electrode was between two S-shaped curves.

threshold, it was marked as the start of a strike. This was done as single spikes could trigger the crossing of this threshold when it was clear that the snake was not striking or in the pre-strike phase. To help decrease computational cost associated with the sliding window, and to decrease false spike-start attributions, the sliding window was started 250 ms prior to the point of visual strike start. The results of this method were visually inspected and found to provide superior results.

As shown in Young (2010), the outside of an S-shaped curve fired before the inside of the curve. Figure 4.4 shows the aggregation of all position pairs of bipolar electrodes from all trials for each snake and the distribution of firing. The outside of a curve fired, predominantly, first. Furthermore, the majority of the time this happened before the start of the strike. There were also activations that occurred on the outside of the curve after the start of the strike. This can happen as all of the muscles do not fire at once, but rather in a sequence. The distribution of these firings is better seen in figure 4.5A_1,B_1, where the aggregate statistics of position firing times in relation to the visual start of the strike are

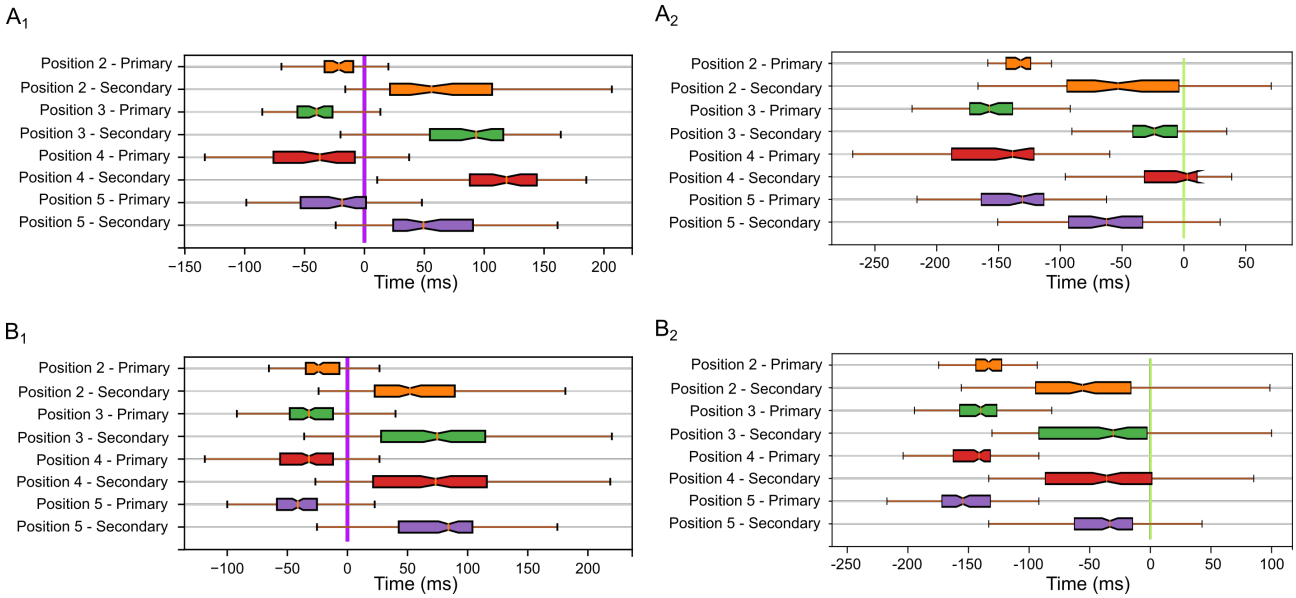

Figure 4.5: Primary and secondary, i.e. fast and slow side, muscle activation statistics in relation to start of strike and point of maximum acceleration. (A) Time of muscle activation, for snakes whose anchor point was at position 5, relative to two events. It consisted of 4 snakes and 59 strikes with a minimum of 11 strikes contributed per snake and a maximum of 23. A_1 shows the start of strike event using a purple vertical line, and A_2 shows the point of maximum velocity event using a lime green line. (B) Same criteria as the data shown in A, except where the anchor point was located posterior to position 5. These data consisted of 5 snakes and 140 strikes with a minimum of 10 strikes contributed per snake and a maximum of 50. B_1 shows the start of strike event using a purple vertical line, and B_2 shows the point of maximum velocity event using a lime green line.

shown.

Visually, the development of a snake strike has been described as starting at the head and continuing caudally through subsequent body coils that lengthen to propel the head of the snake forwards (Young (2010)). With this sort of movement, one might assume that muscle activation also followed the same regime. However, muscle activation during strikes seemed to originate more caudally and move towards the cranium, figure 4.5. Though the data from Young (2010) only focused on the body curve closest to the cranium, similar activity was seen within that curve; the more caudal portion of the curve fired before the more rostral portion for the same muscle.

Point of Maximum Velocity

In Herrel et al. (2011) the maximum velocity for juveniles was at, or near, prey contact. For adults, this value was 15–20 ms before prey contact. While the current pilot data

does not include prey contact, the maximum velocity of the snake occurred prior to full extension. As noted in Herrel et al. (2011), the snake continued to move through the prey target with some force, displacing the target. This could mean that in these data the snake was expecting to contact the stimulus device sooner, or that the majority of strikes were defensive in nature and the snake was merely attempting to scare off the stimulus.

Figure 4.5 shows primary and secondary muscle activations for each position where electrodes were inserted. In this sense, primary refers to the first muscle to show activation in an electrode implantation position, and secondary refers to the muscle activation that follows the primary for that same position. This verbiage has been adopted because the outside of an S-shaped curve was not always the first to fire prior to a strike. The top plots, figure 4.5A_1,A_2 show the muscle activations when the anchor position was at position 5, while B_1 and B_2 show the activations when the anchor position was posterior to position 5. Furthermore, A_1 and B_1 show the activations in relation to the visual start of the strike, i.e. purple vertical line at time 0. A_2 and B_2 show the point of maximum acceleration in relation to the commencement of muscle activity on opposing sides of the snake, i.e. the vertical green line at time 0.

Figure 4.5 shows that in the vast majority of cases the snake was activating the opposing side of its musculature prior to reaching the maximum velocity state. Furthermore, depending on where the anchor position was located, the duration of primary firing for position 5 changed as well as the secondary firing. In A_1 and A_2 the primary activation for position 4 and position 5 occurred at approximately the same time, however, the secondary activation of position 5 occurred much sooner than the activation of position 4. When position 5 was moved anterior to the anchor position, the firing of the primary and secondary muscle activations for position 4 and 5 were comparable. This lends credit to the idea that the posterior portions of the body near the anchor were providing a stabilizing function. The shorter the separation of the primary and secondary activation start, the less that position increased in distance and the more the position functioned as a stabilizer. A similar activity in position 2, i.e. 6 cm behind the head of the snake was seen. This position was usually the last to fire its primary activation, and with short separation, it then usually fired its secondary activation. This behavior was consistent across both figures 4.5A and B. This makes sense as the amount of distance that the last small anterior curve of the snake adds to distance was minimal, and the secondary activation occurred slightly before maximum acceleration was achieved. This supports the idea that this position is also stabilizing the strike vector, and perhaps adding extra rigidity to the neck of the snake

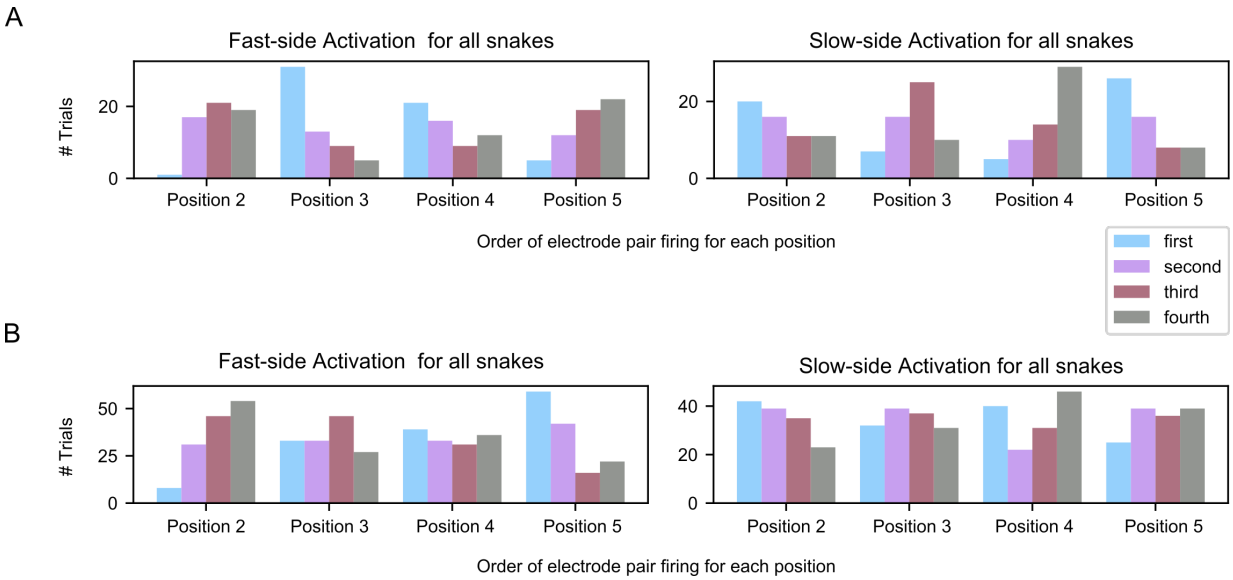

Figure 4.6: The order in which the electrodes in a specific position fire in relation to other positions. First means that amongst the four positions on the snake where electrodes were implanted on lateral sides of the spinal column, it was the first to have EMG activity exceeding a threshold of 1.5 standard deviations above the mean of resting activity. (**A**) Fast-side (primary) and slow-side (secondary) positional firing order for strikes where position 5 was anchored at the tree branch. These data comprise 4 snakes and 59 strikes with a minimum of 11 strikes contributed per snake and a maximum of 23. (**B**) Fast-side (primary) and slow-side (secondary) positional firing order for strikes where position 5 was located rostral to the anchor position. These data consist of 5 snakes and 140 strikes with a minimum of 10 strikes contributed per snake and a maximum of 50.

immediately caudal to the cranium shortly before prey impact.

Activation Sequence

In figure 4.6, the left hand column shows whichever of the two bipolar electrodes that composed a position fired first in relation to the visual strike start (fast-side activation). The right column is thus the channel that fired second (slow-side activation). For each of the four positions (with two bipolar electrodes per position, i.e. an electrode on the left side of the spinal column and an electrode on the right side of the spinal column) the distribution for how often that position in relation to all the other positions fired first, second, third, or fourth is shown. When viewing all of the aggregate data of the snake muscle firing, it was hard to discern a pattern. However, when the snake strike trials were separated by where the snake anchored itself to the branch, a pattern emerged. In figure 4.6 A, position 5 was the anchor point and in B position 5 was anterior to the anchor point.

While variation existed across the snakes, looking at the aggregate of all the snakes that had their anchor position at position 5, position 5 was predominantly one of the last to be activated (Figure 4.6A_1). When the anchor position was moved posterior to position 5, the firing behavior at position 5 became similar to that at positions 3 and 4, i.e. initial/secondary activation. The standing hypothesis of a wave-like activation from caudal to rostral cannot be confirmed, as it can be seen that the positions between the anchor and the head do not always activate in a sequential fashion. This is shown in the distribution of activation positions in A_1 and B_1. For example, if the positions were activated in a wave-like fashion, one would expect the firing order to correlate more strongly with the position. This means that the motor pattern of activation was not fixed, but was dependent on the body configuration of the snake. I hypothesize that the activation order was related to the distance each curve would add to the strike, with larger curves being activated before smaller ones. As the spacing between markers was too large to ensure that a marker was always on the apex of an S-shaped curve, this hypothesis should be addressed in future work. While it was often the case that the S-shaped loops of the snake decreased in size caudally to rostrally, it was not always the case. The data from Young (2010) suggested that the muscle activity in the anterior portion of a single curve lasted longer than the caudal portion of that curve. While the data in this study did not have multiple electrodes in the same curve, it does not support the idea that the anterior portion of the snake was active for a longer period than the caudal. In fact, the opposite was seen.

Another data point that supported the idea that stabilization occurred in areas of the snake posterior to the anchor point can be seen looking at position 5 in Figures 4.6A_1 and A_2. Although position 5 was quite often the last to fire in the fast activation (usually outside) of the curve, here it was often the first to fire in its corresponding slow side. This behavior was not seen when position 5 was rostral to the anchor point, as shown in Figures B_1 and B_2. Instead, like position 3 and 4, the firing happened in a quasi-inverse order. However, one must be careful drawing conclusions about the ordering of the muscle activation for positions 2, 3, and 4, as the variance of times quite often overlap.

Frequency and Power

Chapter 3.4.3 examined the frequency spectrum of the snakes' muscles under perturbatory movement. Figure 4.7 shows the frequencies and power spectral density of different stages of the strike, as described by figure I-3 in the introduction. Prior to pre-strike, pre-strike, strike, and post-strike phases are shown in A, B, C, and D, respectively. Similar to what

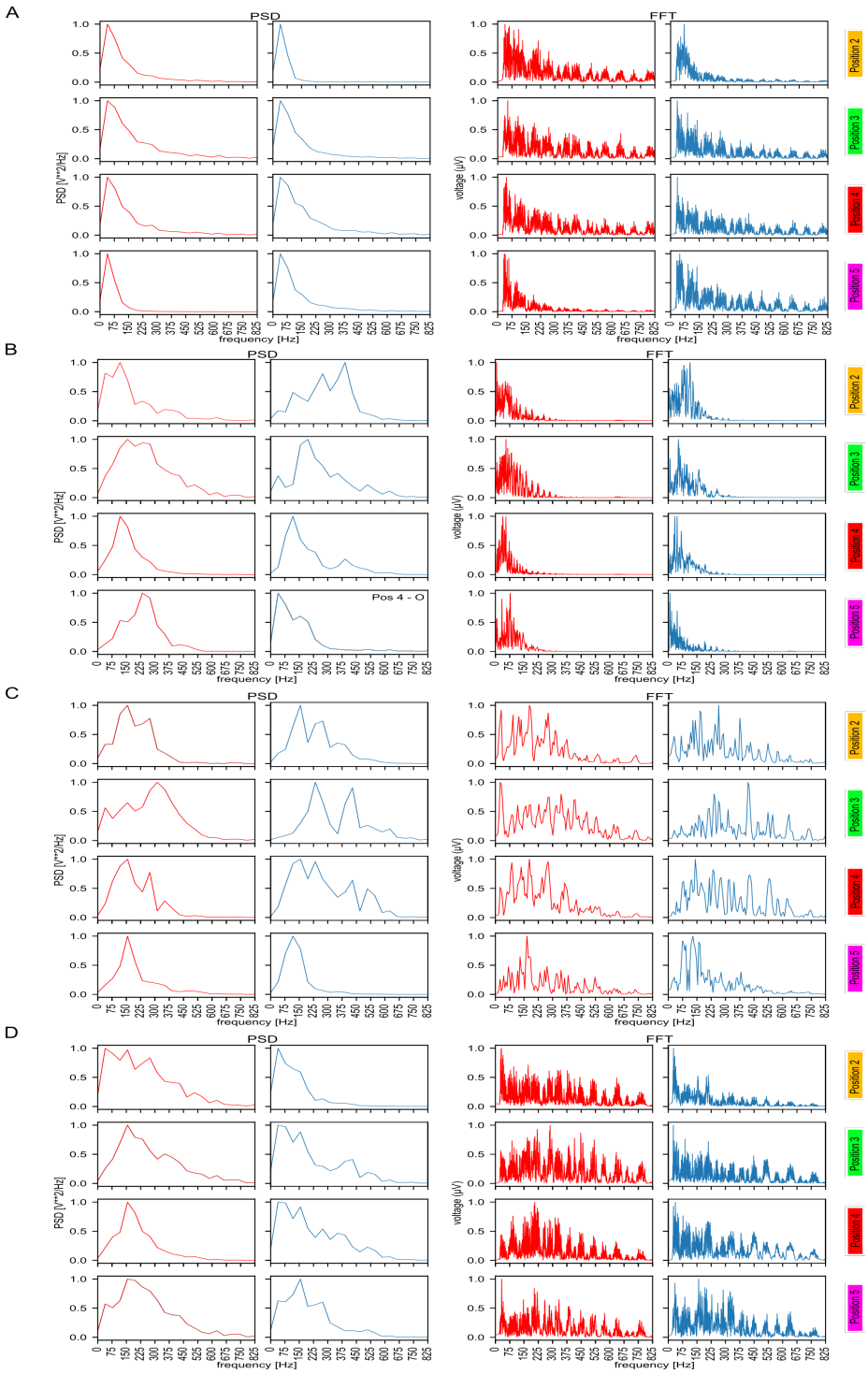

Figure 4.7: Normalized power spectral density of all non-excluded strike captures along with the matching frequency spectrum of the signal. The red plot indicates the position of the electrode was on the inside of a curve; blue represents the outside. The signal was processed with a band-pass filter between 20 and 850 Hz, and clipped to include only the muscle activation during the respective segment of the strike. The segments were defined by phases from figure I-3 and are as follows: (A) Prior to pre-strike, (B) pre-strike, (C) strike, and (D) post-strike.

was seen in the turntable data, figure 4.7A shows a wide range of signals, but the majority of the power of the signal was concentrated in the lower frequencies. In figure 4.7B, there was a shift of the power of the frequencies to higher frequencies.

The largest observed shift was at position 2 near the head of the snake. This makes sense as typically the pre-strike activity of the snake involved an adjustment of the head towards the prey stimulus. In figure 4.7C, a further shift towards the higher frequencies was seen for almost all positions, except for position 5. There was a shift for position 5, but it was not as large in frequency difference. This was different to the turntable data shown in chapter 3.4.3. The turntable data had an increase in the frequencies for position 4 and 5 and not much of an increase for positions 2 and 3. This was easily explained by the different types of movements required for the two activities and how they relate to body movement of the snake. The turntable motion consisted of more body movement in positions 4 and 5, while a striking movement had the vast majority of its body movement accomplished by positions rostral to position 5, and sometimes position 4. For the final set of plots, i.e. post-strike, the power was shifting, but in this case in the direction of lower frequencies. This was to be expected as the retracting of the snake back into its S-shaped curves required, presumably, a lot of energy, as well as time.

4.4.5 Elastic Energy Storing Hypothesis

The puff adders used by Young (2010) were approximately the same length as the amazon tree boas used in our pilot study, but the mass of the two was very different. The body mass of some snakes used by Young were as heavy as 5 kg, while the weight of the amazon tree boa was, on average, around 120 g. As seen in table 4.1, the fastest measured velocity of the *Corallus hortulanus* during strike is 2.3136 m/s.

The strikes of the amazon tree boa, were considerably slower than the puff adder. Therefore, the need for a high-power output muscle system does not seem to be overtly profound in the amazon tree boa. But, as the work of Young (2010) was the only study looking at muscle coordination during the striking of any species of snake, one should start with this mechanism as the baseline to see if different species of snake conserve this mechanism. Figure 4.8 shows a representative EMG trace of 8 electrodes. Although the exact position of the placement of the electrodes from Young (2010) isn't known, the closest comparable set of two electrodes are Channel 1 and 2, i.e. position 2. This position was approximately 6 cm caudal to the cranium of the snake and was often the first loop of the snake. The differently colored vertical lines show the start of different phases of the snake

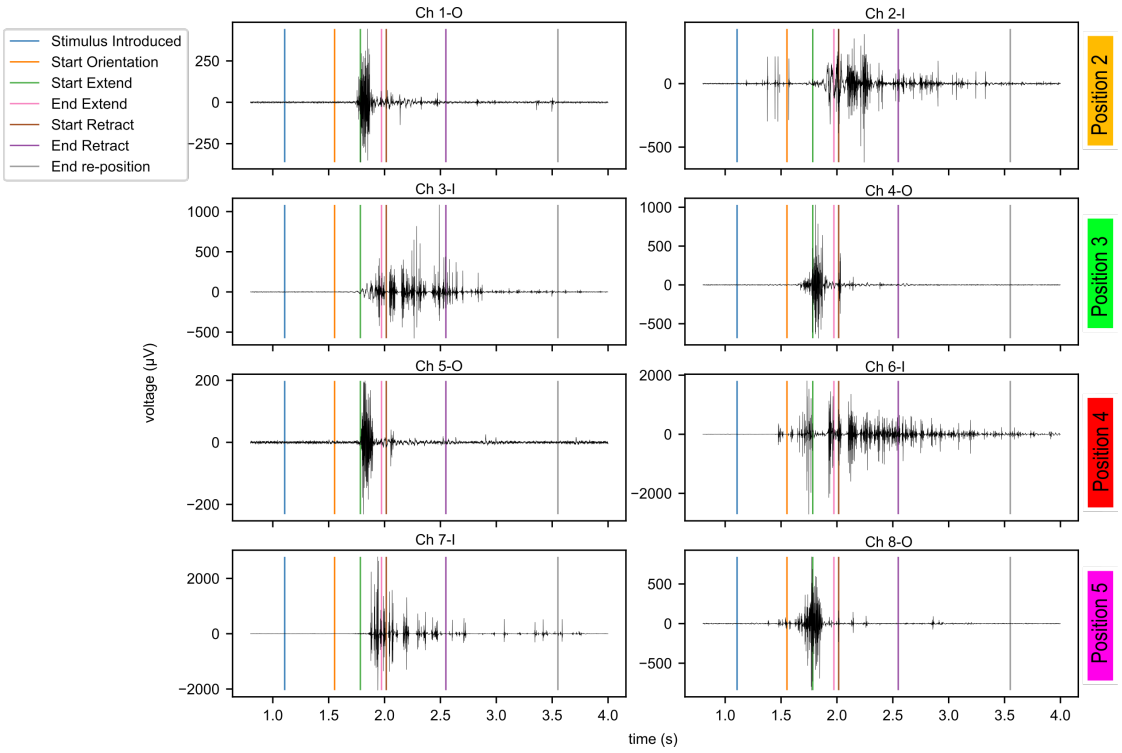

Figure 4.8: 8-Channel EMG of an amazon tree boa (*Corallus hortulanus*) strike. This strike is representative of the strikes collected during the pilot study. An I or an O next to the channel number specifies if that electrode was on the inside or outside of a curve.

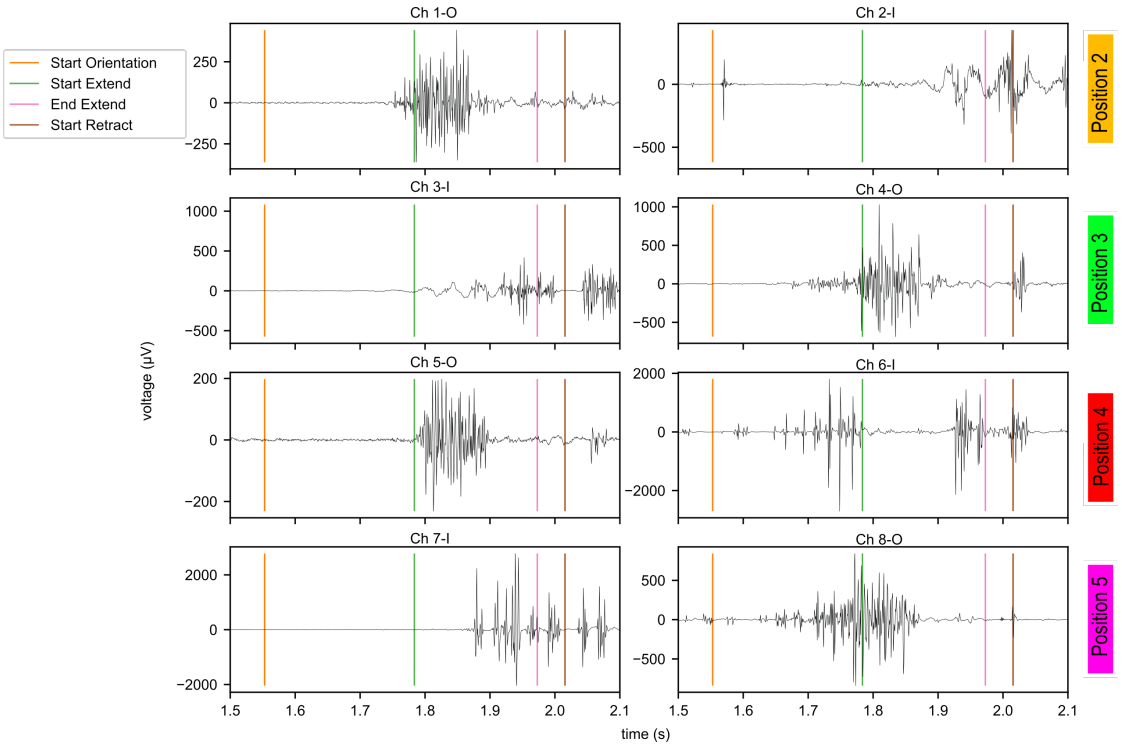

Figure 4.9: The same data as shown in figure 4.8 but with finer timescale granularity surrounding the visual start of the strike. An I or an O next to the channel number specifies if that electrode was on the inside or outside of a curve.

strike, described by figure I-3. In figure 4.9, the same data as figure 4.8 is shown, except the data is zoomed in on the timesteps surrounding the visual start of the strike (green line). In this figure it is clear that there was no common 'pre-loading' activity visible in the EMGs of each channel. Channel 6 appeared to show data similar to that shown in Young (2010), but this electrode was on the inside of the S-shaped curve, not the outside, so this was not the activity that one would expect. Comparable activity in the onset of muscle activation was seen. As shown in section 4.4.4, the outside of a curve fired, for the majority of time, before the inside of the curve. As two electrodes were not placed into the same muscle on the same side of the snake close enough such that both were on the same curve of the snake, the results of Young (2010) concerning the order and duration of muscle activation in a single curve could not be verified.

Since Young (2010) reported that the activity from the *Musculus longissimus dorsi* (LD) and the *Musculus semispinalis* (SSP) were similar in appearance, duration, and relation to the onset of the strike, this current work assumed that the muscle activity using the method of chapter 2 did not affect the interpretation of the EMG data. That is, even in the case that the sub-dermal method of EMG collection used in this study was collecting activity from both the LD and the SSP, it shouldn't have affected the results. The EMG results implied that in some species of snakes there wasn't a need for a high-power muscle output strategy. The simple activation of the outside of S-shaped curves lengthened the anterior portion of the snake towards its target. The interior portion of the curve typically fired later to prevent over extension of the curve, and thus a decrease in strike distance. For muscles near or posterior to the point of anchor, these muscles appeared to anchor the snake to the branch and did not follow the activation schedule seen in more anterior muscles. In the only other study of arboreal strike speeds (Herrel et al. (2011)), the strike speeds of the snakes, in the upper range of capability, were similar to the speeds of the puff adder. This suggests that this energy storing mechanism might be conserved in the context of this arboreal viper. However, from a specialization and evolutionary perspective, this is hard to support as one would expect that arboreal species would have more in common than arboreal and terrestrial given their different preferred environments. This then, instead, suggests that there are multiple strike muscular motor patterns. More data from different species are needed to better understand the muscular coordination of the snake during striking behavior.

4.5 Conclusion

This dataset was the largest set of boid strikes ever recorded as well as the first dataset of any non-viperid, either arboreal or terrestrial, snake strikes that included motion capture and EMG data. It was also the first data showing muscle coordination during a strike that included electrodes along the length of the extending portion of the snake. The gate-model of strike that was presented visually by the amazon tree boa was well described by the muscular activations of the outside and inside of the S-shaped curves of the snake. The data were not able to explicitly confirm that the EMG implantation method of chapter 2 did not affect the performance indicators of the strike, and a better metric for a change in behavior is needed. However, personal observations from the researchers indicate that there was no observable change in behavior, and thus supported that the method did not hinder natural motion. The data suggested that the amazon tree boa did not have the same strike requirements as viperid species given that their speeds were considerably slower. It was shown that the strike vector of this snake was not always a straight line, but could have skew depending on how the snake was positioned. However, the body configuration in which the snake placed itself did not appear to be consistent across individuals. This means that the strike motor pattern was not fixed, but dependent on body configuration and anchor point of the cantilevering snake. Analogous to the stabilizing behavior described in chapter 3, it was shown that stabilizing behavior occurred in the caudally located electrode positions near the anchor point of the snake. While the activation of the outside of the S-shaped curve before the inside, as described by Young (2010), was verified along with these data, the idea that the anterior portion of the snake was active longer than the caudal portion was not. Furthermore, while an elastic mechanism for high-power muscular output may be needed in the puff adder, these data showed no support for the assumption that this mechanism exists in the amazon tree boa.

General Discussion and Future Research Directions

Recording images is a vital part of data collection; when the data collection concerns a motion that is faster than the blink of a human eye, even more so. This recording using a high-speed camera can often be done with free or opensource software, but if one would like to get three dimensional (3D) points from the video when they are using more than one camera, there are limited options. Quite often one must cobble two or more of these free or opensource software programs together to encompass the experimental pipeline of data collection, saving, processing, and viewing. If 3D positions of corresponding points from the images of multiple cameras are needed, then triangulation must be done. This requires calibration of the cameras themselves and finding the relative position of the cameras to each other in the presence of noise. Again, opensource libraries exist to help with this task, but they often require an understanding of computer vision and high-performance programming; skills that are not the focus of every researcher. Commercial options exist to perform this task, but they are expensive. Furthermore, only a few companies offer cameras with speeds higher than 500 Hz and the additional increase in camera speed can raise the cost by tens of thousands of dollars.

SnakeStrike, developed as part of this thesis and presented in chapter 1, is an opensource software framework that solves these problems for researchers from any field who need to capture high-speed video from multiple cameras and perform triangulation on markers. While it is similar to other software such as DLTdv (Hedrick (2008)), it doesn't require any additional software programs as it fully encompasses the data collection pipeline. Furthermore, as it is optimized for the large amounts of data that are produced by multiple high-speed cameras used to track markers, it can process the data faster than DLTdv, i.e. $\sim$12 times faster. When processing large sets of data, this can mean the difference between a week of data processing and 3 months. As SnakeStrike was developed with diversity and cost in mind, it can be configured to use any commercially available cameras that conform to the GenICam programming standard, as long as a suitable application programming interface (API) exists and dynamic library following the SnakeStrike interface is written. The GenICam standard ensures that all compliant cameras function in a similar manner,

and the SnakeStrike dynamic library interface allows customizing the cameras that are used. By default, all Basler cameras are supported in the base functionality.

While SnakeStrike is free, the cameras, computer, and other accessories needed to set up a successful multi-camera motion capture system are not. Fortunately, the major source of cost for the system is a high-powered computer that does not need to be dedicated to the task of image collection and can be used for any other task, as is not often the case with commercial products and their dedicated hardware. This computer cost is also significantly smaller than the cost of a commercial system. Some drawbacks to the system are that, unlike commercial systems, it stores raw image data and not just the triangulated points which requires a large amount of storage space on the computer. On the other hand, having this raw data allows reanalysis or reprocessing of data at any time. This is important because tracking points across multiple camera views is an active area of research and reprocessing the data using newer algorithms may provide new insights. The fixed error of SnakeStrike is low compared to other sources of error that can occur in an experimental setup. SnakeStrike makes the collection of high-speed video with 3D tracking feasible to researchers who work with non-standard and especially fast-moving animals. As described in section 1.3.2 of chapter 1, it has already permitted the collection of previously unattainable data in coordination with a 3D X-ray system, was the first data to show a strike profile for a boid snake, and was a cornerstone of the methods needed to collect the data during the pilot study discussed in the subsequent chapters.

The other method that was essential for collecting the data of the pilot study was the chronic multi-electrode electromyography (EMG) technique developed as part of this thesis and described in chapter 2. This technique was essential to solving the conundrum of how to keep electrodes safely and securely implanted in a snake while the snake had free-range to move and strike. This technique uses a unique method of sub-dermal implantation to position bipolar electrodes above superficial muscles of the snakes axial musculature. This allows the collection of EMG data in a method analogous to surface EMG, only underneath the skin of the snake.

To prevent the removal of wires and keep the open ends of the bipolar electrode in position, the two cables are fixed to each other using cyanoacrylate and sodium bicarbonate. The sodium bicarbonate allows for instant drying and fixing of the glue while also facilitating the formation of structure. This structure is formed into a small spherical shape that, when sutured in position, prevents the cables from being removed. This implantation method produces EMG with a strong signal to noise ratio and is suitable for one day of

recording when using an arboreal snake like the amazon tree boa (*Corallus hortulanus*). For multiple days with this snake, a snake 'sleeping bag' is needed to prevent harm to the snake. The 'sleeping bag' covers the implantation sites on the animal and prevents the animal from removing the covering, and thus removing electrodes, but still allows some restricted movement. This implantation method, in coordination with a snake 'sleeping bag' of unique design, was pivotal in the collection of the first chronic EMG movement data of any snake species.

Combining the opensource motion capture system of chapter 1 with the method for chronic multi-electrode EMG enabled a pilot study where high-speed video of snake movement in two different forms could be collected along with valuable muscle coordination information via EMG. In chapter 3, these data were discussed in the context of compensatory movement in response to a perturbing stimulus. In this case, the perturbing stimulus was simulating a non-stationary environment. While not a typical situation encountered in the wild by terrestrial species of snake, this is a common environment for arboreal species, as these snakes anchor themselves to branches in trees. These branches are constantly subject to wind forces that move them around, but the snake is able to counteract these motions. When the perturbation was provided by a programmable turntable, the ability to record data of stereotypical response behavior became possible. In chapter 3, the compensatory behavior of the amazon tree boa in this situation was first described in coordination with the head fixing behavior mentioned in chapter 2 (section 2.3). This compensatory behavior was found to consist of two main strategies: 1) modifying the angle of S-shaped loops to keep the head position stable and 2) changing the plane in which the snake configures its body to achieve more movement. It was shown that the muscle activity of the snake during this perturbation differed depending on how close that muscle was to the anchor point of the snake to its branch. This difference was hypothesized to be the result of stabilizing activity occurring near the anchor point, which was additionally addressed in the pilot data focusing on snake strikes.

The snake strike video data that were collected were the largest set ever recorded on boid snake strikes, and the only that combined motion capture with EMG. Only one other study previously combined EMG with video information (Young (2010)). The data from this other study was composed of strikes from puff adders (*Bitis arietans*) and gave the first muscle activation description for the strike of any snake. This muscle activation included the following descriptions: muscle activation starts on the outside of a curve and is followed by activation on the inside, the rostral portion of an S-shaped curve is active longer than

the caudal portion, and muscle activity exists in the caudal portion of a curve before the rostral portion. Furthermore, the EMG activity for the strike showed that there was activity prior to the launch of the strike, no activity during extension, and then activity shortly after contact. Until now this was the only muscle activation data for a snake strike.

The data shown here show that, when viewing muscle coordination over a larger portion of the anterior part of the snake, activity most often started on the outside of an S-shaped curve and was followed by activity on the corresponding inside, but not always. The activity in the electrode positions located more posteriorly seemed to have longer activation times, i.e. the time between the first side to activate and when its opposing side activates. Additionally, the strike seemed to start more caudally, but at some point near the anchor point of the snake to the branch, this typical strike activity ceased and an activity described as stabilizing activity starts. Furthermore, this stabilizing activity sometimes appeared in the neck of the snake which could mean that the neck was stiffening prior to impact with the prey. The muscle coordination EMG data also did not replicate the description of that for the puff adder. Activity was both seen prior to and during the launch of the strike. This suggested that there was not a single snake strike muscular activation pattern, and that the pattern of the arboreal amazon tree boa was quite different compared to the terrestrial puff adder.

The methods and techniques described in part I are a solid platform for future research in this area. Solving the problems with the locomotion data collected in this work would allow the collection of locomotion data along with strike data for the same body positions. This would help to shed light on the hypothesis that the gate-model of strike uses similar neuromuscular activations as the concertina movements of the snake. Placing more electrodes in the caudal portion of the snake and systematically moving the anchor point of the snake should validate the stablization hypothesis, first described here. Other questions such as how was the snake able to keep EMG activations low while in a cantilevered positions, did the snake take gravity into account when striking, and where exactly was the snake aiming could all be better understood using these methods and techniques.

Research into the mechanisms of snake striking behavior has been previously hindered by a lack of access to technology as well as methods to support the safe capture of muscular activation information during this movement. This work presents the combination of tools and methods required to collect these interesting data. Furthermore, this combination was used to collect novel new datasets that revealed previously non-described behavior in a non-static environment as well as substantially furthered the understanding of snake strike

behavior and its mechanics.

The pilot study described in chapters 3 and 4 provides a valuable resource for further study. The method for chronic multi-electrode EMG, richness of the video and tracking data, as well as the diversity of snake movements is unlike any other snake movement dataset available. This was the first study where different styles of movement can be directly compared across days, but also to each other because the EMG and video collection methods remained consistent within each snake, and very similar across snakes. The muscle activation required to compensate for a turntable movement can now be compared to strike movements as the EMG covered the same position.

Appendices

A Supplemental figures from Ch. 1

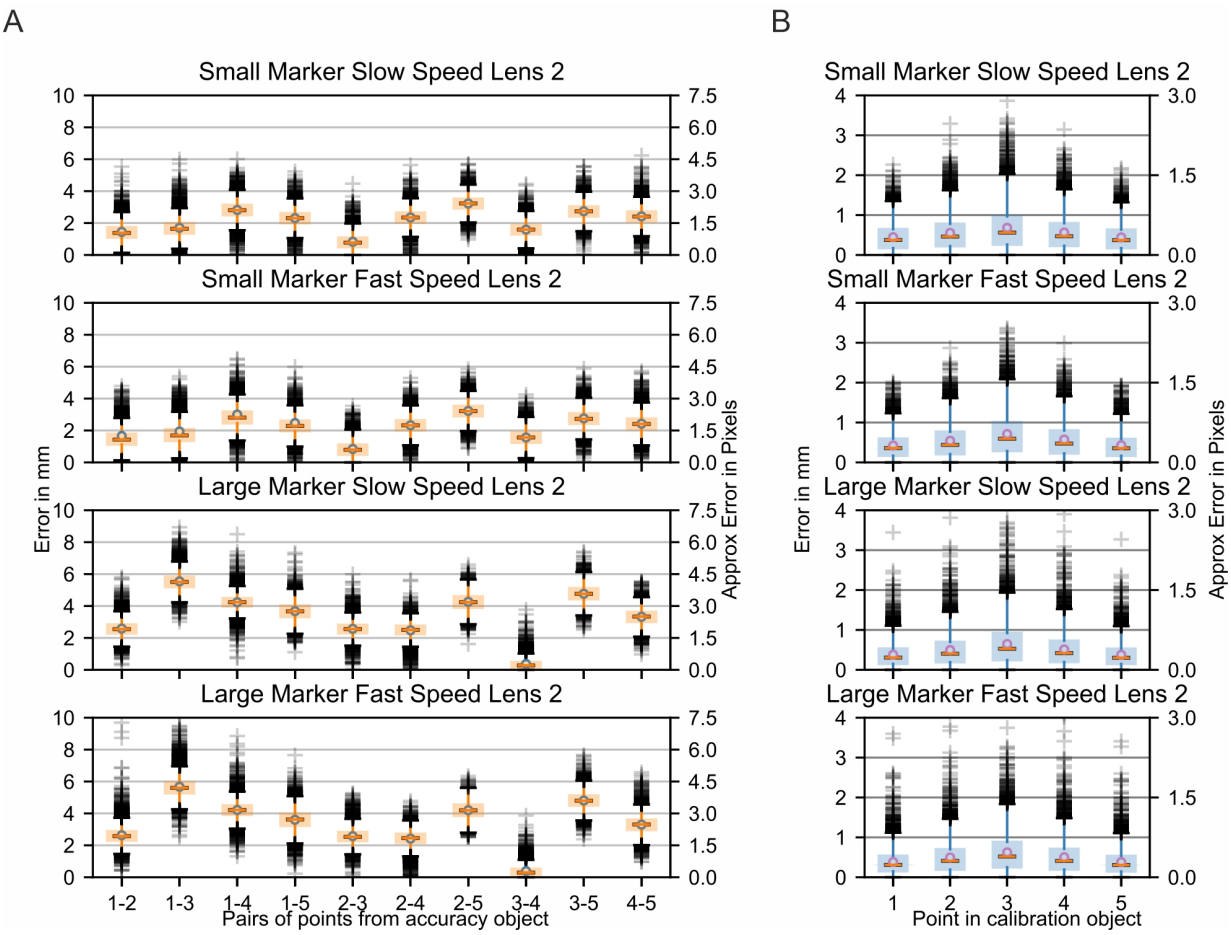

Figure A-1: Study 1: Error in marker location while the fiberboard with attached markers was moved through space by the Franka Emika Panda robotic arm. Parameters: two marker sizes and two relative speeds of movement of the markers. Data is shown for one camera lens (Ricoh FL-CC0614A-2M) (**A**) Each boxplot refers to an interpoint distance error between two points of known distance (Table 1) in the calibration object; the numbers on the x-axis represent the points and are separated by a hyphen. (**B**) Marker distance from the best-fitting plane for all markers. Image source: Jensen et al. (2020a).

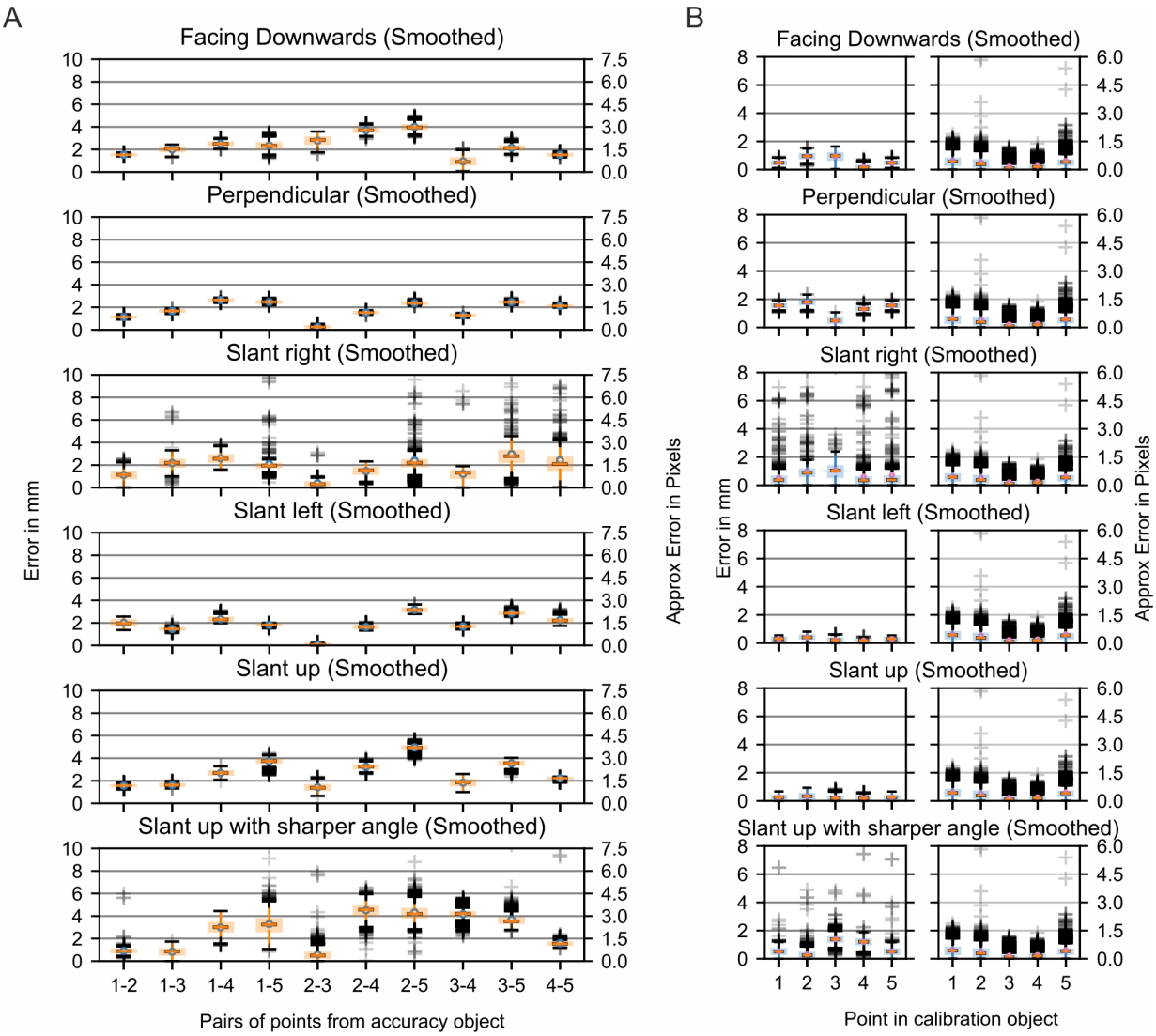

Figure A-2: Same data as shown in figure 1.5A,B, but post-processed with a Kalman filter to illustrate the improvement by filtering or smoothing of the triangulated data for the analysis. (**A**) Each boxplot refers to an interpoint distance error between two points of known distance in the calibration object (Table 1.1). The numbers on the x-axis represent the points and are separated by a hyphen. (**B**) Distance of markers from best-fitting plane for all markers (left). Movement of triangulated points in 3D from their mean while markers were stationary (right). Image source: Jensen et al. (2020a).

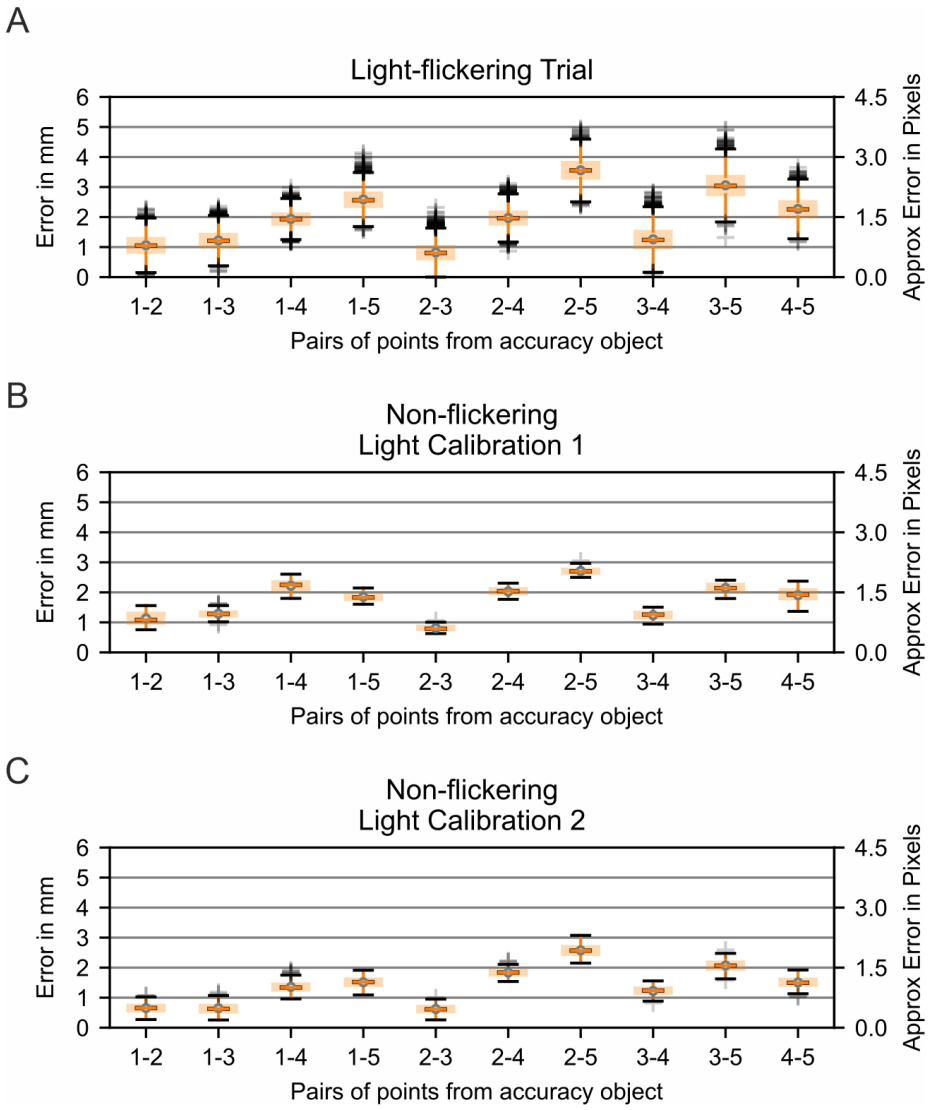

Figure A-3: Study 1: Effect of light-flickering on inter-marker distance error variance. The markers were stationary and perpendicular to the cameras' position. Each boxplot refers to an interpoint distance error between two points of known distance in the calibration object (Table 1.1). The numbers on the x-axis represent the points and are separated by a hyphen. (**A**) Example of a trial where flickering was present in the light source. (**B**) Example of a trial in a different setting where light-flickering was absent. (**C**) Example of a trial in the same setup as in B, but with a different camera calibration. Image source: Jensen et al. (2020a).

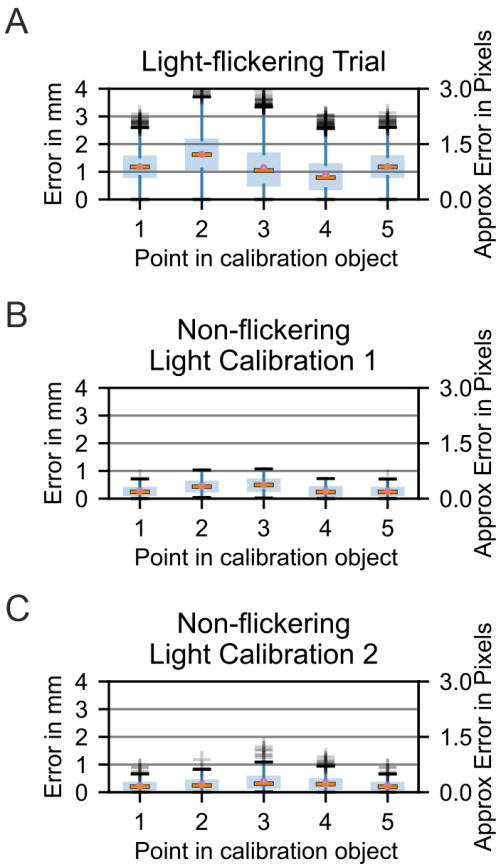

Figure A-4: Study 1: Same data as in figure A-3, but with the error displayed as the distance of the marker from the best-fitting plane for all of markers. (**A**) Example of a trial where flickering was present in the light source. (**B**) Example of a trial in a different setup where light-flickering was absent. (**C**) Example of a trial in the same setup as in B, but with a different camera calibration. Image source: Jensen et al. (2020a).

Bibliography

Agarwal, G. C. and Gottlieb, G. L. (1975). An analysis of the electromyogram by fourier, simulation and experimental techniques. *IEEE Transactions on Biomedical Engineering*, BME-22(3):225–229.

Altshuler, D. L., Dickson, W. B., Vance, J. T., Roberts, S. P., and Dickinson, M. H. (2005). Short-amplitude high-frequency wing strokes determine the aerodynamics of honeybee flight. *Proceedings of the National Academy of Sciences*, 102(50):18213–18218.

Bay, H., Ess, A., Tuytelaars, T., and Van Gool, L. (2008). Speeded-up robust features (surf). *Comput. Vis. Image Underst.*, 110(3):346–359.

Bayraktaroglu, Z. (2009). Snake-like locomotion: Experimentations with a biologically inspired wheel-less snake robot. *Mechanism and Machine Theory*, 44(3):591 – 602. Special Issue on Bio-Inspired Mechanism Engineering.

Berzuini, C., Maranzana-Figini, M., and Bernardinelli, L. (1982). Effective use of emg parameters in the assessment of neuromuscular diseases. *International Journal of Bio-Medical Computing*, 13(6):481 – 499.

Betke, M. and Wu, Z. (2017). *Data Association for Multi-Object Visual Tracking*. Morgan and Claypool, 1st edition.

Boeddeker, N., Dittmar, L., Stürzl, W., and Egelhaaf, M. (2010). The fine structure of honeybee head and body yaw movements in a homing task. *Proceedings of the Royal Society B: Biological Sciences*, 277(1689):1899–1906.

Bourgeois, F. and Lassalle, J.-C. (1971). An extension of the munkres algorithm for the assignment problem to rectangular matrices. *Commun. ACM*, 14(12):802–804.

Bradski, G. (2000). The OpenCV Library. *Dr. Dobb's Journal of Software Tools*.

Cao, Z., Hidalgo, G., Simon, T., Wei, S., and Sheikh, Y. (2018). Openpose: Realtime multi-person 2d pose estimation using part affinity fields. *CoRR*, abs/1812.08008.

Catania, K. C. (2009). Tentacled snakes turn c-starts to their advantage and predict future prey behavior. *Proceedings of the National Academy of Sciences*, 106(27):11183–11187.

Catania, K. C. (2010). Born knowing: Tentacled snakes innately predict future prey behavior. *PLOS ONE*, 5:1–10.

Catania, K. C., Leitch, D. B., and Gauthier, D. (2010). Function of the appendages in tentacled snakes (erpeton tentaculatus). *Journal of Experimental Biology*, 213(3):359–367.

Christensen, C. B., Christensen-Dalsgaard, J., Brandt, C., and Madsen, P. T. (2012). Hearing with an atympanic ear: good vibration and poor sound-pressure detection in the royal python, python regius. *Journal of Experimental Biology*, 215(2):331–342.

Clark, R. W., Tangco, S., and Barbour, M. A. (2012). Field video recordings reveal factors influencing predatory strike success of free-ranging rattlesnakes (crotalus spp.). *Animal Behaviour*, 84(1):183 – 190.

Crespi, A. and Ijspeert, A. J. (2008). Online optimization of swimming and crawling in an amphibious snake robot. *IEEE Transactions on Robotics*, 24(1):75–87.

Cundall, D. (1983). Activity of head muscles during feeding by snakes: A comparative study. *American Zoologist*, 23(2):383–396.

Cundall, D. and Deufel, A. (1999). Striking patterns in booid snakes. *Copeia*, 1999(4):868–883.

Cundall, D. and Gans, C. (1979). Feeding in water snakes: An electromyographic study. *Journal of Experimental Zoology*, 209(2):189–207.

Cundall, D. and Greene, H. W. (2000). Feeding in snakes. In Schwenk, K., editor, *Feeding: Form, Function and Evolution in Tetrapod Vertebrates*, pages 293–333. Academic Press.

Dahmen, H.-j., Zeil, J., and Longuet-Higgins, H. C. (1984). Recording and reconstructing three-dimensional trajectories: a versatile method for the field biologist. *Proceedings of the Royal Society of London. Series B. Biological Sciences*, 222(1226):107–113.

de Cock Buning, T. (2015). Thermal Sensitivity as a Specialization for Prey Capture and Feeding in Snakes. *American Zoologist*, 23(2):363–375.

Deban, S. M., O'Reilly, J. C., Dicke, U., and van Leeuwen, J. L. (2007). Extremely high-power tongue projection in plethodontid salamanders. *Journal of Experimental Biology*, 210(4):655–667.

Esbérard, C. E. L. and Vrcibradic, D. (2007). Snakes preying on bats: new records from Brazil and a review of recorded cases in the Neotropical Region. *Revista Brasileira de Zoologia*, 24:848 – 853.

Frazzetta, T. H. (1966). Studies on the morphology and function of the skull in the boidae (serpentes). part ii. morphology and function of the jaw apparatus in python sebae and python molurus. *Journal of Morphology*, 118(2):217–295.

Fry, S., Bichsel, M., Müller, P., and Robert, D. (2000). Tracking of flying insects using pan-tilt cameras. *Journal of Neuroscience Methods*, 101(1):59 – 67.

Gans, C. (1986). Locomotion of limbless vertebrates: Pattern and evolution. *Herpetologica*, 42(1):33–46.

Gart, S. W., Mitchel, T. W., and Li, C. (2019). Snakes partition their body to traverse large steps stably. *Journal of Experimental Biology*, 222(8).

Geurten, B. R. H., Kern, R., Braun, E., and Egelhaaf, M. (2010). A syntax of hoverfly flight prototypes. *Journal of Experimental Biology*, 213(14):2461–2475.

Goris, R. C. (2011). Infrared organs of snakes: An integral part of vision. *Journal of Herpetology*, 45(1):2–14.

Gray, J. (1946). The mechanism of locomotion in snakes. *Journal of Experimental Biology*, 23(2):101–120.

Guennebaud, G., Jacob, B., et al. (2010). Eigen v3. http://eigen.tuxfamily.org.

Hartley, R. and Kahl, F. (2007). Optimal algorithms in multiview geometry. In *Proceedings of the 8th Asian Conference on Computer Vision - Volume Part I*, ACCV'07, page 13–34, Berlin, Heidelberg. Springer-Verlag.

Hartley, R. and Zisserman, A. (2003). *Multiple View Geometry in Computer Vision*. Cambridge University Press, USA, 2 edition.

Hartley, R. I. and Sturm, P. (1997). Triangulation. *Computer Vision and Image Understanding*, 68(2):146 – 157.

Hedrick, T. L. (2008). Software techniques for two- and three-dimensional kinematic measurements of biological and biomimetic systems. *Bioinspiration & Biomimetics*, 3(3):034001.

Herrel, A., Huyghe, K., Oković, P., Lisičić, D., and Tadić, Z. (2011). Fast and furious: effects of body size on strike performance in an arboreal viper trimeresurus (cryptelytrops) albolabris. *Journal of Experimental Zoology Part A: Ecological Genetics and Physiology*, 315A(1):22–29.

Hu, D. L., Nirody, J., Scott, T., and Shelley, M. J. (2009). The mechanics of slithering locomotion. *Proceedings of the National Academy of Sciences*, 106(25):10081–10085.

Inbar, G. F. and Noujaim, A. E. (1984). On surface emg spectral characterization and its application to diagnostic classification. *IEEE Transactions on Biomedical Engineering*, BME-31(9):597–604.

Insafutdinov, E., Andriluka, M., Pishchulin, L., Tang, S., Levinkov, E., Andres, B., and Schiele, B. (2016a). Articulated multi-person tracking in the wild. *CoRR*, abs/1612.01465.

Insafutdinov, E., Pishchulin, L., Andres, B., Andriluka, M., and Schiele, B. (2016b). Deepercut: A deeper, stronger, and faster multi-person pose estimation model. *CoRR*, abs/1605.03170.

Jayne, B. C. (1986). Kinematics of terrestrial snake locomotion. *Copeia*, 1986(4):915–927.

Jayne, B. C. (1988). Muscular mechanisms of snake locomotion: an electromyographic study of the sidewinding and concertina modes of crotalus cerastes, nerodia fasciata and elaphe obsoleta. *Journal of Experimental Biology*, 140(1):1–33.

Jayne, B. C. and Riley, M. A. (2007). Scaling of the axial morphology and gap-bridging ability of the brown tree snake, boiga irregularis. *Journal of Experimental Biology*, 210(7):1148–1160.

Jena, G., Berkhoudtl, H., Kardong, K., and Zweers, G. (1995). Mechanics of drinking in the brown tree snake, boiga irregularis. *Zool. Anal. Complex Syst*, 98.

Jensen, G. W., van der Smagt, P., Heiss, E., Straka, H., and Kohl, T. (2020a). Snakestrike: A low-cost open-source high-speed multi-camera motion capture system. *Frontiers in Behavioral Neuroscience*, 14:116.

Jensen, G. W., van der Smagt, P., Luksch, H., Straka, H., and Kohl, T. (2020b). Tentative title: Chronic multi-electrode electromyography in snakes.

Jorgensen, R. M. and Jayne, B. C. (2017). Three-dimensional trajectories affect the epaxial muscle activity of arboreal snakes crossing gaps. *Journal of Experimental Biology*, 220(19):3545–3555.

Kalman, R. E. (1960). A New Approach to Linear Filtering and Prediction Problems. *Journal of Basic Engineering*, 82(1):35–45.

Kanatani, K., Sugaya, Y., and Kanazawa, Y. (2016). *Guide to 3D Vision Computation: Geometric Analysis and Implementation*. Springer Publishing Company, Incorporated, 1st edition.

Kanatani, K., Sugaya, Y., and Niitsuma, H. (2008). Triangulation from two views revisited: Hartley-sturm vs. optimal correction. 2008 19th British Machine Vision Conference, BMVC 2008 ; Conference date: 01-09-2008 Through 04-09-2008.

Kardong, K. V. and Bels, V. L. (1998). Rattlesnake strike behavior: kinematics. *Journal of Experimental Biology*, 201(6):837–850.

Kardong, K. V. and Smit, T. L. (2002). Proximate factors involved in rattlesnake predatory behavior: A review. In Schuett, G., Höggren, M., Douglas, M., and Greene, H., editors, *Biology of the Vipers*, pages 253–266. Eagle Mountain Publishing, Eagle Mountain.

Kuhn, H. W. (1956). Variants of the hungarian method for assignment problems. *Naval Research Logistics Quarterly*, 3(4):253–258.

LaDuc, T. J. (2002). Does a quick offense equal a quick defense? kinematic comparisons of predatory and defensive strikes in the western diamond-backed rattlesnake (crotalus atrox). In Schuett, G., Höggren, M., Douglas, M., and Greene, H., editors, *Biology of the Vipers*, chapter 18, pages 267–278. Eagle Mountain Publishing, Eagle Mountain.

Li, B., Heng, L., Köser, K., and Pollefeys, M. (2013). A multiple-camera system calibration toolbox using a feature descriptor-based calibration pattern. In *IROS*, pages 1301–1307. IEEE.

Liljebäck, P., Stavdahl, O., Pettersen, K. Y., and Gravdahl, J. T. (2014). Mamba - a waterproof snake robot with tactile sensing. In *2014 IEEE/RSJ International Conference on Intelligent Robots and Systems*, pages 294–301.

Lillywhite, H. B., LaFrentz, J. R., Lin, Y. C., and Tu, M. C. (2000). The cantilever abilities of snakes. *Journal of Herpetology*, 34(4):523–528.

Lissmann, H. W. (1950). Rectilinear locomotion in a snake (boa occidentalis). *Journal of Experimental Biology*, 26(4):368–379.

Martínez-Marcos, A., Lanuza, E., and Halpern, M. (2002). Neural substrates for processing chemosensory information in snakes. *Brain Research Bulletin*, 57(3):543 – 546.

Mathis, A., Mamidanna, P., Cury, K. M., Abe, T., Murthy, V. N., Mathis, M. W., and Bethge, M. (2018). Deeplabcut: markerless pose estimation of user-defined body parts with deep learning. *Nature Neuroscience*, 21(9):1281–1289.

Merletti, R. (1999). Standards for reporting emg data. *Journal of Electromyography and Kinesiology*, 9(1):III.

Moon, B. and Gans, C. (1998). Kinematics, muscular activity and propulsion in gopher snakes. *Journal of Experimental Biology*, 201(19):2669–2684.

Moon, B. R. (2000). The mechanics and muscular control of constriction in gopher snakes (pituophis melanoleucus) and a king snake (lampropeltis getula). *Journal of Zoology*, 252(1):83–98.

Moon, B. R., Penning, D. A., Segall, M., and Herrel, A. (2019). Feeding in snakes:form, function, and evolution of the feeding system. In Bels, V. and Whishaw, I. Q., editors, *Feeding in Vertebrates*, chapter 14, pages 527–574. Springer.

Moulon, P., Monasse, P., Marlet, R., and Others (2013). Openmvg. an open multiple view geometry library. https://github.com/openMVG/openMVG.

Munkres, J. (1957). Algorithms for the assignment and transportation problems. *Journal of the Society of Industrial and Applied Mathematics*, 5(1):32–38.

Newman, S. J. and Jayne, B. C. (2018). Crawling without wiggling: muscular mechanisms and kinematics of rectilinear locomotion in boa constrictors. *Journal of Experimental Biology*, 221(4).

Nilsson, M. (1998). Snake robot-free climbing. *IEEE Control Systems Magazine*, 18(1):21–26.

Patek, S. N., Korff, W. L., and Caldwell, R. L. (2004). Deadly strike mechanism of a mantis shrimp. *Nature*, 428(6985):819–820.

Penning, D. A., Sawvel, B., and Moon, B. R. (2016). Debunking the viper's strike: harmless snakes kill a common assumption. *Biology Letters*, 12(3):20160011.

Pereira, T. D., Aldarondo, D. E., Willmore, L., Kislin, M., Wang, S. S.-H., Murthy, M., and Shaevitz, J. W. (2019). Fast animal pose estimation using deep neural networks. *Nature Methods*, 16(1):117–125.

Robie, A. A., Seagraves, K. M., Egnor, S. E. R., and Branson, K. (2017). Machine vision methods for analyzing social interactions. *Journal of Experimental Biology*, 220(1):25–34.

Rusu, R. and Cousins, S. (2011). 3d is here: Point cloud library (pcl). In *Robotics and Automation (ICRA), 2011 IEEE International Conference on*, pages 1–4.

Ryerson, W. G. and Tan, W. (2017). Strike kinematics and performance in juvenile ball pythons (python regius). *Journal of Experimental Zoology Part A: Ecological and Integrative Physiology*, 327(7):453–457.

Sadoyama, T. and Miyano, H. (1981). Frequency analysis of surface emg to evaluation of muscle fatigue. *European Journal of Applied Physiology and Occupational Physiology*, 47(3):239–246.

Schneider, C. A., Rasband, W. S., and Eliceiri, K. W. (2012). Nih image to imagej: 25 years of image analysis. *Nature Methods*, 9(7):671–675.

Schroeder, W., Martin, K., and Lorensen, B. (2006). *The Visualization Toolkit–An Object-Oriented Approach To 3D Graphics*. Kitware, Inc., fourth edition.

Seid, M. A., Scheffrahn, R. H., and Niven, J. E. (2008). The rapid mandible strike of a termite soldier. *Current Biology*, 18(22):R1049–R1050.

Simões, B. F., Sampaio, F. L., Loew, E. R., Sanders, K. L., Fisher, R. N., Hart, N. S., Hunt, D. M., Partridge, J. C., and Gower, D. J. (2016). Multiple rod–cone and cone–rod photoreceptor transmutations in snakes: evidence from visual opsin gene expression. *Proceedings of the Royal Society B: Biological Sciences*, 283(1823):20152624.

Stewenius, H., Schaffalitzky, F., and Nister, D. (2005). How hard is 3-view triangulation really? In *Tenth IEEE International Conference on Computer Vision (ICCV'05) Volume 1*, volume 1, pages 686–693 Vol. 1.

Straw, A. D., Branson, K., Neumann, T. R., and Dickinson, M. H. (2011). Multi-camera real-time three-dimensional tracking of multiple flying animals. *Journal of The Royal Society Interface*, 8(56):395–409.

Sutherland, I. E. (1974). Three-dimensional data input by tablet. *Proceedings of the IEEE*, 62(4):453–461.

Theunissen, L. M. and Dürr, V. (2013). Insects use two distinct classes of steps during unrestrained locomotion. *PLOS ONE*, 8(12).

Theunissen, L. M., Reid, T., and Troje, N. F. (2017). Pigeons use distinct stop phases to control pecking. *Journal of Experimental Biology*, 220(3):437–444.

Tian, W., Cong, Q., and Menon, C. (2011). Investigation on walking and pacing stability of german shepherd dog for different locomotion speeds. *Journal of Bionic Engineering*, 8(1):18 – 24.

Tobalske, B. W., Warrick, D. R., Clark, C. J., Powers, D. R., Hedrick, T. L., Hyder, G. A., and Biewener, A. A. (2007). Three-dimensional kinematics of hummingbird flight. *Journal of Experimental Biology*, 210(13):2368–2382.

Toshev, A. and Szegedy, C. (2014). Deeppose: Human pose estimation via deep neural networks. In *2014 IEEE Conference on Computer Vision and Pattern Recognition*, pages 1653–1660.

Westhoff, G., Fry, B. G., and Bleckmann, H. (2005). Sea snakes (lapemis curtus) are sensitive to low-amplitude water motions. *Zoology*, 108(3):195 – 200.

Wright, C., Johnson, A., Peck, A., McCord, Z., Naaktgeboren, A., Gianfortoni, P., Gonzalez-Rivero, M., Hatton, R., and Choset, H. (2007). Design of a modular snake robot. In *2007 IEEE/RSJ International Conference on Intelligent Robots and Systems*, pages 2609–2614.

Young, B., Boetig, M., and Westhoff, G. (2009). Functional bases of the spatial dispersal of venom during cobra "spitting". *Physiological and Biochemical Zoology*, 82(1):80–89. PMID: 19046067.

Young, B. A. (2010). How a heavy-bodied snake strikes quickly: high-power axial musculature in the puff adder (bitis arietans). *Journal of Experimental Zoology Part A: Ecological Genetics and Physiology*, 313A(2):114–121.

Young, B. A., Dunlap, K., Koenig, K., and Singer, M. (2004). The buccal buckle: the functional morphology of venom spitting in cobras. *Journal of Experimental Biology*, 207(20):3483–3494.

Eidesstattliche Versicherung
Affidavit of author's contributions

Hiermit versichere ich an Eides statt, dass ich die vorliegende Dissertation

Faster than the Blink of an Eye: New insights into neuromuscular activations of arboreal snakes

selbstständig angefertigt habe, mich außer der angegebenen keiner weiteren Hilfsmittel bedient und alle Erkenntnisse, die aus dem Schrifttum ganz oder annähernd übernommen sind, als solche kenntlich gemacht und nach ihrer Herkunft unter Bezeichnung der Fundstelle einzeln nachgewiesen habe.

I hereby confirm that the dissertation

Faster than the Blink of an Eye: New insights into neuromuscular activations of arboreal snakes

is the result of my own work and that I have only used sources or materials listed and specified in the dissertation.

München, den 4 Juni, 2020 Grady Jensen

Munich, date Unterschrift /signature

Declaration of Contribution

Additional authors that contributed to the results presented in this thesis are:

- Dr. Tobias Kohl (TK)
- Prof. Dr. Patrick van der Smagt (PvdS)
- Prof. Dr. Hans Straka (HS)
- Dr. Egon Heiss (EH)
- Prof. Dr. Harald Luksch (HL)

Introduction and Final Discussion

- Writing : GJ;
- Visualization: GJ;

Chapter 1 and associated appendix

- Conceptualization: GJ, HS, PvdS, TK;
- Methodology: GJ;
- Software: GJ;
- Validation: GJ;
- Formal analysis: GJ, HS, EH, PvdS, TK;
- Investigation: GJ,TK,EH;
- Resources: PvdS, TK;
- Data curation: GJ;
- Writing - original draft: GJ;
- Writing - review editing: GJ, HS, EH, PvdS, TK;
- Visualization: GJ, TK;
- Supervision: HS, EH, PvdS, TK;
- Project administration: TK;
- Funding acquisition: HS, PvdS, TK.

Chapter 2

- Conceptualization: GJ, HS, PvdS, TK;
- Methodology: GJ, TK;

- Validation: GJ;
- Formal analysis: GJ, TK;
- Investigation: GJ, TK;
- Resources: PvdS, TK, HL;
- Data curation: GJ;
- Writing - original draft: GJ, TK;
- Writing - review editing: GJ, HS, PvdS, TK;
- Visualization: GJ, TK;
- Supervision: HS, HL, PvdS, TK;
- Project administration: TK;
- Funding acquisition: HS, PvdS, TK.

Chapters 3 and 4

- Conceptualization: GJ, HS, PvdS, TK;
- Methodology: GJ, TK;
- Validation: GJ;
- Formal analysis: GJ;
- Investigation: GJ, TK;
- Resources: PvdS, TK, HL;
- Data curation: GJ;
- Writing: GJ;
- Visualization: GJ;
- Supervision: HS, HL, PvdS, TK;
- Project administration: TK;
- Funding acquisition: HS, PvdS, TK.

I hereby confirm the accuracy of the above declared author contributions.

München, 4 June, 2020, Grady W. Jensen Prof. Dr. Patrick van der Smagt